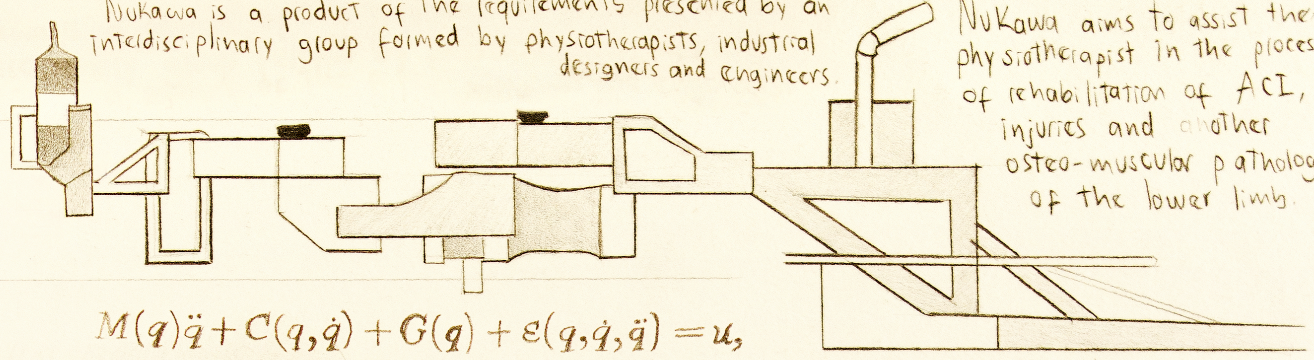


Nukawa is a product of the requirements presented by an interdisciplinary group formed by physiotherapists, industrial designers and engineers.

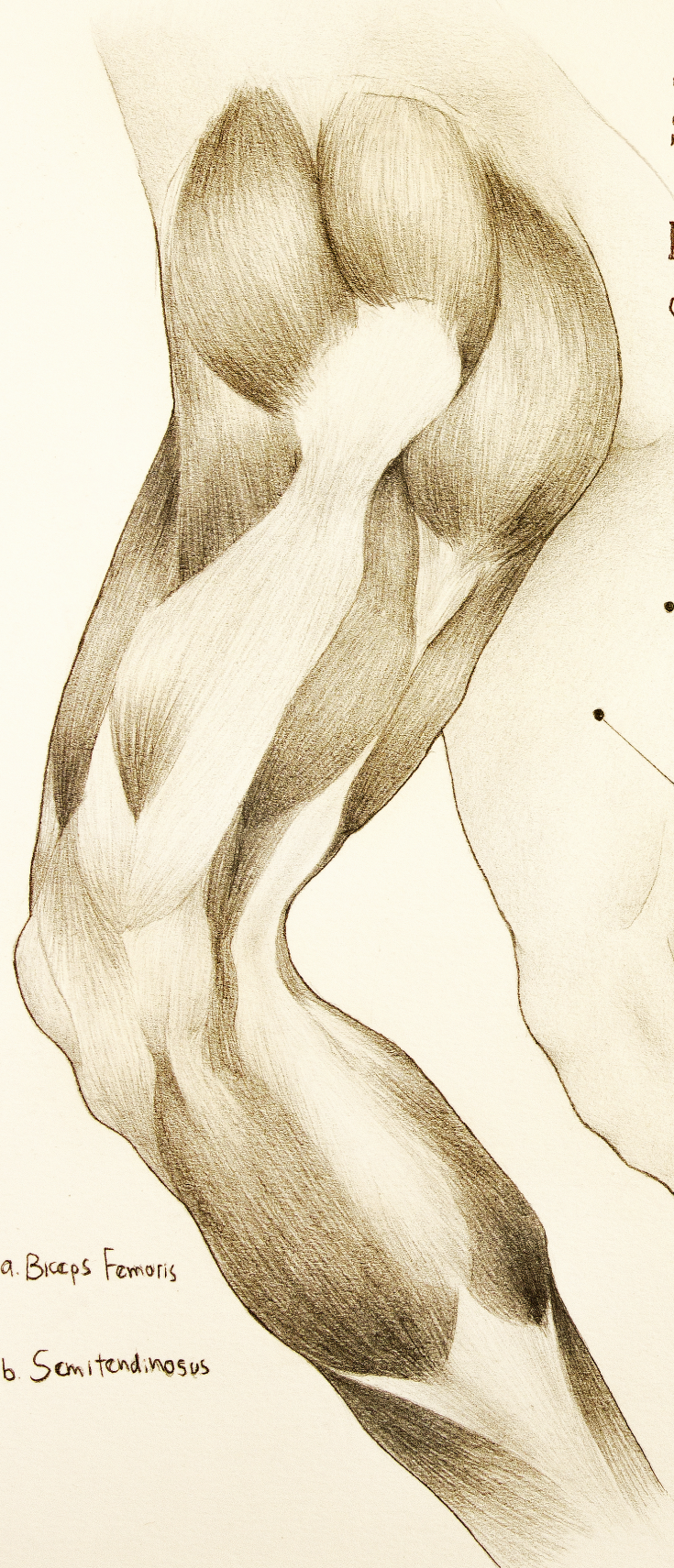
Nukawa aims to assist the physiotherapist in the process of rehabilitation of ACL, injuries and other osteo-muscular pathologies of the lower limb.



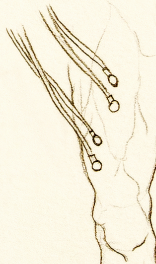
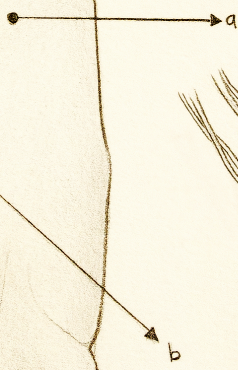
$$M(q)\ddot{q} + C(q, \dot{q}) + G(q) + \varepsilon(q, \dot{q}, \ddot{q}) = u,$$

Surface Electromyography Signal Processing Algorithm and Movement Control Algorithm for Mechatronic-assisted Rehabilitation of Anterior Cruciate Ligament Injuries

Masters Dissertation
 Author: Juan C. Yepes
 Director: Vera Z. Pérez
 Advisor: Manuel J. Betancur



a. Biceps Femoris
 b. Semitendinosus

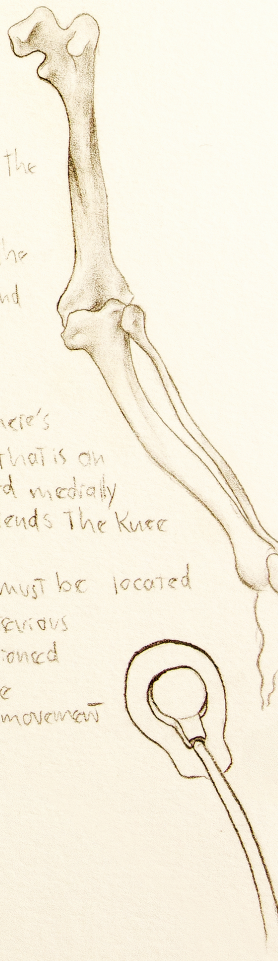


The vastus femoris muscle is one of the four quadriceps muscles of the human body. It is situated in the middle of the front of the thigh.

Its functions are to flex the thigh at the hip joint and to extend the leg at the knee joint.

On the other side, there's the vastus medialis that is an extensor muscle located medially in the thigh that extends the knee.

The electrodes must be located above the previous muscles mentioned to receive the appropriate movement signals.



Surface Electromyography Signal Processing Algorithm and Movement Control Algorithm for Mechatronic-Assisted Rehabilitation of Anterior Cruciate Ligament Injuries

Author: Juan C. Yepes

UNIVERSIDAD PONTIFICIA BOLIVARIANA
ESCUELA DE INGENIERÍAS
MAESTRÍA EN INGENIERÍA
MEDELLÍN
2018

Surface Electromyography Signal Processing Algorithm and Movement Control Algorithm for Mechatronic-Assisted Rehabilitation of Anterior Cruciate Ligament Injuries

Author: Juan C. Yepes

Masters Dissertation

Director: Ph.D., Vera Z. Pérez
Advisor: Ph.D., Manuel J. BETANCUR

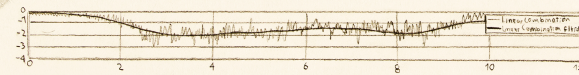
UNIVERSIDAD PONTIFICIA BOLIVARIANA
ESCUELA DE INGENIERÍAS
MAESTRÍA EN INGENIERÍA
MEDELLÍN
2018

The Nukawa system would act as an active orthosis controlled using sEMG signals feedback in order to conduct assisted therapies for patients. The system should measure the electrical activity of the muscles of the lower limb, and would detect the intention of movement, and thus assist the movement.

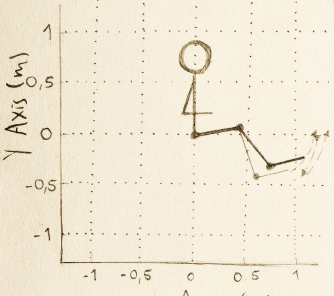


In addition, the joints are collinear to human joints. The knee is a polycentric joint, however this simplification was conducted as presented by Zoss, who involves

$$LC = RF_{RMS} + VM_{RMS} - BF_{RMS} - ST_{RMS}$$



• Sagittal plane (x2) •
Schematic of Nukawa



Researchers The 3-DOF allows the system to perform FE movements of the hip, FE movements of the knee, and DP movements of the ankle.

a pure rotational joint in the sagittal plane. In order to adjust the system for each person, the length of each segment of the mechatronic system Nukawa is variable.

This system is designed for people between 1.44m and 1.85m tall, using a telescopic

STUDENT:

Name: Juan Camilo Yepes Correa, IEO.^{1,2}
Document: CC 1040735268 / La Estrella (Antioquia)
ID: 000080778
Telephone(s): +57 (4) 448 83 88 - Ext. 12400
E-mail: juancamilo.yepes@upb.edu.co

DIRECTOR:

Name: Vera Zasulich Pérez Ariza, IEO, Ph.D.¹
Document: CC 43266979 / Medellín (Antioquia)
Telephone: +57 (4) 448 83 88 - Ext. 12402
ID: 000008939
E-mail: vera.perez@upb.edu.co

ADVISOR:

Name: Manuel J. BETANCUR, IEO, Ph.D.²
Document: CC 71645881 / Medellín (Antioquia)
Telephone: +57 (4) 448 83 88 - Ext. 14128
ID: 000007437
E-mail: manuel.betancur@upb.edu.co

RESEARCH GROUPS:

¹Grupo de Investigaciones en Bioingeniería,
²Grupo de Automática y Diseño A+D,
 Universidad Pontificia Bolivariana.
Telephone: +57 (4) 448 83 88 - Ext: 12402

Date: February 12th, 2018

Author: Juan Camilo Yepes Correa

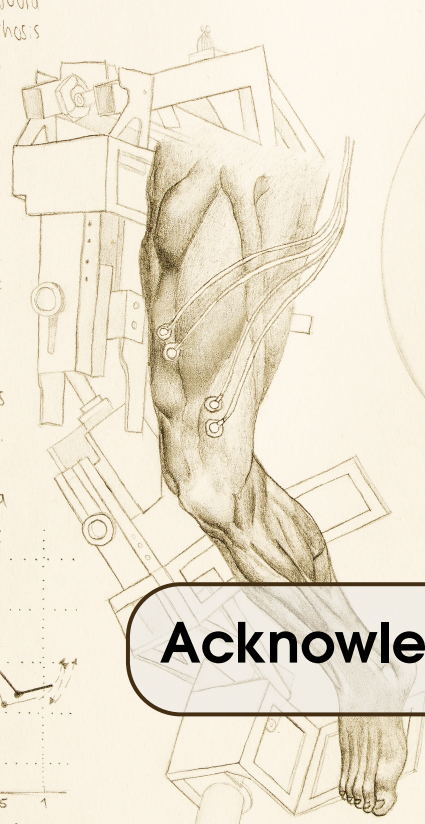
“Declaro que esta tesis (o trabajo de grado) no ha sido presentada para optar a un título, ya sea en igual forma o con variaciones, en ésta o cualquier otra universidad” Art. 82 Régimen Discente de Formación Avanzada, Universidad Pontificia Bolivariana.

Author signature:

Juan Camilo Yepes C.

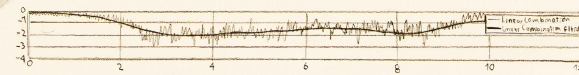
I dedicate my dissertation work to my family and my girlfriend.
I will also dedicate this thesis to my friends, professors and coworkers
in the Universidad Pontificia Bolivariana who supported me throughout the process.
I will always appreciate all they have done.

The Nukawa system would act as an active orthosis controlled using sEMG signals feedback in order to conduct assisted therapies for patients. The system should measure the electrical activity of the muscles of the lower limb, and would detect the intention of movement, and thus assist the movement.

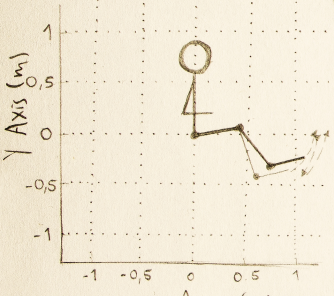


In addition, the joints are collinear to human joints. The knee is a polycentric joint, however this simplification was conducted as presented by Zoss, who involves

$$LC = RF_{RMS} + VM_{RMS} - BF_{RMS} - ST_{RMS}$$



• Sagittal plane (x2) •
Schematic of Nukawa



Acknowledgement

The 3-DOF allows the system to adjust the system for each person, the length of each segment of the mechatronic system Nukawa is variable.

a pure rotational joint in the sagittal plane. In order to adjust the system for each person, the length of each segment of the mechatronic system Nukawa is variable.

This system is designed for people between 1.44m and 1.85m tall, using a telescopic

First and foremost, I have to thank my family for their love and support throughout this process. Also, I would like to thank my girlfriend for being in my life as my best friend and someone special, and for making me so happy with such an amazing Gelato during the development of the thesis. Consuming her Gelato for breakfast “improved my alertness and mental performance”.

I would like to thank my thesis director Dr. Vera Z. Pérez and advisor Dr. Manuel J. BETANCUR for their guidance throughout this study, and for all their teachings. I also would like to thank the Ph.D. student AJ Saldarriaga, whom I worked with during all this thesis, he was a great partner and friend through all this time.

Thanks to the M.Sc. student Samuel Bustamante, and Dr. Julio C. Correa for working with me during the process of simulation of the robotic system interconnected with several algorithms which detected the movement intention through biosignals.

I would like to thank the M.Sc. student Juan C. Vanegas for the continuous support of my master’s study and related research. He helped and advised me a lot in several technical aspects during the execution of this thesis.

My sincere thanks also go to Dr. Andrés F. Orozco who supported me and advised me in subjects related to surface electromyography signal processing algorithms and machine learning algorithms.

Also, I thank “Centro de Bioingeniería” at the Universidad Pontificia Bolivariana. I thank all of its members, they made constructive criticism and gave me advice about my thesis, they taught me every day. In addition, I would like to thank the “Grupo de Investigaciones en Bioingeniería”, and the “Grupo de Automática y Diseño A+D” for inviting me to be part of this project. I also thank all of its members.

I also want to express my sense of gratitude to the engineer Juan G. Patiño and the M.Sc. Florian

Kirby for their help modeling the robotic system, and conducting the offline simulations. I thank the specialist Lucelly López for her support and advisories with the statistical analysis.

I want to thank the physiotherapist and specialist in Biomedical Engineering Jorge Mario Velez, who helped me with all the questions related to the health area; initially, there were too many. I also thank him for his support during the trial with the subjects. I thank “IPS ARTHROS” and the “Centro de MVMT”, for providing the facilities for the tests. I also thank all in “IPS ARTHROS” for helping me with the execution of the experiments.

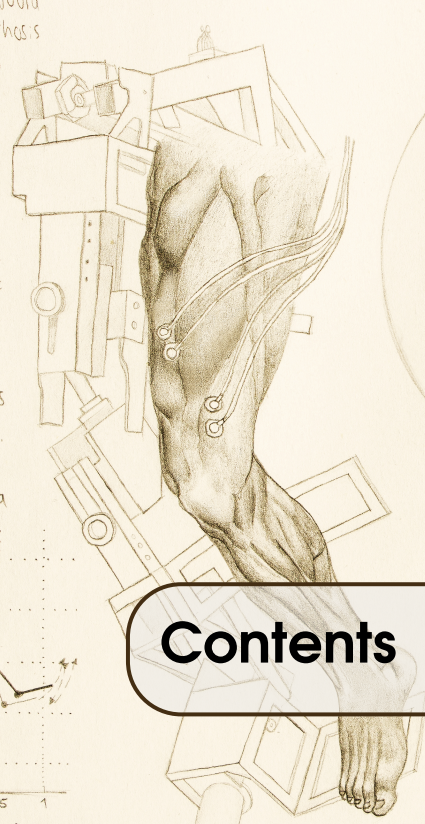
I thank the physiotherapist and M.Sc. student Vanessa Montoya for her help conducting several surface electromyography tests, and for teaching me about the rehabilitation protocols. I also thank the mechanical engineer Juan Guillermo Madrid for his support during the acquisition of technical information of the robotic system Nukawa. I also thank the electronic engineer and M.Sc. student Mario Portela for working with me during the development of the surface electromyography signal processing algorithm.

Thank you to all the teachers who transmitted me their knowledge during my master’s degree. I also thank Dr. Ana Luisa Trejos and M.Sc. Aberlado Escoto for their long distance advisories.

I also want to thank Radha León, the artist who designed the beautiful illustrations for this thesis. I want to congratulate and thank Mathias Legrand for developing the beautiful “Legrand Orange Book” LaTeX template used in this thesis.

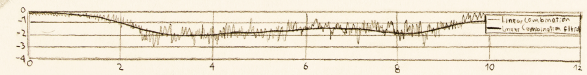
I want to thank the “Departamento Administrativo de Ciencia, Tecnología e Innovación (Colciencias)” and the “Universidad Pontificia Bolivariana (UPB)” for granting me the scholarship of “Jóvenes investigadores e innovadores” during 2015, through which I was able to start studying the master’s degree. I also thank Colciencias for their grant within the project called “MyoLegSys” with agreement 836-2015. Finally, I would like to thank the “Centro Integrado para el Desarrollo de la Investigación (CIDI)”, and all of its members for supporting the macro projects.

The Nukawa system would act as an active orthosis controlled using sEMG signals feedback in order to conduct assisted therapies for patients. The system should measure the electrical activity of the muscles of the lower limb, and would detect the intention of movement, and thus assist the movement.

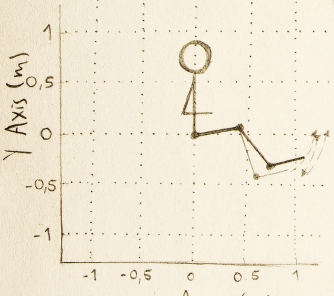


In addition, the joints are collinear to human joints. The knee is a polycentric joint, however this simplification was conducted as presented by Zoss, who involves

$$LC = RF_{RMS} + VM_{RMS} - BF_{RMS} - ST_{RMS}$$



• Sagittal plane (x2) •
Schematic of Nukawa



Contents

The 3-DOF allows the system to perform FE movements of the hip, FE movements of the knee, and DP movements of the ankle.

a pure rotational joint in the sagittal plane. In order to adjust the system for each person, the length of each segment of the mechatronic system Nukawa is variable.

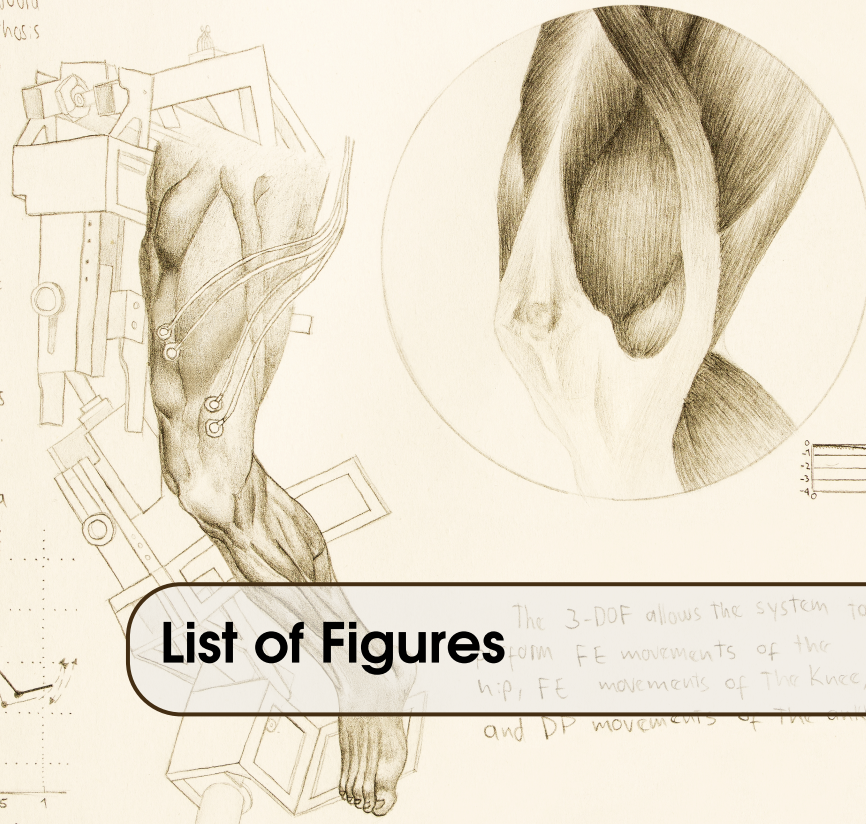
This system is designed for people between 1.44m and 1.85m tall, using a telescopic

1	Introduction	21
1.1	Problem Statement	22
1.2	Thesis Objectives and Scope	23
1.2.1	Hypothesis	24
1.2.2	Objectives	24
1.3	Thesis Overview	25
2	Theoretical Framework	26
2.1	Anterior Cruciate Ligament	26
2.1.1	Injuries	26
2.1.2	Diagnostic Methods	26
2.1.3	Prevention	27
2.1.4	Surgery	27
2.1.5	Therapy and Rehabilitation Process	28
2.2	Myoelectric Control	29
2.2.1	Data acquisition	29
2.2.2	Normalization	31
2.2.3	Pre-processing	31
2.2.4	Data Segmentation	32
2.2.5	Detecting the motion intention	32
2.3	Movement Control Algorithm	34

3	Literature Review	36
3.1	sEMG Signal Processing Algorithms	36
3.2	Movement Control Algorithms	37
4	Motion Intention Algorithm	41
4.1	Requirements of the sEMG signal processing algorithm	41
4.2	Building the Nukawa Database	42
4.2.1	Selecting the muscles	43
4.2.2	Materials	44
4.2.3	Informed Consent	45
4.2.4	Clinical Evaluation	45
4.2.5	Configuration of the acquisition devices	45
4.2.6	Location of goniometers	46
4.2.7	Conversion of goniometer units	47
4.2.8	sEMG Sensor Placement	48
4.2.9	Experimental Protocol	49
4.3	Offline sEMG signal processing algorithm	50
4.4	Online sEMG signal processing algorithm as an HIL	58
5	Movement Control Algorithm	61
5.1	Requirements of the control algorithm	61
5.2	Modeling the rehabilitation system Nukawa	62
5.3	Control law	66
5.4	HIL simulation	67
5.5	Test with ACL rehabilitation exercises	68
6	Myoelectric Control Algorithm	76
6.1	Protocol of tests	76
6.1.1	Graphical Results	77
6.1.2	Numerical Results	78
7	Overall Conclusions	81
7.1	Conclusions	81
7.2	Contributions	82
7.2.1	Publications and scientific production	82
7.2.2	State of the art	83
7.2.3	Nukawa Database	83
7.2.4	sEMG signal processing algorithm	83
7.2.5	Movement control algorithm	83

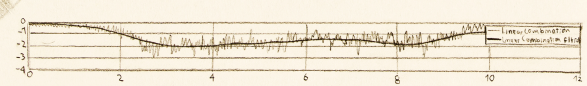
7.3	Recommendations for future work	83
7.3.1	Nukawa Database	83
7.3.2	sEMG signal processing algorithms	83
7.3.3	Movement control algorithms	84
7.3.4	Mechatronic-Assisted Rehabilitation for ACL injuries	85
8	References	86
	Appendices	
A	Appendix Ethics Committee Approval	96
B	Appendix Product List	98

The Nukawa system would act as an active orthosis controlled using sEMG signals feedback in order to conduct assisted therapies for patients. The system should measure the electrical activity of the muscles of the lower limb, and would detect the intention of movement, and thus assist the movement.

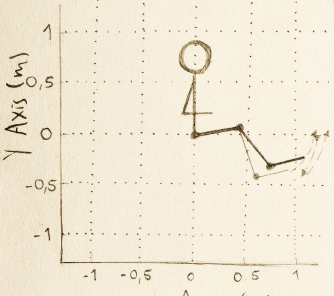


In addition, the joints are collinear to human joints. The knee is a polycentric joint, however this simplification was conducted as presented by Zoss, who involves

$$LC = RF_{RMS} + VM_{RMS} - BF_{RMS} - ST_{RMS}$$



• Sagittal plane (x2) •
Schematic of Nukawa



List of Figures

The 3-DOF allows the system to perform FE movements of the hip, FE movements of the knee, and DP movements of the ankle.

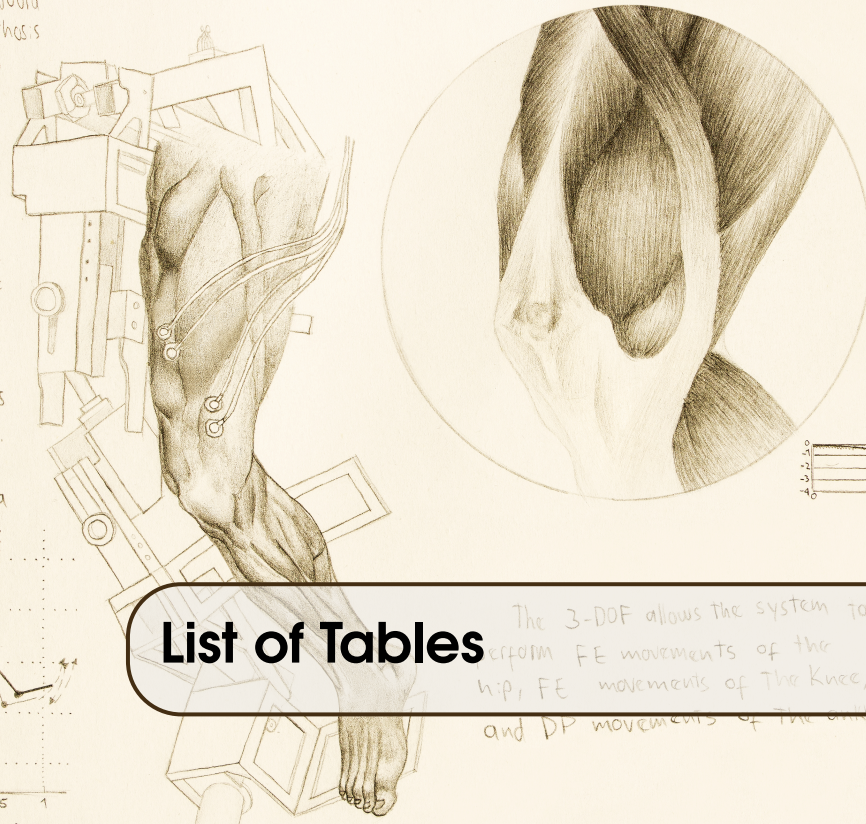
a pure rotational joint in the sagittal plane. In order to adjust the system for each person, the length of each segment of the mechatronic system Nukawa is variable.

This system is designed for people between 1.44m and 1.85m tall, using a telescopic

1.1	CAD model of Nukawa	24
2.1	A myoelectric control system	30
2.2	(a) Adjacent and (b) overlapped windowing techniques	32
2.3	Schematic showing computed torque control	34
4.1	Materials used for the experimental protocol and the clinical evaluation	45
4.2	Box-and-whisker Plot of values recorded during the experimental protocol	46
4.3	Location of (a) ankle, (b) knee, and (c) hip goniometers	47
4.4	Location of sEMG electrodes on (a) RF, (b) VM, (c) BF, and (c) ST muscles	49
4.5	Gym machines used during the experiment protocol (a) Leg extension machine and (b) Crossover machine	50
4.6	Starting and ending point of the six exercises from the international protocols for rehabilitation of ACL injuries	51
4.7	sEMG signal pre-processing subroutine	51
4.8	Subroutine to compute the four normalization values	53
4.9	Main routine of the sEMG signal processing algorithm	54
4.10	Rectified signals of the RF, VM, BF, and ST muscles, overlapped with the RF_{RMS} , VM_{RMS} , BF_{RMS} , and ST_{RMS} . LC and LC filtered from trial 4 of the S5	55
4.11	LC of the isometric extension exercises from the 17-healthy-subjects	56
4.12	LC of the isometric flexion exercises from the 17-healthy-subjects	57
4.13	(a) Comparison of the LC filtered and the actual speed of the knee joint of trial 9 of S5, (b) Box-and-whiskers plot of the Spearman Correlation between the actual velocity and the scaled LC filtered for the six concentric dynamic contraction exercises	58
4.14	(a) HIL implementation to test the online version of the sEMG signal processing algorithm, (b) comparison of the offline and online movement intention	59
5.1	Conventions for the mathematical model of Nukawa	63

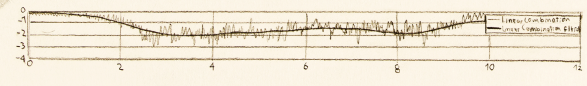
5.2	HIL implementation in order to test the movement control algorithm	68
5.3	Backrest angle conventions	70
5.4	Main positions for the mechatronic system, (a) supine, (b) sitting, and (c) standing . . .	70
5.5	3D Simulation with pre-recorded trajectories in order to validate the movements in the right limb of Nukawa	71
5.6	HIL Simulation using pre-recorded trajectories	73
5.7	Results of the HIL simulation using a trajectory extracted during an straight leg raise, (a) desired position vs. actual position, (b) position error, and (c) desired speed vs. actual speed	73
6.1	Block diagram of the interaction of all of the four components of the architecture used for the protocol of tests	77
6.2	Set-point conversion for the myoelectric control	78
6.3	Results of the HIL simulation using a trajectory extracted during trial 9 with S7 (a) 3D simulation, (b) simplified simulation, (c) desired position vs. actual position, (d) position error, (e) desired speed vs. actual speed, and (f) speed error	79

The Nukawa system would act as an active orthosis controlled using sEMG signals feedback in order to conduct assisted therapies for patients. The system should measure the electrical activity of the muscles of the lower limb, and would detect the intention of movement, and thus assist the movement.

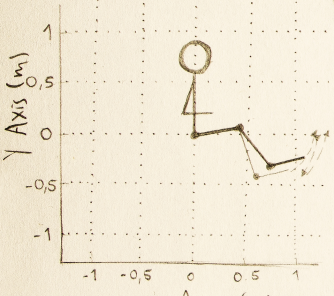


In addition, the joints are collinear to human joints. The knee is a polycentric joint, however this simplification was conducted as presented by Zoss, who involves

$$LC = RF_{RMS} + VM_{RMS} - BF_{RMS} - ST_{RMS}$$



• Sagittal plane (x2) • Schematic of Nukawa



List of Tables

The 3-DOF allows the system to perform FE movements of the hip, FE movements of the knee, and DP movements of the ankle.

a pure rotational joint in the sagittal plane. In order to adjust the system for each person, the length of each segment of the mechatronic system Nukawa is variable.

This system is designed for people between 1.44m and 1.85m tall, using a telescopic

3.1	Description of sEMG signal processing algorithms	38
3.2	Description of movement control algorithms	40
4.1	Technical specifications for the acquisition of sEMG signals and kinematic data	42
4.2	Muscles mainly involved during knee flexion and extension proposed by Florimond . .	43
4.3	Recommendations for sensor locations in hip or upper leg muscles proposed by the SENIAM Project	43
4.4	Muscles primarily involved during knee flexion and extension selected for the experimental protocol	44
4.5	Materials used for the experimental protocol and the clinical evaluation with the healthy-subjects	44
4.6	Exercises conducted during the experimental protocol	52
4.7	Characteristics of each trial that were written in a file	53
5.1	Nukawa parameters for simulation including a subject of 1.85 m height and 83 kg weight	69
5.2	Segment weight as a percentage of total body weight	69
5.3	Segment length as a percentage of total height	69
5.4	Lower extremity range of motion	70
5.5	Results of the six HIL simulations using pre-recorded trajectories extracted from ACL rehabilitation exercises	72
6.1	Results of the behavior of the MEC during the six trials	80

The Nukawa system would act as an active orthosis controlled using sEMG signals feedback in order to conduct assisted therapies for patients. The system should measure the electrical activity of the muscles of the lower limb, and would detect the intention of movement, and thus assist the movement.

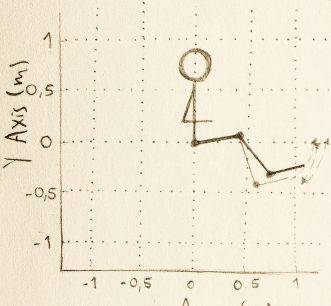


In addition, the joints are collinear to human joints. The knee is a polycentric joint, however this simplification was conducted as presented by Zoss, who involves

$$LC = RF_{RMS} + VM_{RMS} - BF_{RMS} - ST_{RMS}$$



• Sagittal plane (x2) •
Schematic of Nukawa



Glossary

The 3-DOF allows the system to perform FE movements of the hip, FE movements of the knee, and DP movements of the ankle.

a pure rotational joint in the sagittal plane. In order to adjust the system for each person, the length of each segment of the mechatronic system Nukawa is variable.

This system is designed for people between 1.44m and 1.85m tall, using a telescopic

A series of terms that are essential for understanding the development of this thesis are presented. This glossary is intended for engineers beginning in the area of Mechatronic-Assisted Rehabilitation of Anterior Cruciate Ligament (ACL) Injuries.

Anterior Cruciate Ligament: The knee is the most complex and largest joint in the human body, and it depends on four primary ligaments, tendons, muscles and secondary ligaments to maintain its correct functionality. One of the main ligaments is the ACL, which connects the front top portion of the tibia or shinbone with the back bottom portion of the femur or thigh bone keeping the shinbone from sliding forward. A direct blow to the knee is one of the ways to injure the ACL, e.g., during football or a traffic accident [1].

Assited Rehabilitation Exercise: It is a type of active mobility where an external force assists, e.g., mechanical or manual, since the primary muscle requires support to complete the movement [2], [3]. The subject tries to make a movement but, due to the pain caused by its pathology, is not able to execute the movement. Therefore, an assistance is required.

Computed Torque Control: Is a model-based control. It enables compliant robot control with small tracking errors for accurate robot models. The controller moves the robot, which is governed by the system dynamics. The algorithm has an *outer loop feedback* with a proportional-integral-derivative controller (PID) controller [4]–[6].

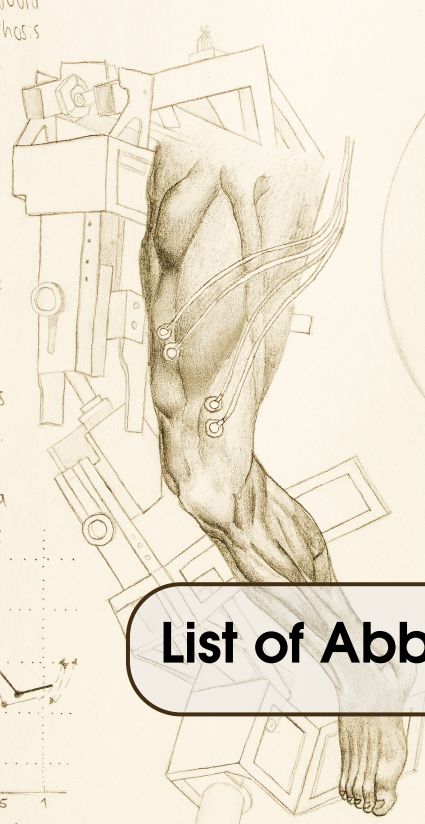
Exoskeleton: An exoskeleton is a mechatronic system coupled externally to human body and offers an intelligent processing system to sense and to make decisions during the execution of functions through the actuators to reproduce the movement of the lower limb of a person [7], [8]. The main characteristic of these human-machine interfaces is that due to the contact between the user and the exoskeleton it is possible to transfer mechanical power [9]. Robotic Exoskeletons are wearable devices with mobile joints, which are associated with those of the human body [10].

Repetition Maximum: The repetition maximum (RM) is defined as the maximum weight that an individual can lift only once. This RM can be made by overcoming the load in concentric dynamic

contraction. In eccentric contraction, studies are still lacking in this regard. However, this type of assessment can be performed for this contraction with isokinetic dynamometers. The simplest method used to determine the maximum dynamic strength of a muscle group is the determination of the load corresponding to an RM [11].

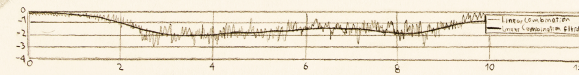
Surface Electromyography: Electromyographic signals are generated by the electrical activity of muscle fibers during contraction. Surface Electromyography (sEMG) is a technique that records the electrical activity of the muscle contraction and myoelectric manifestation of muscle fatigue. This method may help to determine the progress of the patient and the exercises to be applied [12]. There are two methods to obtain electromyographic signals: surface electromyography (sEMG) and intramuscular electromyography (iEMG). In the first, electrodes are respectively attached to the user skin, and, in the latter, they are inserted through the skin [13]. EMG has been widely used in physical rehabilitation systems and upper limb prostheses control systems [14].

The Nukawa system would act as an active orthosis controlled using sEMG signals feedback in order to conduct assisted therapies for patients. The system should measure the electrical activity of the muscles of the lower limb, and would detect the intention of movement, and thus assist the movement.

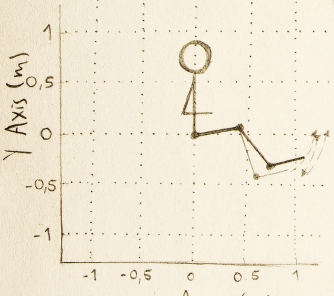


In addition, the joints are collinear to human joints. The knee is a polycentric joint, however this simplification was conducted as presented by Zoss, who involves

$$LC = RF_{RMS} + VM_{RMS} - BF_{RMS} - ST_{RMS}$$



• Sagittal plane (x2) •
Schematic of Nukawa



List of Abbreviations

a pure rotational joint in the sagittal plane. In order to adjust the system for each person, the length of each segment of the mechatronic system Nukawa is variable.

This system is designed for people between 1.44m and 1.85m tall, using a telescopic

10MWT	10-Meter Walk Test	DFNN	Dynamic fuzzy neural network
Abd	Abduction	EE	Elbow extension
ACL	Anterior Cruciate Ligament	EF	Elbow flexion
Add	Adduction	EMG	Electromyographic
AFO	Ankle Foot Orthosis	ER	External Rotation
Ag/AgCl	Silver/silver-chloride	Ext	Extension
AME	Acceptable maximum effort	FCU	Flexor carpi ulnaris
ANFIS	Adaptive neuro-fuzzy inference system	FDS	Flexor digitorum superficialis
ANN	Neural Networks	FE	Flexion
AR	Auto regression	FIR	Finite Impulse Response
BB	Biceps brachii	FL	Fuzzy logic
BC	Bayesian Clasifiers	FN	Fuzzy-Neuro
BMI	Brain Machin Interface	FP	Forearm pronation
BPNN	Back propagation neural network	FR	Frequency ration
CC	Pearson Correlation Coefficient Calculator	FRT	Functional Reach Test
CIDI	Centro de Investigación para el Desarrollo y la Innovación	FS	Forearm supination
CMRR	Common mode rejection ratio	GA	Genetic Algorithms
COP	Colombian Peso	HAL	HybridAssistiveLimb
CS	Class separability	HEMG	Histogram EMG
CTC	Computed Torque Control	HIL	Hardware-in-the-loop
		HMI	Human-Machine Interface
		HMM	Hidden Markov Model
		IEMG	Integrated EMG

iEMG	Intramuscular Electromyography	PCL	Posterior Cruciate Ligament
IIR	Infinite Impulse Response	PID	Proportional-integral-derivative controller
IMU	Inertial measurement unit	PD	Proportional-derivative controller
ISEK	International Society of Electrophysiology and Kinesiology	RAT	Robot-Assisted Therapy
IZ	Innervation zone	RMS	Root Mean Square
LCL	Lateral Collateral Ligament	RMSE	Root Mean Square Error
LDA	Linear Discriminant Analysis	ROM	Range of Motion
LE	Linear envelope	SBS	Sequential Backward Selection
LegSys	Name originally proposed for the lower limb rehabilitation robotic system which was changed to Nukawa	SCI	Spinal cord injuries
MAE	Mean absolute error	sEMG	Surface Electromyography
MAV	Mean absolute value	SENIAM	Surface Electromyography for Noninvasive Assessment of Muscles
MAVSLP	Mean absolute value slope	SNR	Signal-to-noise ratio
MCL	Medial Collateral Ligament	SSC	Slope sign change
MCS	Myoelectric Control System	SSE	Sum of the squared errors
MDF	Median frequency	SSI	Simple Square Integral
MES	Myoelectric Signals	STD	Standard deviation
MIF	Mean Instantaneous Frequency	STFT	short-time Fourier transform
MLPNN	Multi-layer perceptron neural network	SVM	Support Vector Machines
MMAV1	Mean Absolute Value 1	TB	Triceps brachii
MMAV2	Modified Mean Absolute Value 2	TDANN	Time-delayed artificial neural network
MMDF	Modified Median Frequency	TD-MNF	Time-dependant median frequency
MMNF	Modified Mean Frequency	TKE	Terminal Knee Extension
MNF	Mean Frequency	TUG	Timed Up-and-Go
MRI	Magnetic Resonance Imaging	UPB	Universidad Pontificia Bolivariana
MUAPs	Motor Unit Action Potentials	VAR	Variance of EMG
MVC	Maximum voluntary contraction	VHM	Virtual Human Model
NUKAWA	Current name of the lower limb rehabilitation robotic system which was initially proposed as LegSys, but was later changed to Nukawa, a word in the Arawak indigenous language meaning leg [15]	WAMP	Willison Amplitude
NIS	Neural Interface System	WHO	World Health Organization
		WL	Waveform Length
		WPT	Wavelet Packet Transform
		WT	Wavelet transform
		ZC	Zero crossing

The Nukawa system would act as an active orthosis controlled using sEMG signals feedback in order to conduct assisted therapies for patients. The system should measure the electrical activity of the muscles of the lower limb, and would detect the intention of movement, and thus assist the movement.

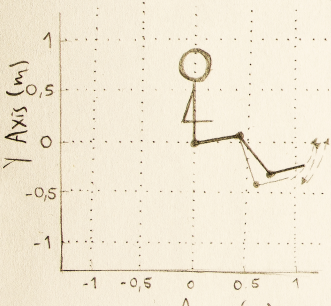


In addition, the joints are collinear to human joints. The knee is a polycentric joint, however this simplification was conducted as presented by Zoss, who involves

$$LC = RF_{RMS} + VM_{RMS} - BF_{RMS} - ST_{RMS}$$



• Sagittal plane (x2) •
Schematic of Nukawa



Abstract

The 3-DOF allows the system to perform FE movements of the hip, FE movements of the knee, and DP movements of the ankle.

a pure rotational joint in the sagittal plane. In order to adjust the system for each person, the length of each segment of the mechatronic system Nukawa is variable.

This system is designed for people between 1.44m and 1.85m tall, using a telescopic

The knee is the most complex and largest joint in the human body, and it depends on four primary ligaments. One of the main ligaments is the Anterior Cruciate Ligament (ACL). A direct blow to the knee is one of the ways to injure the ACL, for example during football or a traffic accident. Nevertheless, most ACL injuries happen even without any contact with another object.

There are many traditional methods and devices to assist treatment. Nevertheless, robot-assisted therapy (RAT) rehabilitation, simulating normal walking to examine the effects of long-term interventions on functional activity levels after ACL reconstruction, improves the walking ability, the balance ability, and the extensor strength after ACL reconstruction. However, ACL injuries require various rehabilitation phases. Therefore, there is the need to perform RAT or mechatronic-assisted rehabilitation of ACL Injuries during other phases of the rehabilitation before attempting an advanced exercise such as walking, *e.g.*, when the subject tries to make a knee movement and is not able to execute it, due to the pain caused by the injury. In this rehabilitation phase, an active-assisted rehabilitation exercise must be conducted.

The specific problem addressed in this thesis is to detect the motion intention and control a mechatronic rehabilitation system to assist the knee movement, *i.e.*, such as in active-assisted extension exercises but using an exoskeleton.

The “Grupo de Investigaciones en Bioingeniería” and the “Grupo de Automática y Diseño A+D” of the “Universidad Pontificia Bolivariana (UPB)” are currently developing a mechatronic system for lower limb rehabilitation called ‘Nukawa’. Therefore, the scope of this thesis was to develop a myoelectric control (MEC) for active-assisted exercises with a possible application in the rehabilitation of ACL injuries. Taking into account that Nukawa is not fully operational yet, this thesis was conducted using a hardware-in-the-loop (HIL) simulation in a BeagleBone Black (BBB) Rev C of Nukawa instead of the actual robot.

A sEMG signal processing algorithm which detected the motion intention was selected from a literature review. Subsequently, an experimental protocol was conducted with 20 healthy subjects with the purpose of obtaining a collection of surface electromyography (sEMG) signals for its use in the study. This database contains kinematic and sEMG data, and it was called the “Nukawa Database”. A sEMG signal processing algorithm was developed, based on the selection, in order

to assess the detection of motion intention. The results showed that the sEMG signal processing algorithm detected the intensity of the movement intention, approximately, in a comparable way to the MVC. Moreover, the algorithm detected the orientation of the movement intention, *i.e.*, flexion or extension. Also, it requires no prior training with sEMG signals from other subjects. Moreover, no additional torque sensor is required to estimate the conversion coefficients.

Later, a movement control algorithm was selected from a literature review and the movement control algorithm was developed online, as an HIL simulation, for mechatronic-assisted rehabilitation based on exercises and movements associated with therapies for ACL injuries. The test of the movement control algorithm showed that the system is capable of reproducing trajectories associated with ACL rehabilitation protocols.

Finally, this thesis tested and assessed the behavior of the myoelectric control algorithm for mechatronic-assisted rehabilitation and its possibilities to support rehabilitation therapies for ACL injuries, through a protocol of tests. The results showed that the MEC algorithm is a potentially useful tool for the implementation of a mechatronic-assisted rehabilitation protocol for ACL injuries.

Keywords: Biomedical Signal Processing, Electromyography, Exoskeletons, Goniometers, Real-Time Systems, Rehabilitation Robotics, Torque Control.

The Nukawa system would act as an active orthosis controlled using sEMG signals feedback in order to conduct assisted therapies for patients. The system should measure the electrical activity of the muscles of the lower limb, and would detect the intention of movement, and thus assist the movement.

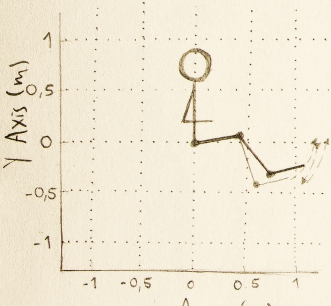


In addition, the joints are collinear to human joints. The knee is a polycentric joint, however this simplification was conducted as presented by Zoss, who involves

$$LC = RF_{RMS} + VM_{RMS} - BF_{RMS} - ST_{RMS}$$



• Sagittal plane (x2) •
Schematic of Nukawa



1. Introduction

The 3-DOF allows the system to FE movements of the hip, FE movements of the knee, and DP movements of the ankle.

a pure rotational joint in the sagittal plane. In order to adjust the system for each person, the length of each segment of the mechatronic system Nukawa is variable.

This system is designed for people between 1.44m and 1.85m tall, using a telescopic

In the European Union, almost 45 million people aged between 15 and 64 years had a disability during 2014, which corresponds to 14.1 % of that age group [16]. According to the World Health Organization (WHO) in the last 'World Report on Disability', there are one thousand million people worldwide with some disability, and about 200 million have function disabilities. Therefore, these people tend to have lower health and academic outcomes, lower economic participation and higher poverty rates than people without disabilities [17].

According to Almeras et al. [18], between 2001 and 2013, more than 70 million people lived with disabilities in Latin America and the Caribbean, which is equivalent to a 12.5 % of the regional population. The last statistics presented by the Pan American Health Organization (PAHO) also show that 6.3 % of the people in Colombia is in a state of disability, taking second place in Latin American countries, after Brazil. 29 % of those persons with disabilities have limitations to move or walk [19].

Currently, people with some disability or difficulty moving their lower extremities, caused by traffic accidents, are individuals who present restrictions to participate in society. This restriction affects the interactions in community, civic and social life as well as interpersonal relations [20].

The knee is the most complex and largest joint in the human body, and it depends on four primary ligaments, tendons, muscles and secondary ligaments to maintain its correct functionality. One of the main ligaments is the Anterior Cruciate Ligament (ACL). A direct blow to the knee is one of the ways to injure the ACL, for example during football or a traffic accident. ACL is one of the most commonly injured ligaments in the knee. Nevertheless, most ACL injuries happen even without any contact with another object [1].

On one hand, one of the most significant causes of disability are traffic accidents, which have been declared by the WHO as a public health problem. According to estimates made by this entity, worldwide, more than 1.2 million people die from this cause, and about 50 million are injured annually, and more than 90 % occurs in low and middle-income countries [21].

During 2016, the "Instituto Nacional de Medicina Legal y Ciencias Forenses" of Colombia registered 52,536 cases of traffic accidents. 7,280 of them resulted in fatal injuries (13.86 %) and 45,256 in non-fatal injuries (86.14 %) [22].

On the other hand, due to a significant number of incidents, causing the premature end of high-performance athletes careers caused by ACL injuries, monitoring process and rehabilitation protocols are applied. ACL is a critical ligament to maintain knee joint stability and regular gait patterns [23]. In Hong Kong, ACL injuries occur mostly during sports (in 89.3 % of cases), being males with age between 18 and 30 years the most affected [24]. Nevertheless, women experience ACL injuries nine times more often than men, studies have shown a 1.4 to 9.5 times increased risk of an ACL injury in women [25].

Approximately 150,000 ACL injuries occur each year in the United States of America and are estimated to cost half-billion dollars each year, due to health care assistance. [1]. Approximately 100,000 ACL reconstructions are applied in that country every year. ACL injuries and reconstructions statistics in Colombia are not accurate due to the lack of a database with the information of all health care centers [26].

ACL does not heal itself, and the standard method of treatment is surgery, but it is optional. After the surgery, a rehabilitation process is developed with the purpose of enabling the athletes to return to sports and their daily activities. Recovering mobility, strength, quality of life and productivity of these persons widely depends on physical rehabilitation therapies [27].

1.1 Problem Statement

There are many traditional methods and devices to assist treatment. Nevertheless, the study of new technologies applied in areas such as Bioengineering and Automation has brought research and experimentation in robotic platforms that enable to replace, enhance or rehabilitate lower limb disabilities. Within these applications, robotic systems have become a benefit for the rehabilitation of lower limb pathologies [28]. These studies have been focused on the development of active orthosis, also defined as exoskeletons [29], [30]. Powered exoskeletons are biomechanical systems coupled outside of the human body to support, align, and correct extremities and have actuators to reproduce therapy movements or gait help [8], [29]. The user is wrapped into the exoskeleton and in constant contact with it [31]. The main characteristic of these human-machine interfaces is that, due to the contact between the user and the exoskeleton, it is possible to transfer mechanical power [9].

For example, in the case of ACL injuries, Hu et al. [32] reported in 2016 an investigation regarding robot-assisted therapy (RAT) rehabilitation, simulating normal walking to examine the effects of long-term interventions using RAT rehabilitation on functional activity levels after ACL reconstruction. The study reported that the RAT treatment improved extensor strength, walking ability, and balance ability.

However, ACL injuries require various rehabilitation phases. These phases are developed with the purpose of controlling pain and swelling, restoring pain-free range of motion (ROM), improving flexibility, normalizing gait mechanics, establishing good and quadriceps activation [33]. There are several international protocols for rehabilitation of ACL injuries such as the Accelerated ACL Reconstruction Rehabilitation Program of the Chester Knee Clinic & Cartilage Repair Center [34], [35], the Classic 1981 Protocol by Lonnie et al. [36], and the ACL Reconstruction Rehabilitation Protocol of the Steadman Clinic [37]. These protocols report several rehabilitation phases for ACL injuries.

For the aforementioned, there is the need to perform RAT or mechatronic-assisted rehabilitation of ACL Injuries during other phases of the rehabilitation before attempting an advanced exercise such as walking, *e.g.*, when the subject tries to make a knee movement and is not able to execute it, due to the pain caused by the injury. In this rehabilitation phase, an active-assisted rehabilitation

exercise must be conducted. During this type of activities, an external force provides assistance, mechanical or manual, since the primary muscle requires support to complete the movement [2], [3]. Moreover, during the traditional rehabilitation process of ACL injuries, the protocol uses knee active-assisted extension exercises. To do so, the subject uses the opposite leg to restore normal ROM, *e.g.*, the healthy leg straightens the non-healthy knee from a 90° flexion to 0° [38].

Therefore, the specific problem addressed in this thesis is to detect the motion intention and control a mechatronic rehabilitation system to assist the knee movement, *i.e.*, such as in active-assisted extension exercises, but using an exoskeleton.

In order to detect the motion intention of a limb or joint, Electromyography (EMG) signals have been used, and with this information, it has been possible to control rehabilitation systems [39]. Regular rehabilitation systems are not as good as using an integrated system that employs human biological signals such as EMG signals because they are unable to provide fast recovery by their own [13].

1.2 Thesis Objectives and Scope

This thesis was framed under the project “MyoLegSys: Pruebas de factibilidad de un sistema robótico de rehabilitación de miembro inferior para víctimas de accidentes de tránsito” granted by the call for projects from “Departamento Administrativo de Ciencia, Tecnología e Innovación (Colciencias)” 711.

The “Grupo de Investigaciones en Bioingeniería” and the “Grupo de Automática y Diseño A+D” of the “Universidad Pontificia Bolivariana (UPB)” are currently developing a mechatronic system for lower limb rehabilitation called Nukawa’. This system has its antecedents in the LegSys system [40], [41]. Figure 1.1 presents the CAD model of Nukawa. The mechatronic system Nukawa is a product of technical requirements proposed by an interdisciplinary group formed by physiotherapists, industrial designers, and engineers. The design consists of two limbs, each one composed of a three-link mechanism and an electronic position and force control, *i.e.*, each leg has 3-DOF. The design also has brushless DC motors, power drivers, position and micro deformation sensors to perform a control strategy capable of generating multiple rehabilitation patterns. Nukawa aims to help the physiotherapist in the process of rehabilitation of musculoskeletal pathologies of the lower limb, *e.g.*, injuries caused by traffic accidents.

The system would may perform flexion/extension (FE) movements of the hip, FE movements of the knee, and dorsi/plantar (DP) flexion movements of the ankle [40]. Also, the joints are collinear to human joints. The knee is a polycentric joint. However, this simplification was conducted as presented by Zoss *et. al.* [43] who involves a pure rotational joint in the sagittal plane. In order to adjust the system for each person, the length of each segment of the mechatronic system Nukawa is variable, *i.e.*, the length between each joint can be adjusted. The system is designed for people between 1.44 m and 1.85 m tall, using a couple of telescopic mechanical systems. Besides, the system was designed for people of no more than 85 kg weight.

The brushless DC motors were selected taking into account that they could compensate the weight of the robot’s links and the subject limbs. The motors were also chosen so that they could generate a resistive opposition to the FE of hip and knee and DP of the ankle.

It is intended that Nukawa would act as an active orthosis controlled using surface electromyography (sEMG) signals feedback to conduct assisted therapies for patients. The system should measure the electrical activity of the muscles of the lower limb, and would detect the motion intention, and thus assist the movement, *i.e.*, as in active-assisted exercises.

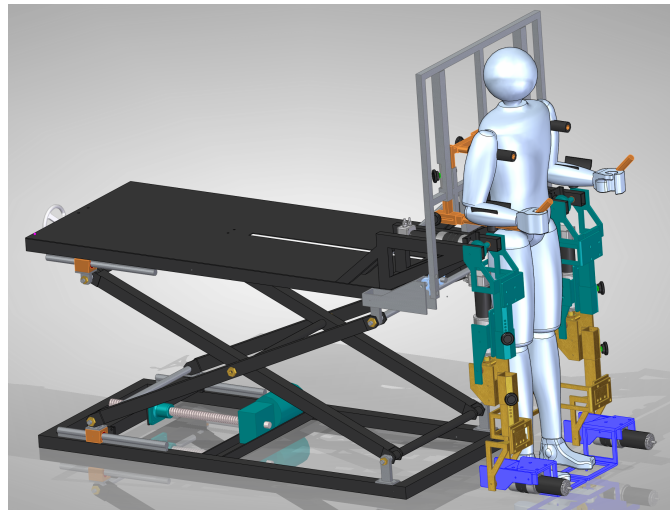


Figure 1.1: CAD model of Nukawa. Made by the author and copyrighted to [42]

The scope of this thesis was to develop a myoelectric control (MEC) for active-assisted exercises with a possible application in the rehabilitation of ACL injuries. Taking into account that Nukawa is not yet fully operational, this thesis was conducted using a simulated model of Nukawa instead of the actual robot. Moreover, the sEMG signal processing algorithm and the movement control algorithm were implemented and tested with the simulated model, using a hardware-in-the-loop (HIL) simulation. The tests were conducted extracting signals from a sEMG signals collection, conducting them into the real-time algorithms, and finally controlling the computational model of Nukawa.

1.2.1 Hypothesis

The hypothesis of this study proposes that an active orthosis controller can be implemented using sEMG signals feedback to conduct assisted therapies for persons with ACL injuries after surgery, where the movement intention of the patient controls the motion of the rehabilitation mechatronic system.

1.2.2 Objectives

This thesis was accomplished by fulfilling the following objectives:

General Objective

To develop a surface electromyography signal processing algorithm and a movement control algorithm for mechatronic-assisted rehabilitation of anterior cruciate ligament injuries.

Specific Objectives

1. To select a surface electromyography signal processing algorithm from a literature review.
2. To develop a surface electromyography signal processing algorithm to assess the detection of intended movement.
3. To select a movement control algorithm for mechatronic-assisted rehabilitation from a literature review.

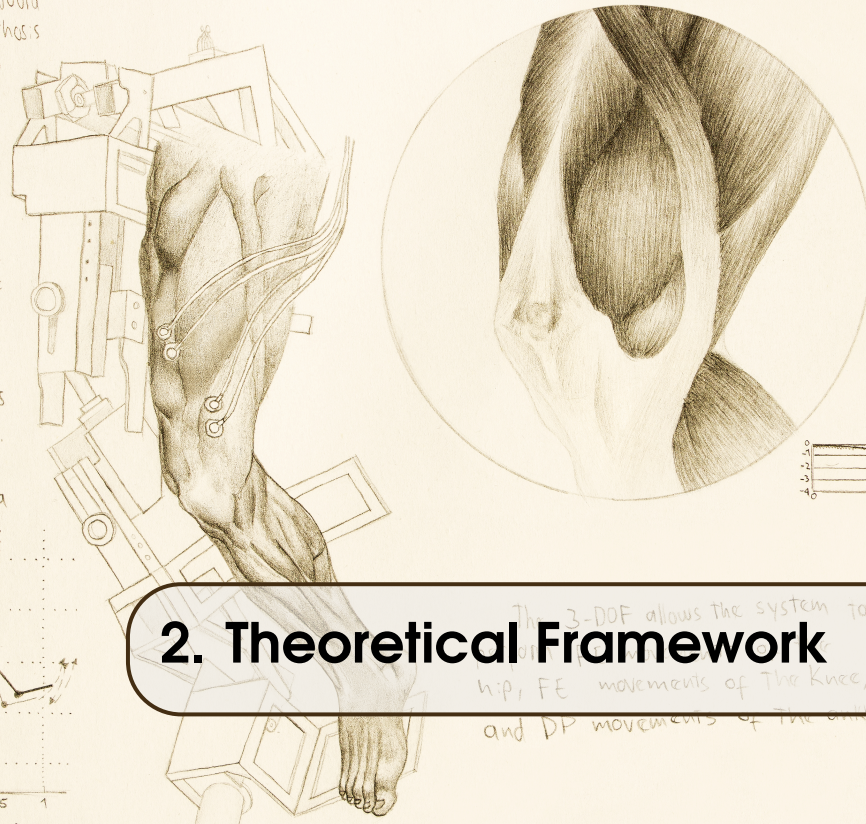
4. To develop a movement control algorithm for mechatronic-assisted rehabilitation based on exercises and movements associated with therapies for anterior cruciate ligament injuries.
5. To assess the behavior of the myoelectric control algorithm for mechatronic-assisted rehabilitation and its possibilities to support rehabilitation therapies for anterior cruciate ligament injuries through a protocol of tests.

1.3 Thesis Overview

The development of this thesis was divided into five methodological aspects according to the fulfillment of each particular objective. Therefore, it is important to mention that each chapter introduces the methodology, results, discussion, and possible future works. This thesis is presented as follows:

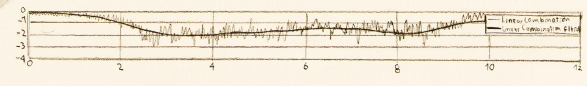
- Chapter 2 contains a theoretical framework, including a review of basic concepts required for the development of this thesis such as ACL injuries, MEC, and movement control algorithms for robotic systems. It is imperative to mention that the theoretical framework is not directly related to any of the specific objectives, but it is a basis to understand the rest of the thesis.
- Chapter 3 presents a literature review to select a sEMG signal processing algorithm, *i.e.*, fulfilling the first objective of this thesis. Also, Chapter 3 presents a literature review of movement control algorithms used in projects related to this thesis in order to select a movement control algorithm for mechatronic-assisted rehabilitation, *i.e.*, fulfilling the third objective of this thesis.
- Chapter 4 presents the experimental protocol conducted with healthy subjects with the purpose of obtaining a database of sEMG signals and kinematic data. Afterward, this chapter presents the development of a sEMG signal processing algorithm to assess the detection of movement intention, *i.e.*, fulfilling the second objective of this thesis. The tests of the sEMG signal processing algorithm were conducted in the offline programming environment Matlab, and as an HIL simulation in Python within a BBB Rev C.
- Chapter 5 explains the development of a movement control algorithm for mechatronic-assisted rehabilitation based on exercises and movements associated with therapies for ACL injuries, *i.e.*, fulfilling the fourth objective of this thesis. Moreover, this chapter presents the tests of the movement control algorithm, *i.e.*, the mathematical modeling of the mechatronic system Nukawa, and a wide description of each test that was conducted to assess the movement control algorithm. During these tests, the movement control algorithm followed the actual movements performed by a physiotherapist during several exercises that belong to international protocols for rehabilitation of ACL injuries.
- Chapter 6 presents the test protocol that was designed to assess the behavior of the MEC algorithm for mechatronic-assisted rehabilitation and its possibilities to support rehabilitation therapies for ACL injuries, *i.e.*, fulfilling the fifth objective of this thesis. The protocol of tests was carried out as an HIL simulation conducting pre-recorded sEMG signals from a database to the myoelectric control system (MCS).
- Chapter 7 presents the overall conclusion of developing a sEMG signal processing algorithm and a movement control algorithm for mechatronic-assisted rehabilitation of ACL injuries. This chapter also presents the contributions and recommendations for future work, *i.e.*, fulfilling the general objective of this thesis.

The Nukawa system would act as an active orthosis controlled using sEMG signals feedback in order to conduct assisted therapies for patients. The system should measure the electrical activity of the muscles of the lower limb, and would detect the intention of movement, and thus assist the movement.

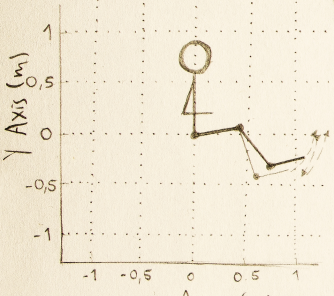


In addition, the joints are collinear to human joints. The knee is a polycentric joint, however this simplification was conducted as presented by Zoss, who involves

$$LC = RF_{RMS} + VM_{RMS} - BF_{RMS} - ST_{RMS}$$



• Sagittal plane (x2) •
Schematic of Nukawa



2. Theoretical Framework

The 3-DOF allows the system to hip, FE movements of the knee, and DP movements of the ankle.

a pure rotational joint in the sagittal plane. In order to adjust the system for each person, the length of each segment of the mechatronic system Nukawa is variable.

This system is designed for people between 1.44m and 1.85m tall, using a telescopic

In order to present a theoretical framework, this chapter contains a review of basic concepts required for the development of this thesis. The review is intended for engineers beginning in the area of mechatronic-assisted rehabilitation of ACL Injuries. First, an overview related to ACL Injuries is presented. Afterward, a review of sEMG related issues and signal processing algorithms is shown. Finally, the topic of movement control algorithms for robotic systems is described.

2.1 Anterior Cruciate Ligament

It is important to mention that this section presents concepts that are considered as the general culture around the problem statement and, it is not intended for people from the health area. However, it is designed for engineers that do not have the context of this injury.

One of the main ligaments of the knee is the ACL. The ACL connects the front top portion of the tibia or shinbone with the back bottom portion of the femur or thigh bone keeping the shinbone from sliding forward [1].

2.1.1 Injuries

A direct blow forces the knee to an abnormal position that results in the tearing of one or more ligaments, e.g., during football or a traffic accident. Nevertheless, most ACL injuries happen even without any contact with another object. These non-contact injuries occur if a subject hyperextend their knee during changes of direction while running or when landing from a jump, which are common movements in agility sports [1]. Contact injuries occur 30 % of all cases, 70 % of ACL tears occur primarily during deceleration of the lower limb [25].

2.1.2 Diagnostic Methods

The physician must examine the knee to diagnose this pathology, and to determine which ligaments are injured. Nevertheless, many injuries are difficult to diagnose manually. Therefore, the use of a magnetic resonance imaging (MRI) scan or an arthroscopy may be applied to ensure an accurate diagnosis [1].

There have been many physical examination tests proposed to assess ACL stability, both as a diagnostic tool or after ACL reconstruction. The most frequent physical examinations are the Anterior Drawer Test, Lachman Test, and Pivot Shift Test [44]–[46]. A complete and proper knee examination is more than 80 % sensitive for an ACL injury. The evaluation should begin observing the gait pattern, and the physician should look for asymmetry [25].

One-repetition-maximum test

The one-repetition-maximum (1RM) test, evaluates the maximum weight that an individual can lift only once for an exercise. Conducting the 1RM may be contraindicated for some populations or preexisting medical conditions. Therefore, several 1RM strength prediction equations have been proposed, *i.e.*, the 1RM can be predicted lifting the greatest weight possible for a certain number of repetitions, until fatigue [11], [47]. Some of the formulas were proposed by Lander [48], Brzycki [49], O'Connor et al. [50], and Epley [51]. Epley proposed that

$$1RM = w(1 + \frac{r}{30}) = (0.0333w)r + w \quad (2.1)$$

where w represents the weight lifted by the subject and r is the number of repetitions achieved, until fatigue. Equation (2.1) is widely employed due to its ease of use.

2.1.3 Prevention

Several programs have been developed to prevent, and to decrease the incidence of non-contact ACL injuries. The focus of these preventions is to obtain a proper nerve/muscle control of the knee. Plyometric exercises consist in a rapid, powerful movement with an eccentric and concentric phase where the subject would jump from a small box and immediately jump back into the air after the contact. Balance training consists of the use of wobble or balance boards. Other balance exercises are throwing a ball with a partner while balancing on one leg. To improve strength and stability, athletes jump, and land on one leg with the knee flexed, followed by a momentary position maintenance [1]. For example, the Hospital for Special Surgery presented complementary tips and exercises to prevent ACL injuries [52]:

- Always warm up before a game or practice to get the blood circulating through the muscles.
- Include stretch exercises for thighs, calves, and hips.
- Strengthen the hips through squats and lunges.

2.1.4 Surgery

Other ligaments heal by scar formation. However, ACL is located through the joint and is surrounded by joint fluid and due to its location, the bleeding cannot be contained, and it fills the joint causing pain and swelling. Synovial fluid is then produced by the irritation of the knee produced by the blood. This fluid prevents blood clotting. Therefore, scar tissues do not form [53].

Considering that surgical treatment is optional, conservative treatment (without surgery) is recommended for patients that have ruptured ACL and are related to activities that require little side stepping, *e.g.*, running in straight lines, swimming, and cycling. Patients who are related to activities that demand a stable knee are at risk of repetitive injuries, resulting in tears to the menisci, damage to the articular surface turning into degenerative arthritis that evolves in a disability [54].

Conservative treatment is executed through physical treatment with the purpose of reducing swelling, restoring muscle power and restoring the ROM of the knee joint [54]. ACL reconstruction

surgery is not a repair procedure because it cannot be sewn back together, it is a replacement with a new ACL that is grafted in the knee. Recovery process varies on every patient, and a rehabilitation process may take from 6 months to a year [33].

2.1.5 Therapy and Rehabilitation Process

ACL injuries may be rehabilitated using both, traditional rehabilitation process [33] and RAT rehabilitation [32]. The following is a brief theoretical framework of both:

Traditional rehabilitation process

Traditional rehabilitation process consists of various phases, which are developed with the purpose of controlling pain and swelling, restoring pain-free ROM, improving flexibility, normalizing gait mechanics, establishing good quadriceps activation [33].

The initial phase of the treatment includes rest, anti-inflammatory actions, and activity modification. Subsequently, after swelling, the normal motion and strength are achieved, and physical therapy is given. Immediately after the injury ice should be applied 3-5 times a day during 10 – 20 min at a time [33].

Exercises such as patella mobilization, belt stretch, heel slides, cycle with minimum resistance are intended to recover the ROM. Other exercises like hip abduction, adduction, extension, external rotation, body weight squats, standing terminal knee extension (TKE) with Theraband/cable column, standing or prone hamstring curls, heel raises are executed with the purpose of strength recovery [33].

There are several international protocols for rehabilitation of ACL injuries, for example, the Accelerated ACL Reconstruction Rehabilitation Program of the Chester Knee Clinic & Cartilage Repair Center [34], [35], the Classic 1981 Protocol by Lonnie et al. [36], and the ACL Reconstruction Rehabilitation Protocol of the Steadman Clinic [37]. These protocols report several rehabilitation phases for ACL injuries. However, in order to exemplify one version of the rehabilitation process, the ACL Non-Operative Protocol from the South Shore Hospital is presented below [53]:

- Phase 1 is given from weeks 0 to 1 and involves to recover the full ROM of the knee. Full extension is the most important. This phase consists of calf exercises, extension exercises, knee bends, heel slides, static hamstrings and knee bend in standing.
- Phase 2 is given from weeks 1-8, where the goal is to improve muscle strength and to continue to improve full ROM. This phase consists of straight leg raise, leg press, leg raise in side lying, bridging, sit to stand, one leg balance stand, hamstring catches, rope walk, calf stretch, and hamstring stretch.
- Phase 3 is given from weeks 8-16, where the goal is to increase speed, weight, and the number of repetitions. This phase consists of skipping, step-ups and downs, quadriceps stretch, jogging, cycling, swimming, gym work, wobble board and single leg squats.
- Phase 4 is given from week 16 onwards, where the rehabilitation can be intended to return to sports.

Robot-assisted therapy rehabilitation

Current research studies in areas such as Bioengineering and Automation are investigating about robotic platforms to rehabilitate lower limb pathologies. For example, in the case of ACL injuries, Hu et al. [32] reported in 2016 an investigation regarding RAT rehabilitation, simulating normal walking to examine the effects of long-term interventions using RAT rehabilitation on functional activity levels after ACL reconstruction. In the research, eight subjects (6 males and 2 females)

participated in RAT for one month. Walking ability was assessed using the 10-Meter Walk Test (10MWT) and the Timed Up-and-Go (TUG) test. Also, balance ability was evaluated using the Functional Reach Test (FRT). They also used sEMG to examine the extensor strength. The tests showed that the RAT treatment improved the walking ability, the balance ability, and the extensor strength.

2.2 Myoelectric Control

There are two methods to obtain EMG signals: sEMG and intramuscular electromyography (iEMG). In the first, electrodes are attached to the user skin, and, in the latter, they are inserted through the skin [13]. sEMG signals have been effectively used for controlling rehabilitation systems [14].

sEMG is a technique that records the electrical intensity of the muscle contraction and myoelectric manifestation of muscle fatigue. This method may help to determine the progress of the patient and the exercises to be applied [12]. Factors such as electrode type, correct electrode placement on the muscle fiber, muscle variability to perform the same exercise repeatedly and signal processing to reduce noise, must be taken into account to succeed using this acquisition technique [55]–[57].

There are two main standards to acquire and report EMG data for publications. Dr. Roberto Merletti wrote the Standards for Reporting EMG Data which are approved by the International Society of Electrophysiology and Kinesiology (ISEK) [58]. Additionally, the Surface Electromyography for Noninvasive Assessment of Muscles project (SENIAM) is a European initiative which pretends to establish a standard for electrode placement, dimensions, shape with the purpose of generalizing the technique that enables to compare and share biosignal results [59].

Nowadays there are several EMG signal databases available for research. EMGLAB is a forum to share algorithms, data and information related to EMG decomposition sponsored by the Veterans Affairs Palo Alto Rehabilitation Research and Development Center, and the National Institute of Neurological Disorders and Stroke [60]. PhysioNet has free web access to a collection of physiologic signals called PhysioBank [61]. They have a small signal database, but it is possible to contribute.

The development of advanced human-machine interfaces (HMI) has been a frequent and exciting research topic in the field of rehabilitation, and many biosignals such as myoelectric signals (MES) have been used. Figure 2.1 presents a basic block diagram employed in a MCS to control rehabilitation devices or assistive robots. The most significant advantage of MCS is the hands-free control according to the movement intention of the user [62]. An MCS is typically composed of several modules including data segmentation, pre-processing, feature extraction and classification [63], other studies have used black box, white box, and gray box models to develop a MEC instead of using machine learning algorithms [64], [65].

The following is a brief description of the theoretical framework related to sEMG signal processing algorithms to assess the detection of motion intention. The review is a basis for engineers beginning in this area. The information presented talks about data acquisition, normalization, pre-processing, data segmentation, and detecting the motion intention using sEMG signals. The explanation is presented so that the reader can understand the next chapters.

2.2.1 Data acquisition

A raw sEMG signal is an unfiltered and unprocessed signal detecting the superposed Motor Unit Action Potentials (MUAPs), but it may have been passed by a bandpass filter amplifier. The EMG baseline noise depends on factors such as the quality of the amplifier or the environment. When the muscle is relaxed, a more or less noisy EMG baseline is obtained. Typically, with a proper skin

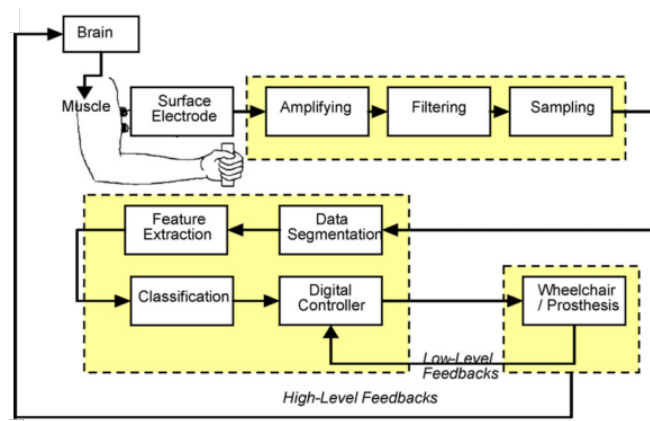


Figure 2.1: A myoelectric control system. Taken from [62]

preparation and using a state-of-the-art amplifier, the averaged baseline should be no more than 3 or $5 \mu\text{v}$, but 1 to 2 should be preferred. The healthy relaxed muscle shows no significant EMG activity since there is a lack of depolarization and action potentials [66].

The Raw sEMG can range between $\pm 0.005 \text{ v}$ including athletes, and the typical frequency range is between 6 and 500 Hz, with its most frequency power between 10 and 250 Hz. In order to accurately record or acquire the complete frequency spectrum of the MES, the sampling frequency must take into account the Nyquist-Shannon sampling theorem avoiding aliasing effects. According to the SENIAM Project, a bandpass amplifier of between 10 to 500 Hz should be used. Therefore, the sampling frequency should be at least 1,000 Hz or even 1,500 Hz to avoid signal loss [66]. The standard presented by Merletti establishes the importance of reporting the characteristics of the electrode used during the biosignal acquisition, among others. For studies using surface electrodes, the report must include the electrode material, electrode shape, size, use of gel or paste, alcohol applied to cleanse skin, skin abrasion, shaving of hair, inter-electrode distance, electrode location orientation over muscle considering tendons, motor point, and fiber direction [58].

The ISEK standard requires reporting the detection mode and amplification including the type of electrodes such as monopolar, differential, or others. Also, ISEK standard suggests reporting the input impedance, common mode rejection ratio (CMRR), signal-to-noise ratio (SNR), and the actual gain range [58]. The CMRR should be as high as possible to eliminate interfering signals, and it is proposed to be greater than 95 dB [66].

The amplification of the signal is set by a factor of at least 500 when using pre-amplifiers and at least to 1,000 when using passive cable units. Also, the input impedance of the amplifier should be at least ten times greater than the impedance of the electrode. Some reports suggest an input impedance of 1 – 10 $\text{M}\Omega$ [66].

The EMG signal must be converted from an analog voltage to a digital signal. This process is called A/D conversion. A 12 bit Analog to Digital Converter (ADC) is sufficient for most kinesiological setups [66].

The quality of the EMG signals depends on a proper skin preparation. There are plenty procedures which first includes removing the hair. Afterward, an abrasive paste may be used to remove dead skin cells. Moreover, a soft controlled pressure with sand papers and alcohol cleaning pads may be used. However, the area may be cleaned only with alcohol. These procedures are intended to reduce the skin impedance to a level of 5 and 50 $\text{k}\Omega$ between pairs of electrodes. This impedance can be

checked with a regular multi-meter or specialized impedance meters. Also, if the movements during the EMG signals acquisition tend to generate a lot of movement artifacts, an extensive preparation is imperative [66].

The SENIAM project recommends using Silver/silver-chloride (Ag/AgCl) pre-gelled electrodes for surface recordings. Besides, this electrode material is the most used. Also, the conductive area of the electrode should be sized to 1cm or smaller. This increases the selectivity of measurements avoiding cross-talk with other muscle. There are two types of commercial disposable electrodes, wet-gel or adhesive electrodes. Wet-gel electrodes have a lower impedance than adhesive gel electrodes. However, adhesive gel electrodes can be repositioned [66].

The recommendation for the inter-electrode distance is 2 cm (center point to center point). Also, the electrodes must be applied parallel to the muscle fiber direction to have the best selectivity, using the dominant middle portion of the muscle belly. It is imperative to avoid the region of motor points. Moreover, it is important to keep in mind that the electrode remains on the active muscle mass during the muscle shortening. Although, is important to keep in mind the possible muscle migration below the electrode during dynamic studies [66].

Furthermore, the cables must be secured for dynamic studies to avoid cable movement artifacts. This procedure should be done using regular tape, elastic straps or net bandages. Nevertheless, too much tension must be prevented. At least one reference electrode, also called ground electrode, should be utilized. Moreover, this electrode must be positioned in an electrically neutral tissue, such as joints, bony area, frontal head, Processus Spinosus, Christa Iliaca, Tibia Bone, and others [66].

Scientific recommendations from the SENIAM and the ISEK, reports that EMG recordings should not use any hardware filters such as notch filters, except a bandpass filter within the 10 to 500 Hz bandwidth [66].

2.2.2 Normalization

The amplitude of an EMG signal is strongly affected by the given detection condition. The inter-subject and intra-subject amplitude variation are the biggest problems of any EMG analysis. The maximum voluntary contraction (MVC) value of a reference contraction is used to normalize and to calibrate the micro volts value into a unique calibration unit with physiological relevance, and it represents a percent of the maximum innervation capacity of the subject. This normalization process does not affect the shape of the EMG curves, only their Y axis scaling. In order to develop an MVC normalization process, the healthy subject produces a maximal contraction using static resistance, but patients should not perform MVCs. Therefore the acceptable maximum effort (AME) may be applied [66].

In investigations that use EMG data, the normalization process of the EMG data must be reported including relevant information such as joint angles, muscle lengths, isometric contractions, and others. Furthermore, other information to report must include how subjects were trained to obtain MVC, joint angle, muscle length, conditions, and angles of adjoining joint [58].

2.2.3 Pre-processing

Scientific recommendations for research studies such as the ones provided by the SENIAM Project or the ISEK Standards present a standard to use a bandpass filter between 10 to 500 Hz. These Standards deny any narrower band setting, even the use of a notch filter, to cancel out 50 or 60 Hz noise, is not accepted because it destroys the sEMG signal power. However, some research projects use Finite Impulse Response (FIR) Filters or Infinite Impulse Response (IIR) Filters to filter artifact

movements. Moreover, other studies have used low-pass filters at 6 Hz to create a linear envelope sEMG [66].

2.2.4 Data Segmentation

The response of the system is directly affected by the data segmentation and the processing and control algorithms. A segment is a time slot of the MES, and it is used for feature extraction. Real-time MCS must have a response less than 300 ms to have a latency unrecognizable by the user [62]. Although, it is reported that real-time computing and high-speed microprocessors may take up to 50 ms or less to process signals [62].

The segmentation is performed after the data acquisition in both, overlapping or disjoint techniques. Figure 2.2a presents an adjacent windowing technique which uses segments with predefined length for feature extraction [67]. On the use of this technique, a motion intention is obtained after a certain process delay. Furthermore, the processor is idle during a small time, since the processing time is a small portion of segment length. Figure 2.2b presents an overlapping windowing, which uses the idle time of the processor to generate more outputs. In order to compute the feature and make a decision, before the next segment arrives, the processing and motion intention algorithm must end before the next window, *i.e.*, it should be available to process another segment. In these figures, W1, W2, and W3 are adjacent and disjoint successive analysis windows and R1, R2 and R3 are overlapped windows. Also, D1, D2, and D3 are a motion intention decisions for each window which are made τ seconds later, where τ is the amount of time required for the motion intention algorithm [68].

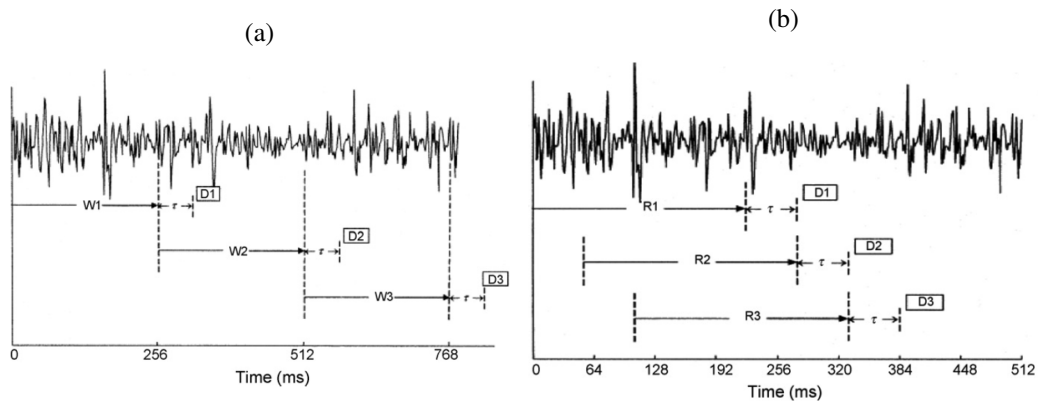


Figure 2.2: (a) Adjacent and (b) overlapped windowing techniques. Taken from [68]

2.2.5 Detecting the motion intention

After data segmentation, the feature extraction process is carried out. This step should be given in order to have suitable features from sEMG raw signals, due to the fact that raw sEMG signals are not appropriate as input signals to the controller. The success of motion intention detection depends on the selected features used to characterize raw signals [69]. The literature presents a broad range of techniques to extract features from sEMG signals that use parameters in the time-domain, frequency-domain and time-frequency domain. Within the time-domain, the most common features

are Mean Absolute Value (MAV) [62], [64], [70], [71], Mean Absolute Value Slope (MAVSLP) [70], Modified Mean Absolute Value 1 (MMAV1) [70], Modified Mean Absolute Value 2 (MMAV2) [70], Zero Crossing (ZC) [70], Simple Square Integral (SSI) [70], Variance of EMG (VAR) [70], Slope Sign Change (SSC) [70], Root Mean Square (RMS) [13], [62], [70], [72]–[78], Waveform Length (WL) [70], [78], Integrated EMG (IEMG) [70], Willison Amplitude (WAMP) [70], [78], Histogram EMG (HEMG) [70], and others. In the frequency-domain features the common techniques are the coefficients of Short-Time Fourier transform (STFT), the Mean Instantaneous Frequency (MIF) [77], the Median Frequency (MDF) [14], [58], [70], [79], [80], the Modified Mean Frequency (MMNF) [70], the Variance of Central Frequency Calculated from spectral moments [77], Modified Median Frequency (MMDF) [70], frequency Ratio (FR), the Mean Frequency (MNF) [14], [58], [70], [79]–[81], the coefficients of Wavelet Transform (WT), and the coefficients of Auto Regression (AR) of the spectrum of EMG signals [70]. The main time-frequency algorithms are the Wavelet Transform (WT), Wavelet Packet Transform (WPT) [67], [74].

Time domain features are the most popular in MEC since they have the lower computational cost. These features are based on the amplitude of the signal. The amplitude of the sEMG signal represents the signal energy, activation level, duration, and force, and it is influenced by many factors such as the electrode location, the distribution of motor units, the thickness of tissues, muscle conduction velocities, and the detection system [62].

RMS

Is based on the square root calculation, the RMS shows the mean power of the signal and is the preferred recommendation for smoothing. It is important to take into account that the higher the window, the higher the risk of phase shift [66]. RMS is a time domain feature and is modeled as amplitude modulated Gaussian random process, and its RMS is related to the constant force and non-fatiguing contraction [74]. The signal is rectified with RMS and is converted into an amplitude envelope [13]. The RMS is calculated one value at the time using

$$RMS_{emg}(n) = \sqrt{\frac{1}{n} \sum_{s=1}^n sEMG(s)^2}, \quad (2.2)$$

where $sEMG(s)$ represents the amplitude recording [82] of the signal in the s_{th} sample and n is the total number of samples in a window from the vector of the signal.

Many assistive robots have used RMS for feature extraction, and it is often used since it can be mapped into the motion intention during non-muscle fatigue conditions and it can be computed in real-time [67], [83], [84].

MAV

Is one of the most used techniques for MES analysis, especially for prostheses and exoskeletons control. The MAV is computed for each window as

$$MAV = \frac{1}{N} \sum_{i=1}^N |x_i|, \quad (2.3)$$

where N is the number of samples of the whole signal, and x_i is each sample of the signal.

The MAV computes the absolute value of all of the values in the window, and afterward, it determines the mean of the resultant values [76].

After the feature extraction a classification algorithm may be used to estimate the motion intention of a joint. There are several classification algorithms, *e.g.*, Fuzzy Logic (FL) [62], [67], Fuzzy-Neuro (FN) [67], Bayesian Classifiers (BC) [67], Linear Discriminant Analysis (LDA) [67], Support Vector Machines (SVM) [67], Hidden Markov Model (HMM) [67] and, Artificial Neural Networks (ANN) [62], [67], K-Nearest Neighbors (KNN), Decision Trees, Deep Learning, Hierarchical Classifier, Multilayer perceptron, Naive Bayes Classifier, Nearest Centroid Classifier, Kalman Filters, Hilbert Huang transform, and others [13], [63], [77], [85].

In addition, white box, and gray-box models are also used to estimate the motion intention of a joint, as a different alternative to classification algorithms. An EMG-driven model which combines Hill-based muscle model with the forward dynamics of joint movement may be utilized for the estimation of continuous joint movements [86], with full knowledge and access to all of the physiological phenomena. Also, a model that uses the myoelectric activity of the flexor and extensor muscles with conversion coefficients from myoelectric activity to motion intention may be employed [65].

2.3 Movement Control Algorithm

In order to control the movement of the joints of a robotic exoskeleton, a control algorithm must be developed. It could be a classic or a modern algorithm; some examples of them are PID controllers [87], Neuro-Fuzzy Control [64], Computed Torque Control (CTC) [5], among others. Also, many control schemes can be used to control robotic exoskeletons such as impedance control, admittance control, force/torque control, position control, hybrid control (force/position). These control schemes depend on a particular application of the robotic system [88]. The following is a brief explanation of the CTC algorithm so that the reader can understand the next chapters.

CTC is a model-based control. It enables compliant robot control with small tracking errors for accurate robot models. The controller moves the robot, which is governed by the system dynamics. The general scheme of the CTC algorithm is shown in Figure 2.3.

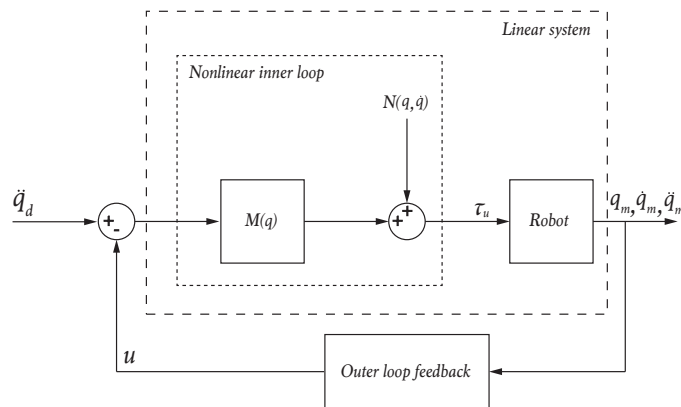


Figure 2.3: Schematic showing computed torque control

The block diagram presented in this figure is decomposed into:

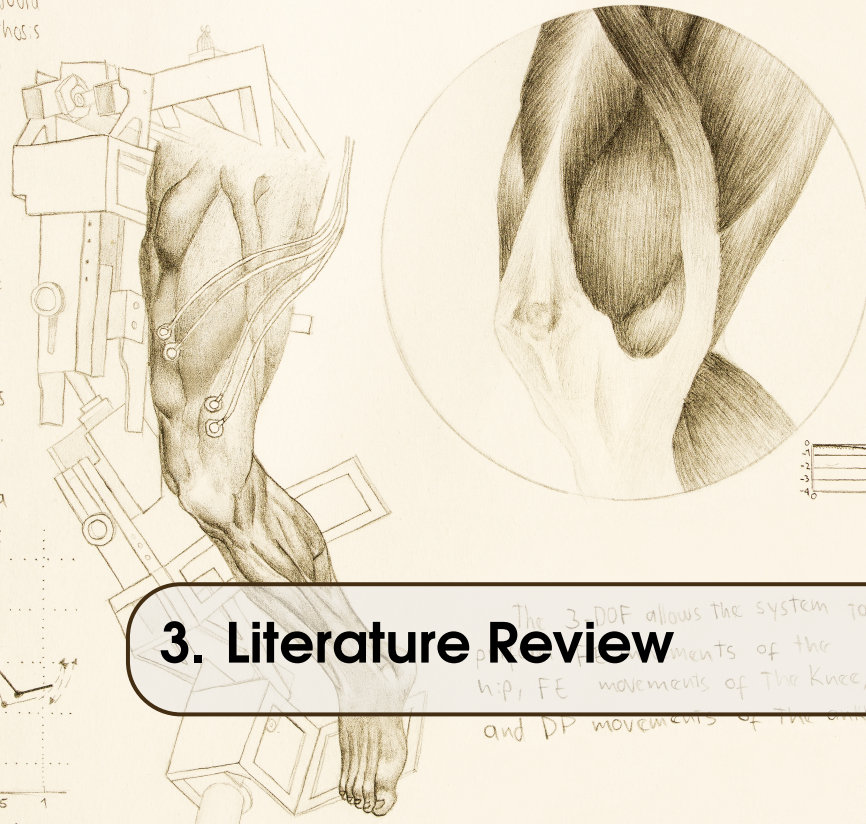
- A *nonlinear inner loop* or nonlinear model-based control law that “cancels” the nonlinearities of the system to be controlled, *i.e.*, this *nonlinear inner loop* reduces the system to a linear system
- An *outer loop feedback* that can control the reduced linear system

The mathematical model of a 3-DOF serial robot is described by the rigid body dynamic equation, stated in [6], as

$$M(q)\ddot{q} + V(q, \dot{q}) + F(\dot{q}) + G(q) + \tau_d = \tau, \quad (2.4)$$

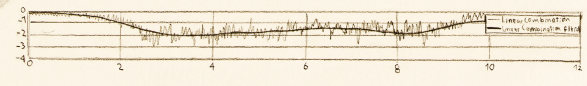
where $q \in \mathbb{R}^{3 \times 1}$, $\dot{q} \in \mathbb{R}^{3 \times 1}$, and $\ddot{q} \in \mathbb{R}^{3 \times 1}$ represent the joint positions, velocities, and accelerations, respectively. $M(q) \in \mathbb{R}^{3 \times 3}$ is the inertia matrix, $V(q, \dot{q}) \in \mathbb{R}^{3 \times 1}$ is the coriolis and centripetal vector, $G(q) \in \mathbb{R}^{3 \times 1}$ gravity vector, $F(\dot{q}) \in \mathbb{R}^{3 \times 1}$ the friction term [6], $\tau \in \mathbb{R}^{3 \times 1}$ is the torque of the actuators, and $\tau_d \in \mathbb{R}^{3 \times 1}$ are the disturbance torques, *e.g.*, the torque exerted by the subject or any inaccurately modeled dynamics. The tracking control determines the joints torque such that the robot follows the desired trajectory.

The Nukawa system would act as an active orthosis controlled using sEMG signals feedback in order to conduct assisted therapies for patients. The system should measure the electrical activity of the muscles of the lower limb, and would detect the intention of movement, and thus assist the movement.

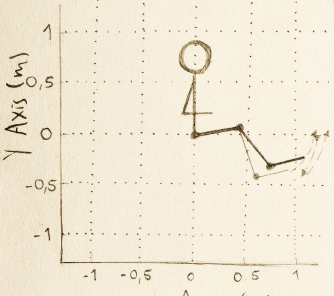


In addition, the joints are collinear to human joints. The knee is a polycentric joint, however this simplification was conducted as presented by Zoss, who involves

$$LC = RF_{RMS} + VM_{RMS} - BF_{RMS} - ST_{RMS}$$



• Sagittal plane (x2) • Schematic of Nukawa



3. Literature Review

a pure rotational joint in the sagittal plane. In order to adjust the system for each person, the length of each segment of the mechatronic system Nukawa is variable.

This system is designed for people between 1.44m and 1.85m tall, using a telescopic

This chapter presents a literature review to select a sEMG signal processing algorithm, *i.e.*, fulfilling the first objective of this thesis. Also, in order to select a movement control algorithm for mechatronic-assisted rehabilitation from a literature review, this chapter presents a report of movement control algorithms used in projects related to this thesis, *i.e.*, fulfilling the third objective.

3.1 sEMG Signal Processing Algorithms

An overview of sEMG signal processing algorithms is shown in Table 3.1. This table presents the description of eight algorithms used in projects related to this thesis. In the Table 3.1 it is observed that two of the algorithms were implemented and tested in an offline fashion [13], [85], four of them were implemented online [65], [72], [86], [89], and in one of them, the type of implementation is not reported [71]. Also, it is observed that six of the algorithms are currently under investigation [13], [71], [72], [85], [86], [89] and only one of them is in the commercial stage [65]. In addition, it is observed that one of them was tested in the knee joint [65] and six of the algorithms detect the motion intention in other joints [13], [71], [72], [85], [86], [89].

The algorithm proposed by Hayashi et al. [65] was selected to be used in this thesis. The selection was made due to the fact that this algorithm was designed, implemented and tested to detect the motion intention in the knee joint. In addition, it was tested in the commercial robotic system HAL, which was designed to assist lower limbs. Finally, this algorithm was also selected due to the fact that it does not require prior training, as in the case of artificial intelligence algorithms.

The sEMG signal processing algorithm of this thesis, should detect approximately the intensity and orientation of the movement intention. With that said, Chapter 4 presents the development and the tests of a sEMG signal processing algorithm to assess the detection of intended movement, based on the algorithm proposed by Hayashi et al. [65], *i.e.*, fulfilling the second objective of this thesis.

Hayashi et al. [65] used an instrumentation amplifier and two electrodes to detect the myoelectricity. The electrodes were located over the skin of the operator, near the flexor and extensor muscles, in charge of performing the movement of the knee joint. Both signals were amplified and

filtered, and the myoelectric activity was computed as

$$E(t) = \sqrt{(1/T) \int_{t-T}^t m^2 dt}, \quad (3.1)$$

where $E(t)$ corresponds to an amplitude envelope of the myoelectricity, m is the measured myoelectricity, and T the number of samples of the whole signal. Equation (3.1) is applied to both signals in an online fashion, *i.e.*, the sEMG signals from the flexor and extensor muscles [65].

Subsequently, the muscle torque $\hat{\mu}$ is computed taking into account that

$$\hat{\mu} = (a_e E_e(t) + b_e) - (a_f E_f(t) + b_f), \quad (3.2)$$

where $E_f(t)$ and $E_e(t)$ are the myoelectric activity of the flexor and extensor muscles, respectively. Moreover, a_f , a_e , b_f and b_e are conversion coefficients from myoelectric activity to contraction torque. Finally, the estimated muscular torque is used, and the torque of the robotic system τ_μ is

$$\tau_\mu = \alpha_\mu \hat{\mu}, \quad (3.3)$$

where α_μ is a gain parameter [65].

The sEMG signal processing algorithm proposed by Hayashi et al. [65] estimates the muscular torque. However, it requires a long calibration process with an additional torque sensor to obtain the conversion coefficients a_f , a_e , b_f and b_e . This calibration process must be conducted separately for both, each subject and each muscle. During the calibration process, HAL outputted a torque pattern as a reference torque, and the subject wearing the HAL system produced a torque to compete against the torque of the robot. Finally, in order to obtain the conversion coefficients, a least-square method was applied. Hayashi et al. also mentioned that these conversion coefficients depend on the physical condition of the subject, and the location of the sensors. Therefore, the long calibration process must be conducted each time that the subject wears the robotic system.

3.2 Movement Control Algorithms

An overview of movement control algorithms is shown in Table 3.2. This table presents the description of nine projects related to this thesis, taking into account the advantages and disadvantages. In the Table 3.2 it is observed that five of the movement control algorithms were designed, implemented and tested on lower limb exoskeletons [5], [41], [87], [91], [92] and four of them on upper limb exoskeletons [93]–[96]. Also, it is observed that six of the algorithms were implemented in an online fashion [87], [92]–[96], one of them was implemented in an offline manner [41], and in two of them, the type of implementation is not reported [5], [91]. Two of the studies used a CTC algorithm [5], [41] and two studies used controllers based on Fuzzy Logic [87], [93]. Also, two studies used controllers based on PID control [87], [92], and the other studies, proposed adaptive controllers [94]–[96] or controllers based on inverse dynamics [91].

The algorithm used by Lasso et al. [5] and Kirby [41] was selected to be used in this thesis. Both studies evaluated the behavior of the CTC algorithm, on lower limb exoskeletons, with simulations. Lasso et al. [5] reported small position tracking errors, and Kirby [41] reported small position, speed, and torque tracking errors. Also, the simulations conducted by Kirby [41] were validated by a

Table 3.1: Description of sEMG signal processing algorithms

Reference	Robot	Application	Sensors	Algorithm	Implementation	Experiments	Calibration process	Current state	Advantages	Disadvantages
[13]	A Virtual Human Model (VHM)	Upper limb movements	The sEMG signals were collected from the anterior deltoid, posterior deltoid, biceps brachii (BB) and triceps brachii (TB).	The signals were rectified with RMS to obtain an amplitude envelope. Subsequently, a low pass filter was implemented, and the signals were normalized. The raw and pre-processed signals were the input of a three layer back propagation neural network (BPNN) controller.	Offline	4-healthy-subjects	Offline training of the algorithm.	Research	It was tested using multiple joints and multiple movements.	It is currently under research stage, it requires to train a machine learning algorithm. Therefore, it requires a training data set. It was tested on upper limb joints. The algorithm was tested in an offline fashion.
[65]	HAL-3	Swinging motion of lower leg	Two sensors near the flexor and extensor muscles.	Signals were filtered and amplified, the myoelectric activity was computed for both channels. Subsequently, the estimated muscle torque was computed as a linear combination of both, taking into account the equation of a straight line. Finally, a gain parameter was used to compute the torque for the actuator.	Online	1-healthy-subject	A calibration process is necessary in order to obtain the conversion coefficients.	Commercial	It uses a simple algorithm and it was tested online in a commercial robotic exoskeleton.	It requires a long calibration process, including additional sensors such as torque sensors.
[71]	None	Upper limb movements	BB and TB.	The MAV was computed. Subsequently, an SVM was used to classify the signals.	Not reported	3-healthy-subjects	Training of the algorithm.	Research	It was tested using multiple joints and multiple movements.	It is currently under research stage, it requires to train a machine learning algorithm. Therefore, it requires a training data set. It was tested on upper limb joints. The type of implementation is not reported.
[72]	Computer model of the index finger and wrist joint	Control of finger and wrist joint models	Flexor digitorum superficialis (FDS) and flexor carpi ulnaris (FCU).	An RMS envelope was computed. Subsequently, a low-pass filter was used and two different functions were used for the finger position.	Online	18-healthy-subjects	Simple calibration process of constants.	Research	It uses a simple algorithm and it was tested in an online fashion. It requires a simple calibration process, and it was tested on 18-healthy-subjects.	It is currently under research stage. It was tested on upper limb joints.
[85]	None	Elbow flexion-extension movements	An accelerometer placed on the forearm and sEMG electrodes on BB and TB.	The raw signal was processed. Subsequently, the signals were rectified and a signal normalization process was developed for each subject according to pre-recorded signals. The neural activity was calculated and a Kalman Filter was used to predict motion.	Offline	12-healthy-subjects	Manual calibration.	Research	It was validated with 12-healthy-subjects, and requires a simple manual calibration.	It is currently under research stage. It was tested on upper limb joints. Moreover, it requires additional sensors. The algorithm was tested in an offline fashion.
[86]	4-FOD robotic arm	Elbow movements	BB.	EMG-driven state space model which combines Hill-based muscle model with the forward dynamics of joint movement for the estimation of continuous joint movements. The raw signal is pre-processed. Subsequently, the neural activation is computed.	Online	1-healthy-subject	The EMG-driven model parameters were estimated.	Research	The calibration process is subject-specific. The algorithm uses a white-box model, which makes it easier to understand. It was tested in an online fashion.	It is currently under research stage. It was tested on upper limb joints.
[89]	NEUROExos	Elbow assistance	BB and TB.	The EMG signals were processed obtaining a linear envelope (LE) through full-wave rectification. Both signals were conducted to a proportional controller to manipulate the flexion and extension of the exoskeleton.	Online	10-healthy-subjects	Subjects selected the gains of the algorithm in a previous procedure.	Research	It requires a simple calibration exercise, it was tested in an online fashion, and it was tested on 10-healthy-subjects.	It is currently under research stage. It was tested on upper limb joints.
[90]	None	Single elbow dynamic movement	BB and TB.	A low-pass filter was used. Subsequently, two time-domain features were extracted and the signals were normalized. A linear state-space model was used to estimate joint motion.	Offline	2-healthy-subjects at two load levels	Offline training of the algorithm.	Research	It overcomes subject-specific problems.	It is currently under research stage, and it was tested in an offline fashion. It was tested on upper limb joints.

group of physiotherapists. The trade off is that CTC algorithm requires an accurate model of the system. However, a mathematical model of Nukawa was reported on [41], since some researchers have previously developed simulations of an offline CTC algorithm for Nukawa in Matlab [40], [41]. These simulations have shown the feasibility of implementing a online CTC algorithm to control the movements of Nukawa [41].

For the aforementioned, Chapter 5 presents the development of an online movement control algorithm for mechatronic-assisted rehabilitation based on the offline algorithm reported by Kirby [41], *i.e.*, fulfilling the fourth objective of this thesis.

Chapter Summary

A literature review of sEMG signal processing algorithms was conducted. This study showed that there are several sEMG signal processing algorithms to detect the motion intention. Moreover, some of them are very complex, and some of them are very simple. The sEMG signal processing algorithm proposed by Hayashi et al. [65] was selected to be used in this thesis. The selection was made due to the fact that it detects the motion intention in the knee joint. Moreover, it was tested in the commercial robotic system HAL. Finally, it is a simple algorithm which requires no prior training with sEMG signals from other subjects. The only problem with this approach is that it requires a long calibration process with an additional torque sensor to estimate the conversion coefficients a_f , a_e , b_f and b_e . However, this problem will be addressed in Chapter 4, where the adaptation of the algorithm is explained.

In addition, a literature review of movement control algorithms for mechatronic-assisted rehabilitation was conducted. There are several movement control algorithms for exoskeletons, some examples of them are PID controllers [87], [92], Fuzzy Control [64], CTC [5], [41], among others [91], [94]–[96]. The CTC algorithm was selected since several studies reported to have a small position, speed, and torque tracking errors [5], [41]. Moreover, the offline simulations presented by Kirby [41] have shown the feasibility of implementing the CTC algorithm to control the movements of Nukawa, and they were validated by a group of physiotherapists. The only problem with this approach is that it requires an accurate model of the system. However, for the purpose of this thesis, the parameter uncertainties are neglected, therefore, the performance will be proportional to the precision of the exoskeleton dynamic model.

Table 3.2: Description of movement control algorithms

Reference	Robot	Application	DOF	Algorithm	Implementation	Experiments	Observations
[5]	Robotic exoskeleton for lower limb rehabilitation	Lower limb rehabilitation of patients with profound sensory impairment.	10-DOF	CTC algorithm	Not reported	Simulation	Small position error of maximum 3.55°. The trade off is that it requires an accurate model of the system.
[93]	Upper limb exoskeleton	To assist patients during rehabilitation.	5-DOF	Disturbance Observer-Based Fuzzy Control of Uncertain MIMO Mechanical Systems with input Nonlinearities	Online	Test were conducted without subjects	The stability was proved mathematically. The algorithm rejects disturbances by dead zone and saturation. The trajectories were apparently chosen arbitrarily.
[41]	Legsys, currently Nukawa	Lower limb rehabilitation.	Each leg has 3-DOF	CTC algorithm	Offline	Simulation	The simulations of the CTC algorithm present a small position, speed, and torque tracking error. The simulations conducted within this study were validated by six physiotherapists. The trade off is that it requires an accurate model of the system.
[94]	ETS-MARSE	Upper Limb Neurorehabilitation.	7-DOF	Estimated Time Delay Controller based on sliding mode and Jacobian transpose (JSTDE) controller"	Online	Tests with 3-healthy-subjects were conducted	The stability was proved mathematically. Precise information about the dynamic of ETS-MARSE robot is not required. The trajectories were chosen taking into account an upper limb rehabilitation protocol.
[95]	ULEL	Upper limb rehabilitation of post-stroke patients.	7-DOF	Control strategy for an upper limb exoskeleton based on an online dynamic parameter estimator	Online	No se hicieron pruebas en pacientes	The stability was proved mathematically. No experimental tests were conducted. The authors do not report the sampling period or convergence time.
[96]	Upper limb exoskeleton robot	Training of activities of daily Living (ADL).	5-DOF	Adaptive control with improved safety	Online	Test were conducted without patients	A safety-improved adaptive controller was proposed. However, the trajectories were apparently chosen arbitrarily without considering the pathology.
[91]	BLEEX	Augment human strength and endurance during locomotion.	Each leg has 7-DOF	Sensitivity Amplification Controller (SAC)	Not reported	No experiments reported	Works without any measurement from the wearer. It requires a good model of the system, and it is poorly robust to parameter variations.
[92]	EiCoSI	Lower limb exoskeleton for rehabilitation or assistance.	1-DOF	PSO-PID adaptive controller	Online	Test were conducted with 3-healthy-subjects	The algorithm adapts and guarantees a minimum control energy without chattering. The trajectories were apparently chosen arbitrarily.
[87]	Lower limb exoskeleton with series-parallel topology	Walking, stair ascent, stair descent, side kick, squatting down and standing up.	Each leg has 6-DOF	fuzzy-PID/PID movement control algorithms	Online	Not reported	It was difficult to design fuzzy rules and fuzzy parameters. However, the performance and effectiveness of the movement control algorithm was validated.

The Nukawa system would act as an active orthosis controlled using sEMG signals feedback in order to conduct assisted therapies for patients. The system should measure the electrical activity of the muscles of the lower limb, and would detect the intention of movement, and thus assist the movement.

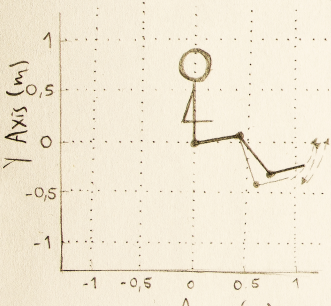


In addition, the joints are collinear to human joints. The knee is a polycentric joint, however this simplification was conducted as presented by Zoss, who involves

$$LC = RF_{RMS} + VM_{RMS} - BF_{RMS} - ST_{RMS}$$



• Sagittal plane (x2) •
Schematic of Nukawa



4. Motion Intention Algorithm

The 3 DOF allows the system to hip, FE movements of the knee, and DP movements of the ankle.

a pure rotational joint in the sagittal plane. In order to adjust the system for each person, the length of each segment of the mechatronic system Nukawa is variable.

This system is designed for people between 1.44m and 1.85m tall, using a telescopic

In order to select the sEMG signal processing algorithm, a literature review was presented in Section 3.1. In that section the sEMG signal processing algorithm proposed by Hayashi et al. [65] was selected. That algorithm estimates the muscular torque. However, a long calibration process with an additional torque sensor is necessary each time that the system is used. Therefore, this chapter presents the development of a sEMG signal processing algorithm to assess the detection of intended movement, based on the algorithm proposed by Hayashi et al. [65], *i.e.*, fulfilling the second objective of this thesis. The tests of the algorithm were conducted in the offline programming environment Matlab and as an HIL simulation in Python within a BBB Rev C, which is a development platform.

4.1 Requirements of the sEMG signal processing algorithm

The following is a list of requirements to be met by the sEMG signal processing algorithm:

- The algorithm should detect the motion intention orientation, *i.e.*, when the subject intends to perform a knee flexion or extension.
- The algorithm should detect the intensity of the movement intention, *i.e.*, when the subject has a weak intention, the algorithm should detect a soft intention, and when a subject has a strong intention, the algorithm should detect a hard intention.
- The mean computational time of the algorithm must be lower than the sampling period.
- The sampling period of the algorithm should be lower than 300 ms.
- The sEMG signal processing algorithm should be fast and light so it may be implemented in real-time.
- The sEMG signal processing algorithm should be tested offline.
- The sEMG signal processing algorithm should be implemented online as an HIL simulation.
- The detection of the movement intention should be useful to control the movement of a computational model of Nukawa.

4.2 Building the Nukawa Database

Experimental tests with healthy-subjects were conducted with the purpose of obtaining a collection of sEMG signals for its use in the study. This database contains kinematic and sEMG data, and it will be called the “Nukawa Database”. The experimental tests were conducted to acquire and record sEMG signals and its corresponding kinematics associated with rehabilitation body movements for ACL injuries. These tests were approved by the ethics committee of the UPB as presented in Appendix A. The tests were framed under the MyoLegSys¹ project.

The Nukawa Database was obtained with the purpose of developing and testing sEMG signal processing algorithms to assess the detection of intended movement. This acquisition was executed with the support of professionals in the area of medicine and physiotherapy, considering their expertise in the assessment of people with lower limb injuries using sEMG signal acquisition, among others. The Nukawa Database was given since open-source databases do not fulfill the requirements of the project mentioned on Section 4.1.

The healthy-subjects were recruited in the “Centro de Movimiento MVMT” and the “IPS ARTHROS”. However, not all the subjects who wanted to be part of the study and assisted voluntarily could be included as subjects of study, *i.e.*, a selection was made conducted before the procedures. The selection of subjects was carried out with the support of a physiotherapist. To do so, the physiotherapist followed the technical specifications of the study population.

Technical specifications for the acquisition of sEMG signals and kinematic data are described in Table 4.1.

Table 4.1: Technical specifications for the acquisition of sEMG signals and kinematic data

Characteristic	Description
Universe	Healthy-subjects
Population	Subjects of the Universe between 18 and 60 years
Unit of study	Subjects of the Population who decide voluntarily and Ad honorem to participate in the study and that they agree and sign the Document of Informed Consent

It is important to clarify that healthy-subjects, for the present thesis, are defined as those who do not have mental disorders or physical disabilities. Moreover, a healthy-subject possess the following variables of control within normal ranges according to their sex and age: heart rate, respiratory rate, peripheral body temperature, blood pressure and body weight.

The experimental protocol was conducted in a group of 20-healthy-subjects. However, the usable Nukawa Database is just composed by 17-healthy-subjects, since the files of three of the subjects had errors when being saved. The information about each trial was recorded in a file in order to recognize the experiment.

¹Project approved under the call for projects Colciencias 711 to develop the myoelectric control

4.2.1 Selecting the muscles

In order to select the muscles involved during knee flexo extension, and determine which of them should be acquired for the Nukawa Database, a selection process was conducted. Florimond [97] reported the muscles involved in the movements of each of the joints. Table 4.2 presents the muscles mainly comprised in the flexion and extension of the knee proposed by Florimond.

However, the SENIAM project [59] proposed recommendations for locating sensors on the muscles of the upper leg. Table 4.3 presents this proposal.

Table 4.2: Muscles mainly involved during knee flexion and extension proposed by Florimond [97]

Movement	Flexion	Extension
Involved Muscles	Biceps Femoris (BF)	
	Gastrocnemius	Rectus Femoris (RF)
	Gracilis	Tensor Fascia latae (TFL)
	Popliteus	Vastus Intermedius
	Sartorius	Vastus Lateralis (VL)
	Semimembranosus	Vastus Medialis (VM)
	Semitendinosus (ST)	

Table 4.3: Recommendations for sensor locations proposed by the SENIAM Project [59]

Muscles	Function
Gluteus Maximus	Adduction of the hip and helps to stabilise the knee in extension
Gluteus Medius.	Abduction of the hip joint and may assist in flexion and extension of the hip joint.
TFL	May assist in knee extension.
RF	Extension of the knee joint and flexion of the hip joint.
VM	Extension of the knee joint.
VL	Involved in the extension of the knee joint.
BF	Flexion and lateral rotation of the knee joint.
ST	Is the flexion and medial rotation of the knee joint.

The list of muscles presented on Table 4.3 is slightly different from the proposed by Florimond [97] presented on Table 4.2 as the ones involved in the flexion and extension of the knee. Therefore, mixing both proposals, the muscles involved during knee flexion are the BF and the ST. Moreover, the muscles involved during knee extension are the RF, TFL, VL, and VM. However, the SENIAM Project [59] proposes that the TFL may assist in knee extension as shown in Table 4.3. Therefore, it is despised for the acquisition. The VM is one of the main muscles affected after an ACL surgery

[98]. Therefore, the VL was also despised for the acquisition. Finally, Table 4.4 presents the four muscles selected to conduct the tests.

Table 4.4: Muscles primarily involved during knee flexion and extension selected for the experimental protocol

Movement	Flexion	Extension
Involved Muscles	BF	RF
	ST	VM

4.2.2 Materials

Table 4.5 and Figure 4.1 presents the materials used for the experimental protocol with the healthy-subjects.

Table 4.5: Materials used for the experimental protocol and the clinical evaluation with the healthy-subjects

Material	Quantity
Thermometer	1
Tensiometer	1
Pulse oximeter	1
Chronometer	1
Bascule	1
Analog goniometer	1
BiosignalPlux	1
AC Adapter	1
Electrogoniometer	3
Micropore	20 m
Double sided adhesive tape	20 m
Cable for electrode	4
Cable for reference electrode	1
sEMG electrodes	180
Computer	2
OpenSignals Software	1
Pen	2
Alcohol	1 bottle
Scissors	1
Cotton	1 bag
Inform consent form	21
Liability insurance	1
Portable stadiometer	1
Tape measure	1



Figure 4.1: Materials used for the experimental protocol and the clinical evaluation

4.2.3 Informed Consent

The informed consent was presented by a medical doctor or a physiotherapist to each of the subjects separately. The Informed consent invited each person to participate voluntarily in the study, to acquire sEMG signals and kinematics data for the Nukawa Database. The informed consent explained the two procedures to be performed. The first procedure was the clinical evaluation, and the second procedure was the experimental protocol.

4.2.4 Clinical Evaluation

In order to verify if the subject was healthy, a clinical evaluation was performed before each test. This assessment was carried out by a medical doctor or a physiotherapist and included the measurement of the following control variables: body weight, body height, blood pressure, heart rate, respiration rate, body temperature. All participants were in a healthy condition. Therefore, all of them were accepted to be part of the study. The tests also recorded the age, suprapatellar perimeter, calf perimeter, inter-joint hip/knee distance, and inter-joint knee/ankle distance. The results of these values are reported in Figure 4.2 as a Box-and-whisker plot. In this figure, it can be observed that age of participants ranged from 19 to 47 years, with a median (interquartile range) of 25.5 years (23 to 30.5 years). Moreover, the body weight ranged from 50.1 to 81.9 kg and the body height ranged from 1.46 to 1.85 m. In addition, the inter-joint hip/knee distance ranged from 0.35 to 0.44 m and the inter-joint knee/ankle distance ranged from 0.35 to 0.47 m. For the aforementioned and Figure 4.2, all subjects would fit in the exoskeleton.

4.2.5 Configuration of the acquisition devices

In order to capture the movements performed by the subjects, the acquisition device was the wearable body sensing platform BiosignalPlux powered by Plux. The BiosignalPlux is a wireless device used to record and send real-time information captured by various sensors that can be connected. The sampling rate was configured to $f_s = 1$ kHz. The sensed data was stored in a text file using the OpenSignals software, also powered by Plux. In order to capture the movements performed

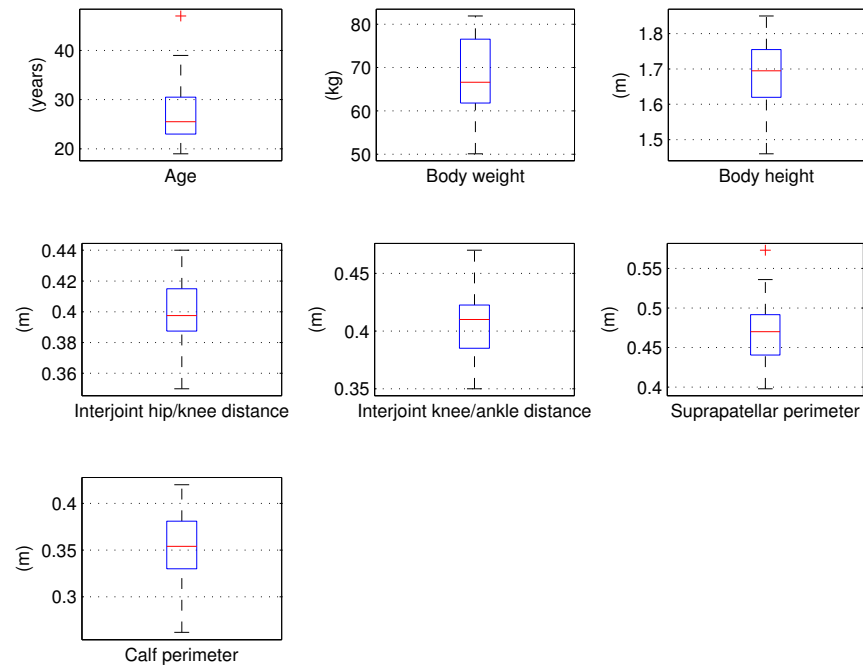


Figure 4.2: Box-and-whisker Plot of values recorded during the experimental protocol

by the subjects during the selected experimental protocol, three twin axis goniometers (SG150) were used. However, the tests only used the FE channels of each goniometer to measure hip FE movements, knee FE movements, and ankle DP flexion movements. The goniometers were located in the dominant lower limb member of the subject. The location of the goniometers was conducted following some of the recommendations of the goniometer and torsionmeter operating manual from Biometrics Ltd [99].

4.2.6 Location of goniometers

The subject wore shorts in order to ease attachment of the goniometers. These sensors were located taking into account that they formed a “simple” bend, without forming an “Oxbow shape”. Also, the sensors were located considering that the distance between the two end-blocks of the goniometers was not reduced. Both precautions were considered not to reduce the accuracy. The end-blocks of the sensors were attached with a double-sided adhesive tape, and then firmly pressed over the subject. Finally, a micropore was located wrapping the goniometer and the subject’s limb. Figure 4.3 presents the location of ankle, knee, and hip goniometers.

In order to monitor DP flexion of the ankle, the distal end-block of the goniometer was attached to the back of the heel of the subject, without the shoes. Subsequently, the subject was asked to execute a dorsiflexion movement, until the subject reached the maximum ROM. At this point, the proximal end-block, attached to the output cables, was fastened at the back of the leg, with collinear axes, as seen in Figure 4.3a.

In order to monitor FE movements of the knee joint, the subject was asked to stand, so that they were standing in the neutral position over a flat surface. The distal end-block of the goniometer was located on the side of the leg, so the axes of the leg and the end-block were coincident when

observed in the sagittal plane. Then, the goniometer was extended and the proximal end-block was attached to the thigh, taking into account that both axes were coincident, as seen in Figure 4.3b.

In order to monitor FE movements of the hip joint, the subject was asked to stand on a flat surface. The proximal end-block of the goniometer was attached to the trunk, in the pelvic region. Subsequently, the goniometer was also extended and the distal end-block was attached to the thigh, taking into account that the axis of the end-block and the axis of the thigh were coincident when observed in the sagittal plane, as seen in Figure 4.3c.

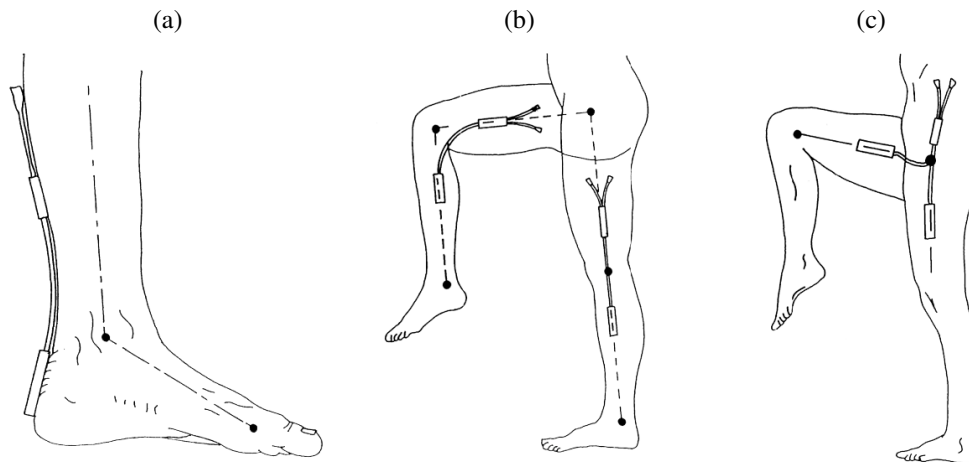


Figure 4.3: Location of (a) ankle, (b) knee, and (c) hip goniometers. Taken from [99]

4.2.7 Conversion of goniometer units

In order to perform a conversion of goniometer units, *i.e.*, from bits to degrees, a test was conducted with the help of an analog goniometer and a pushbutton connected to the BiosignalPlux. To do so, the subject was asked to move each joint separately until they reached the desired position. At this point, the angle was measured with an analog goniometer and the exact time was stored with the push button to do a manual annotation of the events. Both data were recorded to perform the units conversion. It is important to note that during this process numerous spatio-temporal deviations occur because the time of the annotation is left to the subjects. The steps to make this conversion process are the following:

1. The subject was standing on a flat surface.
2. The evaluator started recording the test with the BiosignalPlux.
3. The subject pressed the push-button to register the starting position.
4. The subject performed a hip flexion to 90° .
5. The subject pressed the push-button when they received the indication of the right position.
6. The subject went back to the standing position.
7. The subject performed a knee flexion to 90° .
8. The subject pressed the push-button when they received the indication of the right position.
9. The subject went back to the standing position.
10. The subject performed an ankle plantar flexion to its maximum ROM.
11. The evaluator measured the maximum plantar flexion angle.

12. The subject pressed the push-button when they received the indication of the right position.
13. The evaluator wrote down the maximum plantar flexion angle.
14. The evaluator stopped recording.

4.2.8 sEMG Sensor Placement

The sEMG sensor placement was based on some of the recommendations of the SENIAM Project [59]. According to ISEK Standards for Reporting EMG Data [58] the characteristics of the procedure are shown:

The raw signal was detected using four pairs of commercial, disposable and adhesive gel surface electrodes placed in different parts of the upper leg of a group of healthy-subjects, along with a reference electrode located at the C7 spinal segment. The electrodes had a disc shape and were made of Ag/AgCl. They were placed with an interelectrode distance of approximately 3.5 cm, center point to center point, given the size of the electrodes. The skin of fourteen subjects was shaved, and three subjects were not shaved. The area of interest was cleaned with alcohol before placing the electrodes to reduce the impedance between the electrodes and the skin. The electrodes were placed in order to detect flexion and extension of the knee [97] in the:

- RF muscle, detecting activation when the knee joint was extended.
- VM muscle, detecting activation when the knee joint was extended.
- BF muscle, detecting activation when the knee joint was flexed.
- ST muscle, detecting activation when the knee joint was flexed.

The electrodes were fixed in parallel to the muscle fiber direction using the dominant middle portion of the muscle belly for best selectivity and avoiding the region of motor points. The signals were acquired using an eight channel wearable body sensing platform BiosignalPlux Professional powered by Plux[®]. The device has a differential configuration, an input impedance of 100 G Ω , CMRR of 100 dB, and it was configured with a gain of 1,000. The biosignal was sampled at 1 kHz. The sEMG signal acquisition device transmitted the signal through Bluetooth to a PC, within the Open Signals Software, also provided by Plux[®]. This software was in charge of recording the biosignals. The reference electrode was located on the Processus Spinosus of C7. The reference electrode was located in an electrically unaffected area.

In order to place the electrodes of the RF, the subject was sitting with the knee flexed, and the upper body bent backward, as shown in Figure 4.4a. The electrodes were placed at 50 % on the line from the Anterior Superior Spina Iliaca (ASIS) to the superior part of the Patella, in the direction of the line from the ASIS to the superior part of the Patella [59], the location of the electrodes is represented by a yellow circle in Figure 4.4a.

In order to place the electrodes of the VM, the subject was sitting with the knees flexed and the upper body bent backward, as shown in Figure 4.4b. The electrodes were placed at 80 % on the line between the ASIS and the joint space in front of the anterior border of the ML. The electrode was placed almost perpendicular to the line between the ASIS and the joint space in front of the anterior border of the ML, the location of the electrodes is represented by a yellow circle in Figure 4.4b.

In order to place the electrodes of the BF, the subject was in prone position and the knees flexed, to less than 90°, with the thigh in slight lateral rotation and the leg in slight lateral rotation with respect to the thigh, as shown in Figure 4.4c. The electrodes were placed at 50 % on the line between the ischial tuberosity and the lateral epicondyle of the tibia, the location of the electrodes is represented by a yellow circle in Figure 4.4c.

In order to place the electrodes of the ST, the subject was in prone position and the knee was flexed to less than 90° , as shown in Figure 4.4d. The electrodes were placed at 50 % on the line between the Ischial Tuberosity and the Medial Epicondyle of the Tibia, the location of the electrodes is represented by a yellow circle in Figure 4.4d.

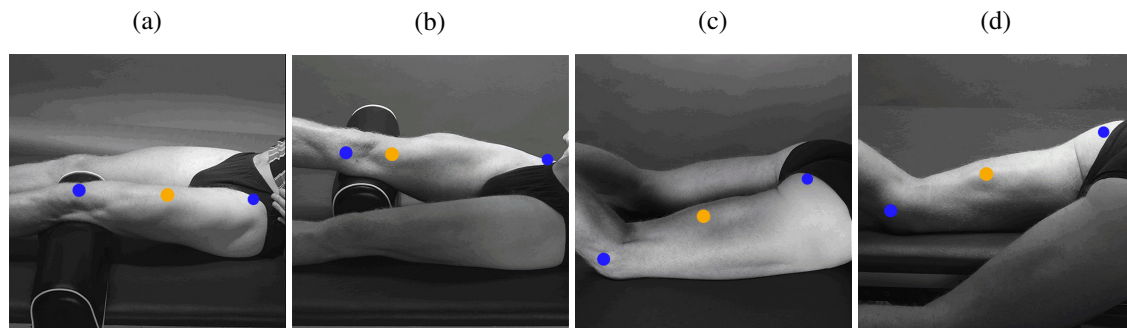


Figure 4.4: Location of sEMG electrodes on (a) RF, (b) VM, (c) BF, and (d) ST muscles. Taken from [59]

4.2.9 Experimental Protocol

In order to acquire the sEMG signal collection regarding ACL rehabilitation exercises, *i.e.*, the Nukawa Database, 19 tests were conducted with each subject. Table 4.6 presents a description of the 19 exercises that were selected with the assistance of a physiotherapist with a specialization in Biomedical Engineering. The test took approximately 2 hours with each participant. It is important to mention that exercises that include movements of the other joints, such as hip and ankle, are also used during ACL rehabilitation protocols. For the aforementioned, It is also interesting to include exercises involving these other joints.

Six isometric exercises (1 to 6) and six concentric dynamic contraction exercises (7 to 12) were selected by the physiotherapist. Figure 4.5 presents two gym machines that were used during the experimental protocol for these two types of exercises. Moreover, Figure 4.5a and Figure 4.5b presents the leg extension machine and the crossover machine, respectively.

A selection process of the exercises belonging to international protocols for rehabilitation of ACL injuries was performed with the assistance of the physiotherapist. The Accelerated ACL Reconstruction Rehabilitation Program of the Chester Knee Clinic & Cartilage Repair Center [34], [35], the Classic 1981 Protocol by Paulos et al. [36], and the ACL Reconstruction Rehabilitation Protocol of the Steadman Clinic [37] were taken into account.

Inclusion criteria

- Exercises that only involve movements in the sagittal plane.
- Exercises involving only the movement of a leg.
- Exercises that are repeated at least in two phases considering the Accelerated ACL Reconstruction Rehabilitation Program of the Chester Knee Clinic & Cartilage Repair Center [34], [35], the Classic 1981 Protocol by Lonnie et al. [36], and the ACL Reconstruction Rehabilitation Protocol of the Steadman Clinic [37].
- Assisted, resisted, and active exercises.
- Isokinetic movements.

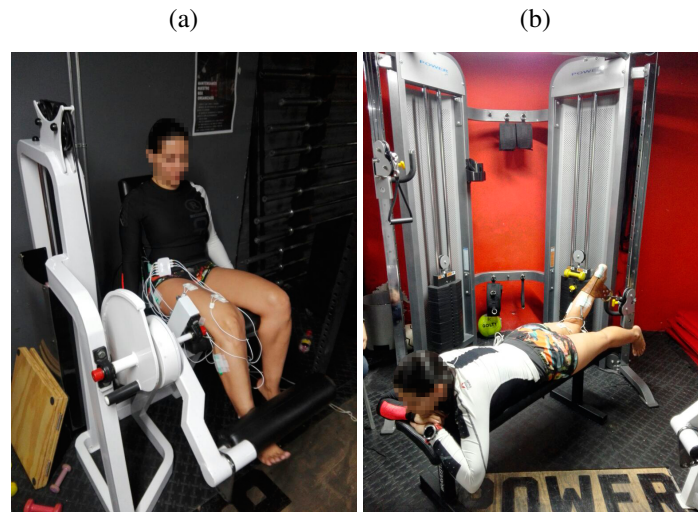


Figure 4.5: Gym machines used during the experiment protocol
(a) Leg extension machine and (b) Crossover machine

Exclusion criteria

- Exercises involving trunk movements.

Taking into account the inclusion and exclusion criteria, six exercises (13 to 18) from the international protocols for rehabilitation of ACL injuries were selected. Figure 4.6 presents the starting point and the ending point of the six exercises. Figure 4.6a and 4.6g presents the starting point and the ending point of a straight leg raise exercise, respectively. Figure 4.6b and 4.6h presents the starting point and the ending point of an unilateral leg press exercise, respectively. Figure 4.6c and 4.6i presents the starting point and the ending point of an active-assisted extension exercise, respectively. Figure 4.6d and 4.6j presents the starting point and the ending point of a resisted knee extension exercise, respectively. Figure 4.6e and 4.6k presents the starting point and the ending point of a resisted knee flexion exercise, respectively. Figure 4.6f and 4.6l presents the starting point and the ending point of heel slides exercise, respectively. Finally, an additional exercise (19) was added to the protocol, as suggested by the physiotherapist.

According to ISEK Standards for Reporting EMG Data, the characteristics of each procedure was written in a file to have sufficient information for reporting data correctly. Table 4.7 presents the data that the file contained.

4.3 Offline sEMG signal processing algorithm

This section proposes a sEMG signal processing algorithm, based on the algorithm stated by Hayashi et al. [65], in order to assess the detection of movement intention. The proposed sEMG signal processing algorithm can detect, approximately, the intensity of the motion intention in a proportionate way to the MVC. In this section the signal processing algorithm was not conducted in real-time. However, tests were carried out with pre-recorded signals as proposed in the simulation-based methodology, stated in [100], [101].

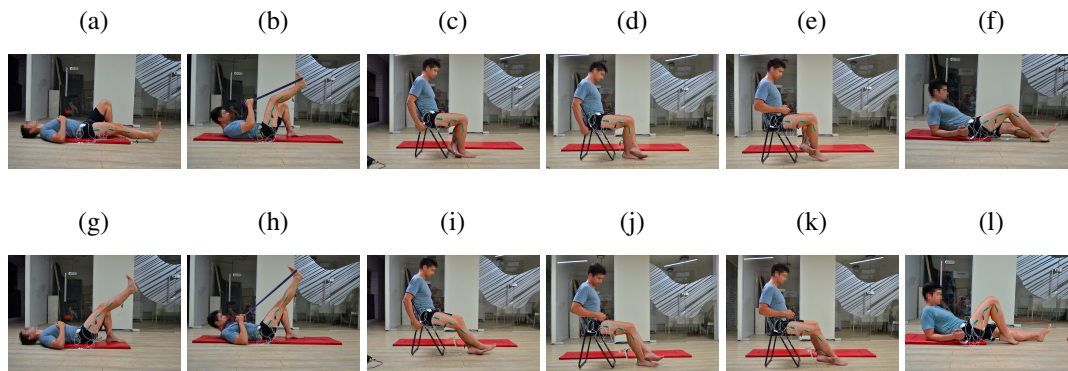


Figure 4.6: Starting and ending point of the six exercises from the international protocols for rehabilitation of ACL injuries. Made by the author and copyrighted to [42].

Figures 4.8, 4.9, and 4.7 present the block diagrams that make up the sEMG signal processing algorithm. In this figures the notation $[n \times m]$ is the size of the signal bus where n is the number of signals and m is the number of samples in the observation window.

Figure 4.7 presents a block diagram containing the principal functions of the sEMG signal pre-processing subroutine. In this figure it is possible to notice that the algorithm has three main blocks which are (1) band-pass filtering, (2) removing DC offset, and (3) full-wave rectification. This subroutine starts filtering the raw sEMG signals. A band-pass Butterworth filter with cut-off frequencies of 10 Hz and 500 Hz was used. A Notch filter was not used, since scientific recommendations from the SENIAM and the ISEK reports that EMG recordings should not use any notch filter. They only recommend a band-pass filter within the 10 Hz and 500 Hz bandwidth [58], [59].

Besides, the mean of the sEMG signals is subtracted, to remove the DC offset. The MAV was extracted to the whole signal taking into account Equation (2.3) given the offline nature of the algorithm. Subsequently, the subroutine performs a full-wave rectification of the signals, computing the absolute value, *i.e.*, all negative amplitudes are converted to positive amplitudes. The rectification process is conducted so that amplitude parameters such as the MAV or RMS can be applied to sEMG signals.

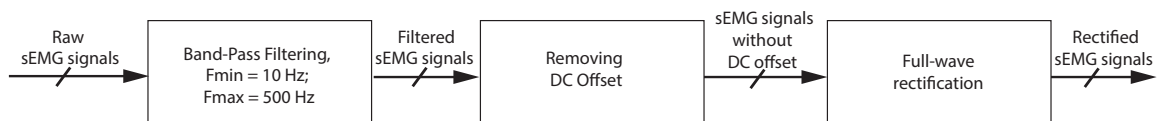


Figure 4.7: sEMG signal pre-processing subroutine

Figure 4.8 presents a block diagram containing the principal functions of the subroutine to compute four normalization values. In this figure it is possible to notice that the algorithm has three main blocks which are (1) sEMG signal pre-processing subroutine explained in Figure 4.7, (2) MAV, and (3) finding and storing maximum values.

The subroutine presented in Figure 4.8 uses RF and VM signals, from trial 4, and BF and ST signals, from trial 1, to compute four normalization values which are later used to normalize the signals of these muscles, respectively. This subroutine uses the adjacent windowing technique

Table 4.6: Exercises conducted during the experimental protocol

Trial	Exercise	Description
1	MVC (flexion) with the knee flexed at 90° and the hip at 0°	The subject was in prone position over a flat bench, and their ankle was fastened with a belt to a crossover machine as shown in Figure 4.5b. The weight to lift was set to the maximum of the machine. The subject was asked to start slowly increasing their knee flexion force, and to reach the maximum effort after 3 to 5 s. The subject was told to hold the maximum effort for 3 s. Afterward, the subject was asked to release the knee flexion force in 3 s.
2	75 % isometric contraction (flexion) with the knee flexed at 90° and the hip at 0°	The subject was in prone position over a flat bench, and their ankle was fastened with a belt to a crossover machine as shown in Figure 4.5b. The weight to lift was set to the 75 % of the total body weight of the subject, e.g., if the total body weight of the subject was 70 kg, the weight to lift was configured to 52 kg, approximately. The subject was asked to start increasing their knee flexion force until they raised the weight. The subject was asked to hold the weight for 5 s. Afterward, the subject was asked to release the knee flexion force.
3	50 % isometric contraction (flexion) with the knee flexed at 90° and the hip at 0°	The subject was in prone position over a flat bench, and their ankle was fastened with a belt to a crossover machine as shown in Figure 4.5b. The weight to lift was set to the 50 % of the total body weight of the subject, e.g., if the total body weight of the subject was 70 kg, the weight to lift was configured to 35 kg, approximately. The subject was asked to start increasing their flexion force until they raised the weight. The subject was asked to hold the weight for 5 s. Afterward, the subject was asked to release the knee flexion force.
4	MVC (extension) with the knee flexed at 90° and the hip flexed at 90°	The subject was sitting on a leg extension machine as shown in Figure 4.5a. The weight to lift was set to the maximum of the machine. The subject was asked to start increasing their knee extension force, and to reach the maximum effort after 3 to 5 s. The subject was told to hold the maximum effort for 3 s. Afterward, the subject was asked to release the knee extension force in 3 s.
5	75 % isometric contraction (extension) with the knee flexed 90° and the hip flexed 90°.	The subject was sitting on a leg extension machine as shown in Figure 4.5a. The weight to lift was set to the 75 % of the total body weight of the subject, e.g., if the total body weight of the subject was 70 kg, the weight to lift was configured to 52 kg, approximately. The subject was asked to start increasing their extension force until they raised the weight. The subject was asked to hold the weight for 5 s. Afterward, the subject was asked to release the knee extension force.
6	50 % isometric contraction (extension) with the knee flexed at 90° and the hip flexed at 90°.	The subject was sitting on a leg extension machine as shown in Figure 4.5a. The weight to lift was set to the 50 % of the total body weight of the subject, e.g., if the body weight of the subject was 70 kg, the machine was configured to 35 kg, approximately. The subject was asked to start increasing the extension force until they raised the weight. The subject was asked to hold the weight for 5 s. Afterward, the subject was asked to release the knee extension force.
7	IRM (flexion) test with the knee flexed at 90° and the hip at 0°.	The subject was in prone position over a flat bench, and their ankle was fastened with a belt to a crossover machine as shown in Figure 4.5b. The subject was asked: what weight can you lift approximately eight times, so that you are not able to perform the ninth repetition due to fatigue? Therefore, the weight to lift was set for each subject, so they could perform approximately eight repetitions. The subject was asked to complete the maximum number of repetitions until they could not continue. Even if they performed more or less than eight repetitions. The Epley formula presented in Equation (2.1) was used to estimate the IRM taking into account the weight lifted w and the number of repetitions r .
8	Concentric dynamic contraction (flexion) at 75 % of the IRM estimated in Trial 7, with the knee flexed at 90° and the hip at 0°.	The subject was in prone position over a flat bench, and their ankle was fastened with a belt to a crossover machine as shown in Figure 4.5b. The weight to lift was configured to 75 % of the IRM estimated in Trial 7. The subject was asked to perform 10 flexion repetitions.
9	Concentric dynamic contraction (flexion) at 50 % of the IRM estimated in Trial 7, with the knee flexed at 90° and the hip at 0°.	The subject was in prone position over a flat bench, and their ankle was fastened with a belt to a crossover machine as shown in Figure 4.5b. The weight to lift was configured to 50 % of the IRM estimated in Trial 7. The subject was asked to perform 10 flexion repetitions.
10	IRM (extension) test with the knee flexed at 90° and the hip flexed 90°.	The subject was sitting on a leg extension machine as shown in Figure 4.5a. The subject was asked: what weight can you lift approximately eight times, so that you are not able to perform the ninth repetition due to fatigue? Therefore, the weight to lift was set for each subject, so they could perform approximately eight repetitions. The subject was asked to complete the maximum number of repetitions until they could not continue. Even if they performed more or less than eight repetitions. The Epley formula presented in Equation (2.1) was used to estimate the IRM taking into account the weight lifted w and the number of repetitions r .
11	Concentric dynamic contraction (extension) at 75 % of the IRM estimated in Trial 10, with the knee flexed at 90° and the hip flexed at 0°.	The subject was sitting on a leg extension machine as shown in Figure 4.5a. The weight to lift was configured to 75 % of the IRM estimated in Trial 10. The subject was asked to perform 10 extension repetitions.
12	Concentric dynamic contraction (extension) at 50 % of the IRM estimated in Trial 10, with the knee flexed at 90° and the hip flexed at 90°.	The subject was sitting on a leg extension machine as shown in Figure 4.5a. The weight to lift was configured to 50 % of the IRM estimated in Trial 10. The subject was asked to perform 10 extension repetitions.
13	Straight leg raise (SLR)	The subject was in supine position over an exercise mat with the knee at 0° and the hip at 0° as shown in Figure 4.6a. The subject was asked to raise their dominant leg maintaining the knee extended at 0° as seen in Figure 4.6g. The subject performed 10 hip flexions until the hip was at 45°, approximately. In this case the right leg was the dominant leg.
14	Unilateral leg press	The subject was in supine position over an exercise mat with the knee flexed at 45° as shown in Figure 4.6b. The subject was asked to perform 10 resisted repetitions with the dominant leg on an exercise band as shown in Figure 4.6h, i.e., as if they were in a leg press machine. In this case the right leg was the dominant leg.
15	Knee active-assisted extension exercise	The subject was sitting on a chair with the knee flexed at 90° as shown in Figure 4.6c. The subject was asked to assist the dominant leg with their opposite leg to straighten the knee from the 90° to 0° as shown in Figure 4.6i. The subject was asked to perform 10 repetitions. In this case the right leg was the dominant leg.
16	Resisted knee extension	The subject was sitting on a chair with the knee flexed at 90° as shown in Figure 4.6d. The subject was asked to resist the extension movement of the dominant leg with the non-dominant leg as shown in Figure 4.6j. In this case the right leg was the dominant leg.
17	Resisted knee flexion	The subject was sitting on a chair with the knee flexed at 90° as shown in Figure 4.6e. The subject was asked to resist the flexion movement of the dominant leg with the non-dominant leg as shown in Figure 4.6k. In this case the right leg was the dominant leg.
18	Heel slides	The subject was in supine position over an exercise mat as shown in Figure 4.6f. The subject was asked to pull the heel of their dominant leg toward the buttocks, flexing the knee as shown in Figure 4.6l. Subsequently, the subject was asked to straighten the leg by sliding the heel downward. The subject was asked to perform 10 repetitions.
19	Knee extension	The subject was sitting on a chair with the knee flexed at 90°. The subject was asked to straighten the knee from the 90° to 0°. The subject was asked to perform 10 repetitions. In this case the right leg was the dominant leg.

presented in Section 2.2.4. In the four cases, the algorithm extracts the MAV for each of the adjacent window of 500 ms, later the algorithm finds the maximum MAV, and it stores the maximum value obtained for each signal.

Figure 4.9 presents a block diagram containing the principal functions of the main routine. In this figure it is possible to notice that the algorithm has five main blocks which are (1) sEMG signal pre-processing subroutine explained in Figure 4.7, (2) RMS envelope, (3) normalization, (4) linear combination, and (5) low-pass filtering.

The main routine uses the four raw sEMG signals from the RF, VM, BF, and ST of current trial (Exercices 2-3, 5-19) and conducts them to the sEMG signal pre-processing subroutine. Subsequently, the algorithm extracts an envelope of the four channels computing the Root Mean Square (RMS) with adjacent windows of 20 ms, since the algorithm should be fast and light, i.e., the total number of samples in a window from the vector of the signal was 20 samples. The

Table 4.7: Characteristics of each trial that were written in a file

Data
Timestamp (DDHHMMZ MMM YY)
Anonymizer code
Age of the subject
Weight of the subject (kg)
Height of the subject (m)
Sports activity (weekly hours)
Practicing sport
Health news
Comments
Health changes after the test
Responsible for the test
Identification of the responsible

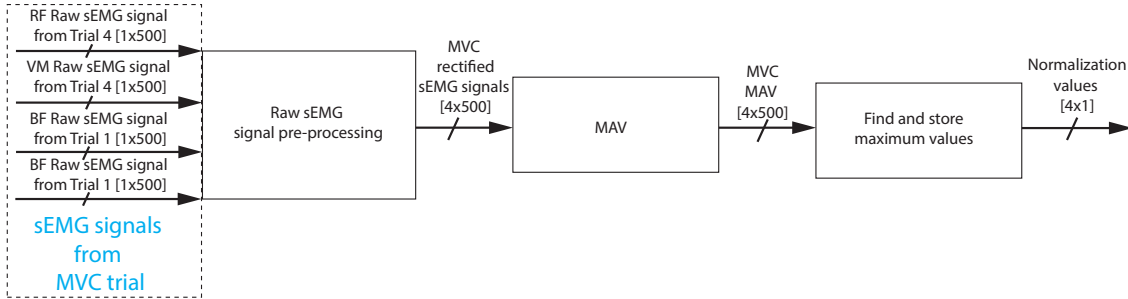


Figure 4.8: Subroutine to compute the four normalization values

RMS is calculated using the Equation (2.2). Afterward, the signals are normalized using the values previously stored for each of the channels during the MVC trial, as previously mentioned in subroutine presented in Figure 4.8. These signals are denoted as RF_{RMS} , VM_{RMS} , BF_{RMS} , and ST_{RMS} , which are the normalized RMS envelopes.

Finally, in order to detect the movement intention a linear combination (LC) of the four RMS envelopes is proposed, *i.e.*, the features of four channels were combined. This LC is based on the Equation (3.2) proposed by Hayashi et al. [65]. However, the conversion coefficients a_f , a_e , b_f , and b_e are not estimated with an additional torque sensor but established heuristically. Moreover, the LC proposed in this thesis uses four sEMG channels instead of two. To do so, the equation

$$LC = RF_{RMS} + VM_{RMS} - BF_{RMS} - ST_{RMS} \quad (4.1)$$

was proposed, where RF_{RMS} , VM_{RMS} , BF_{RMS} , and ST_{RMS} are the processed and normalized signals of the RF, VM, BF, and ST, respectively.

Equation (4.1) was proposed taking into account that the RF and the VM muscles activate more during an extension intention. Moreover, the RMS envelope of these channels would be greater than the RMS envelope of the BF and the ST muscles during an extension intention. Therefore, the conversion coefficients of the RF_{RMS} and the VM_{RMS} have a positive sign, *i.e.*, $a_{RF} = 1$, $b_{RF} = 0$,

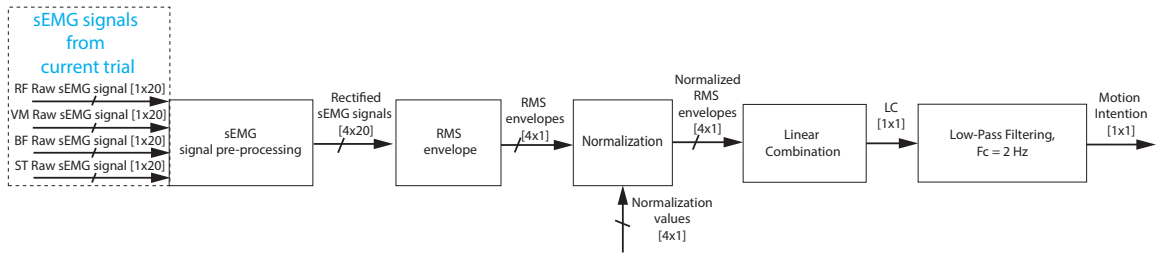


Figure 4.9: Main routine of the sEMG signal processing algorithm

$a_{VM} = 1$, and $b_{VM} = 0$. The BF and the ST muscles activate more during a flexion intention. Therefore, the conversion coefficients of the BF_{RMS} and the ST_{RMS} are negative, since that these muscles are opposed to the RF and the VM muscles, *i.e.*, $a_{BF} = -1$, $b_{BF} = 0$, $a_{ST} = -1$, and $b_{ST} = 0$. Therefore, when the subject intends to perform a knee flexion, the LC is negative in a comparable way to the MVC trial for the flexion, and when the subject intends to carry out a knee extension, the LC is positive in a proportionate way to the MVC trial for the extension. Therefore, the motion intention is a continuous value between -2 and 2, *i.e.*, $LC \in [-2, 2]$, where -2 and 2 means the MVC trial in flexion and extension, respectively.

Finally, the LC was filtered using a low-pass digital Butterworth Filter with a cut-off frequency of 2 Hz, order one, to remove the peaks and smooth the signal.

The tests of the sEMG signal processing algorithm were conducted with the signals acquired from the 17-healthy-subjects. However, to exemplify the algorithm, the implementation with the signals obtained during the tests with the fifth subject (S5) is presented below (randomly selected). Figure 4.10 overlaps the rectified signals of the RF, VM, BF, and ST muscles in light gray, with the RF_{RMS} , VM_{RMS} , BF_{RMS} , and ST_{RMS} , respectively in black. Figure 4.10 also presents the results of the LC in light gray, and the LC filtered in black. In this figure, it can be observed the detection of the subject's intention to perform an extension movement since the LC filtered has a positive sign.

Figure 4.11 presents the results of conducting all three isometric extension signals (Exercises 4 to 6) from the 17-healthy-subjects to the sEMG signal processing algorithm. Moreover, Subfigures 4.11a to 4.11q presents the results for each subject from S1 to S17, respectively. Each subfigure has three lines, one for trial. The red, green, and blue lines represent the detection of the motion intention for the MVC, 75 % isometric contraction, and 50 % isometric contraction exercises, respectively.

Subfigures 4.11a to 4.11q have a similar result. It can be observed that all 51 lines are positive, which means an extension exercise. Therefore, the algorithm detected the orientation of the intention 100 % of the times for the extension exercises (4 to 6). Besides, the red line is greater than the green line, and the green line is higher than the blue line for 16 of the 17 (94 %) subjects, *i.e.*, all but S12 (6 %). Therefore, it is proposed that the algorithm detects the orientation and intensity of the movement intention in a comparable way to the MVC during extension exercises (Exercises 4 to 6).

Figure 4.12 presents the results of conducting all three flexion signals (Exercises 1 to 3) from the 17-healthy-subjects to the sEMG signal processing algorithm. Moreover, Subfigures 4.12a to 4.12q presents the results for each subject from S1 to S17, respectively. Each subfigure has three lines, one for trial. The red, green, and blue lines represent the detection of the motion intention for the MVC, 75 % isometric contraction, and 50 % isometric contraction exercises, respectively.

Furthermore, in Subfigures 4.12a to 4.12q all 51 lines are negative, by means of a flexion exercise. Therefore, the algorithm detected the orientation of the intention 100 % of the times for the flexion exercises (1 to 3). Also, the red line is greater than the green line, and the green line is higher than

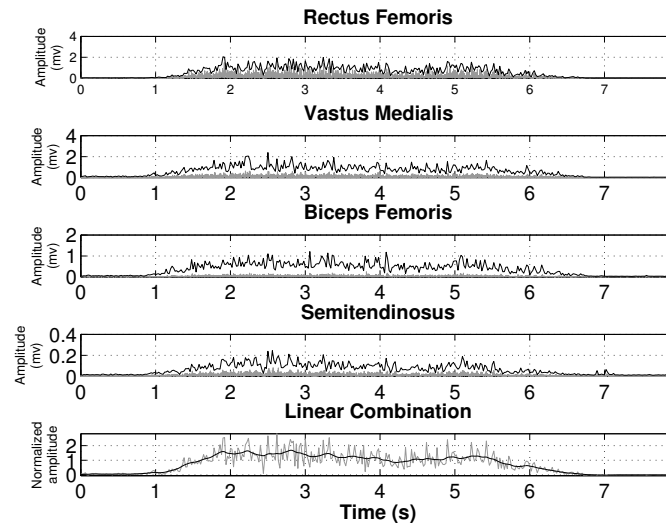


Figure 4.10: Rectified signals of the RF, VM, BF, and ST muscles, overlapped with the RF_{RMS} , VM_{RMS} , BF_{RMS} , and ST_{RMS} . LC and LC filtered from trial 4 of the S5

the blue line for 10 of the 17 (59 %) subjects, *i.e.*, S1, S2, S3, S4, S7, S8, S9, S10, S11, and S17. However, the intensity of the flexion exercises for 7 of 17 (41 %) the subjects was not recognizable, *i.e.*, S5, S6, S12, S13, S14, S15, and S16. Therefore, it is proposed that the algorithm detects the orientation and intensity of the movement intention in a comparable way to the MVC during flexion exercises (Exercises 1 to 3).

The algorithm could not detect the intensity but the orientation of the intention in some of the flexion tests, due to two possible explanations. The first one is that the subjects were performing a co-contraction of the muscles, *i.e.*, a simultaneous contraction of agonist and antagonist muscles around the target joint. The second one is that the impedance between the electrodes and the skin influenced the sEMG signals acquisition. This impedance was not measured or controlled during the experimental protocol. Therefore, it could have changed during the tests. For the aforementioned, the algorithm may detect when the subject intends to perform a flexion and the intensity of the movement intention in most cases.

Unexpectedly, a relation between the movement intention detected, and the actual movement of the knee in the concentric dynamic contractions (exercises 7 to 12) was observed. Therefore, the LC filtered of the concentric dynamic contractions was scaled. Figure 4.13a shows in gray the actual angular velocity of the knee during trial 9 of s5, and in black the scaled LC filtered obtained with the sEMG signal processing algorithm. Both curves are similar in shape but are slightly different in amplitude. In addition, Figure 4.13b shows a Box-and-whiskers plot of the Spearman Correlation between the actual velocity measured, with goniometers, and the scaled LC filtered for the six concentric dynamic contraction exercises. This figure shows that the best correlation was trial 12 where the median correlation was $r = 0.72, p < 0.05$ and the exercise with the worst correlation was trial 7 with a median correlation of $r = 0.64, p < 0.05$. Therefore, it is possible to propose that there may be a relationship between them.

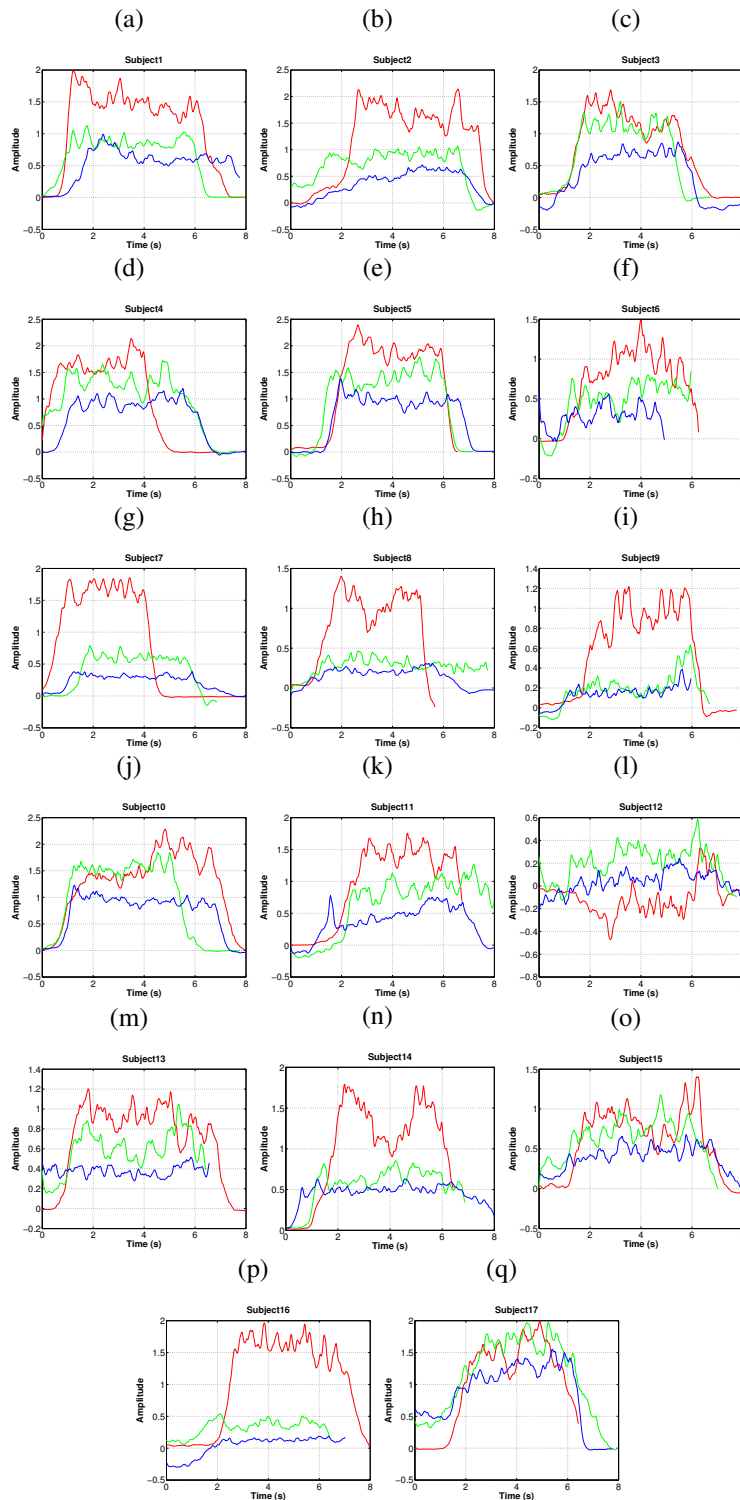


Figure 4.11: LC of the isometric extension exercises from the 17-healthy-subjects

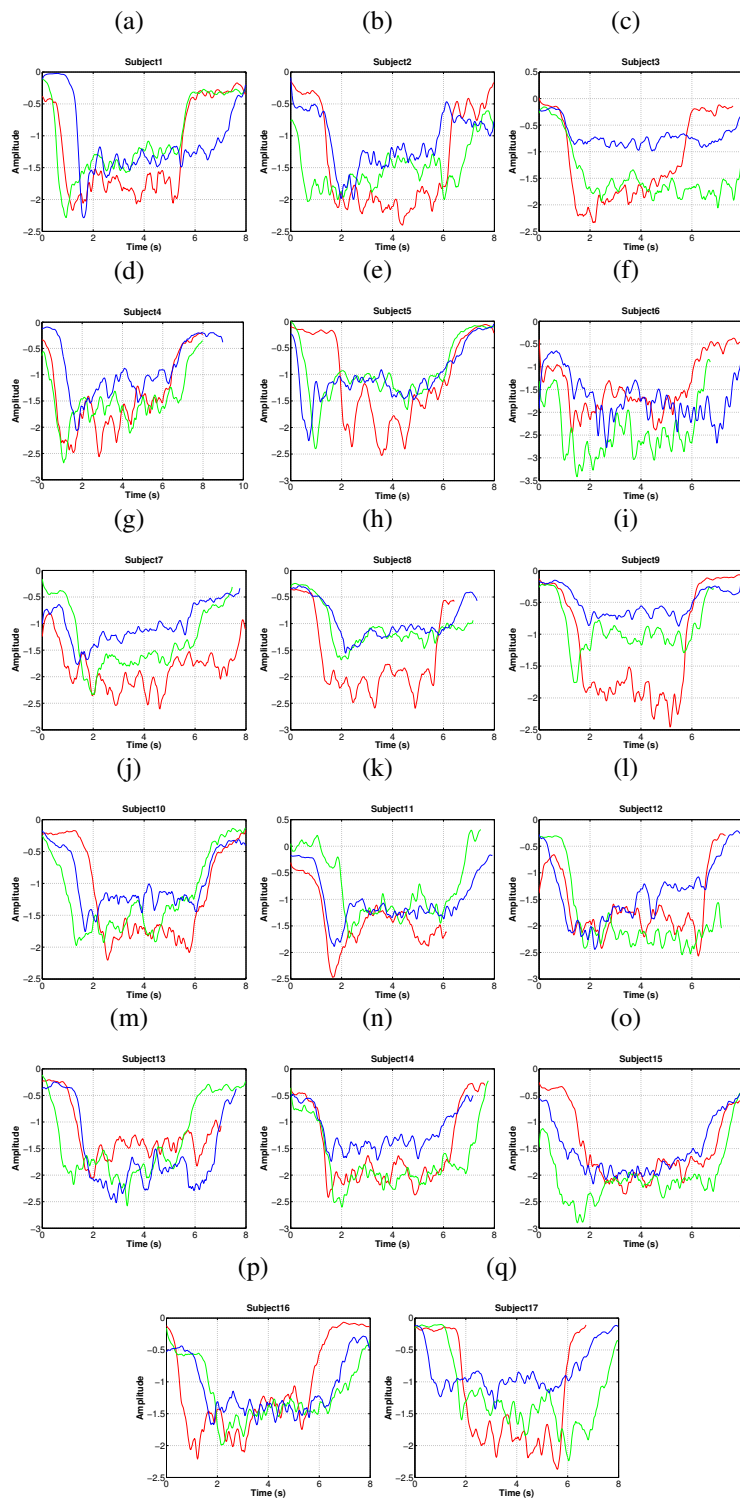


Figure 4.12: *LC* of the isometric flexion exercises from the 17-healthy-subjects

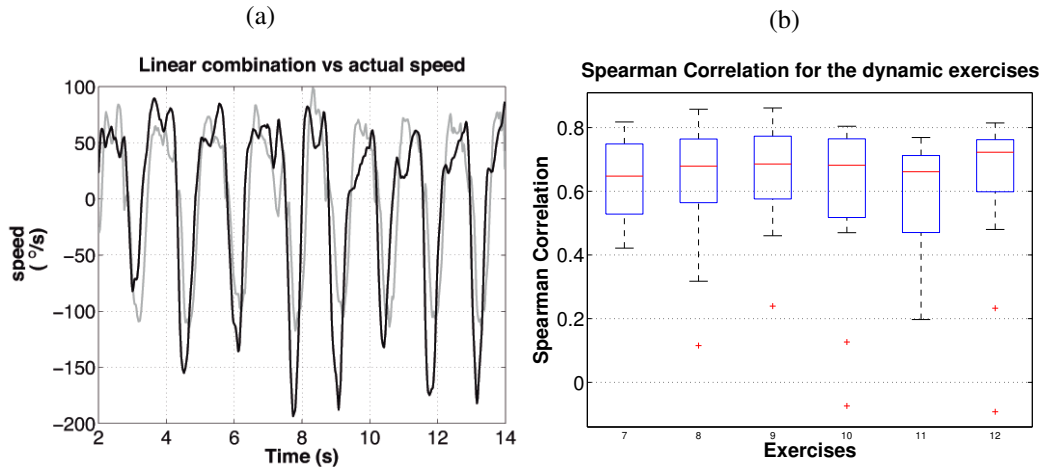


Figure 4.13: (a) Comparison of the *LC* filtered and the actual speed of the knee joint of trial 9 of S5, (b) Box-and-whiskers plot of the Spearman Correlation between the actual velocity and the scaled *LC* filtered for the six concentric dynamic contraction exercises

4.4 Online sEMG signal processing algorithm as an HIL

Subsequently, the sEMG signal processing algorithm was implemented in real-time in a BBB which has an AM335x 1 GHz ARM[®] Cortex-8512 MB processor and a 512 MB DDR3 Memory RAM. This implementation was conducted using Python, a high-level programming language. The sEMG signal processing algorithm was developed in real-time as an HIL simulation, *i.e.*, tests were performed using pre-recorded signals from the Nukawa Database. Moreover, tests were carried out as proposed in the simulation-based methodology stated in [100], [101]. A custom-made sEMG signal simulator was developed in Python in a computer. The custom-made sEMG signal simulator extracted the signals from the Nukawa Database, and send them to the BBB. The computer used for the tests was an Intel[®] Core[™] i5 with a 4 GB DD3 memory RAM. The computer communicates with the BBB through TCP/IP within a predefined communication port as shown in Figure 4.14a. The sampling period was set to $TS = 0.02$ s. Therefore, the signals were extracted using a window of 20 ms each time. The signals were conducted to the real-time algorithm to detect the motion intention of the knee.

Figure 4.14b presents in red the offline movement intention, and in green the online movement intention. In this figure, it is possible to observe that the two curves have a similar shape and amplitude. Moreover, the Spearman correlation between the offline movement intention and online movement intention was $r = 0.86, p < 0.05$. However, the small differences may be due to the fact that the offline algorithm has the pre-recorded data, therefore, the behavior of the signals is known a priori, however, the online algorithm does not have access to the entire signal, as expected in real-time systems.

The mean execution time (*M*) and the standard deviation (*SD*) taken by sEMG signal processing algorithm within the BBB was measured. The mean execution time for the sEMG signal processing algorithm does not take more than $M = 27.1$ ms on average with a maximum standard deviation of $SD = 7.5$. The sEMG signal processing algorithm would add a delay during the execution in the BBB. Therefore, the execution time of the sEMG signal processing was tested in the computer, and

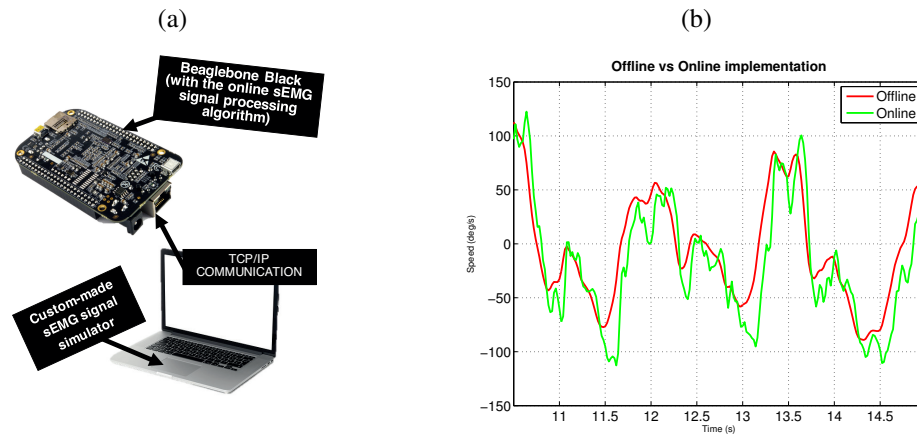


Figure 4.14: (a) HIL implementation to test the online version of the sEMG signal processing algorithm, (b) comparison of the offline and online movement intention

it does not take more than $M = 1.4$ ms on average with a maximum standard deviation of $SD = 0.4$. Therefore, it is proposed that the sEMG signal processing algorithm may be executed in the computer for the tests with the real-time system, taking into account that the algorithm was developed in Python, which is a cross-platform high-level programming language.

Chapter Summary

A sEMG signal processing algorithm, based on the algorithm stated in [65], was proposed. This algorithm detects the motion intention in the knee joint and requires no prior training with sEMG signals from other subjects. Moreover, no additional torque sensor is required to estimate the conversion coefficients.

The results showed that the *LC* algorithm detected the intensity of the movement intention, approximately, in a comparable way to the *MVC*. It is possible to conclude about the similarity since the *MVC* tests had greater amplitude than the 75 % isometric contraction tests. Also, the 75 % isometric contraction tests had greater amplitude than 50 % isometric contraction tests.

In addition, the results of the *LC* algorithm showed that when a subject intended to perform a knee flexion or extension, without executing the movement, the algorithm detected the orientation of the movement intention. Moreover, when a subject intended to carry out an extension movement, the algorithm detected a *LC* with a positive sign, and when a subject intended to perform a flexion movement, the algorithm detected a *LC* with a negative sign.

The offline and the online movement intention have small differences, *i.e.*, the online movement intention is noisier than the offline movement intention, however, they are very similar in shape and both are strongly correlated, $r = 0.86, p < 0.05$. Therefore, it is possible to propose that both are helpful for the current application since both represent the intensity and orientation of the movement intention, *i.e.*, flexion or extension.

Also, in the next studies, the detection of the motion intention of the hip and the ankle may be included, to perform mechatronic-assisted rehabilitation exercises which include movements of these joints.

In the future, the sEMG signal processing algorithm may be developed and implemented using several models such as white models or even black-box models.

Future work also includes the evaluation of the behavior of the algorithm using, not just pre-recorded signals extracted from a database, but from healthy-subjects with the BiosignalPlux or any acquisition device. These tests should be given to assess if the intention was detected correctly.

Future work includes to test and evaluate the sEMG signal processing algorithm with signals from patients with ACL injuries with the BiosignalPlux or any acquisition device.

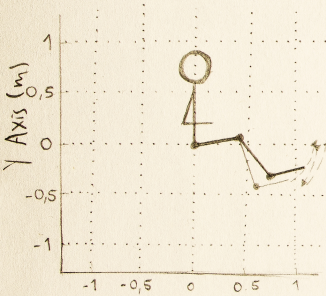
It is considered as a future work the inclusion of mechatronic-resisted rehabilitation exercises, where the algorithm detects the intended movement and does not perform an assistive action, but a resistive.

Future work includes several tests such as 25 % isometric contractions with the knee flexed 90° and the hip flexed 90°. In addition, tests with multiple repetitions of isometric tests may be conducted, *e.g.*, performing an isometric contraction multiple times and in a row.

Future work may include testing the sEMG signal processing algorithm to compute the torque of the knee joint using sEMG signals. The tests may be conducted taking into account the actual torque exerted by the subject. The tests may be conducted using an isokinetic dynamometer or an estimation of the torque using the free-body diagram of the machine and the subject, and the angle of each limb recorded with the goniometers. These tests should be conducted to modify the current algorithm so it can estimate the exact torque exerted by the subject.

The Nukawa system would act as an active orthosis controlled using sEMG signals feedback in order to conduct assisted therapies for patients. The system should measure the electrical activity of the muscles of the lower limb, and would detect the intention of movement, and thus assist the movement.

• Sagittal plane (x2) •
Schematic of Nukawa



In addition, the joints are collinear to human joints. The knee is a polycentric joint, however this simplification was conducted as presented by Zoss, who involves

$$LC = RF_{RMS} + VM_{RMS} - BF_{RMS} - ST_{RMS}$$



5. Movement Control Algorithm

The 3-DOF allows the system to adjust the system for each segment of the mechatronic system Nukawa is variable. hip, FE movements of the knee, and DP movements of the ankle.

a pure rotational joint in the sagittal plane. In order to adjust the system for each segment of the mechatronic system Nukawa is variable.

This system is designed for people between 1.44m and 1.85m tall, using a telescopic

This chapter presents a simulation of a movement control algorithm for mechatronic-assisted rehabilitation based on exercises and movements associated with therapies for ACL injuries, *i.e.*, fulfilling the fourth objective of this thesis. The implementation of the CTC algorithm was conducted as an HIL simulation using a computational model to test the mechatronic system Nukawa without having to use the actual robot.

This chapter is presented as follows. Section 5.1 presents a list of requirements to be met by the movement control algorithm. Section 5.2 explains the mathematical modeling of the mechatronic system Nukawa. Also, Section 5.3 presents the movement control algorithm. In addition, Section 5.4 explains the implementation as an HIL simulation. Subsequently, the following sections present a wide description of each of the tests that were conducted to examine and assess the movement control algorithm implemented as an HIL simulation and the model itself. Section 5.5, the movement algorithm followed the actual movements conducted by a physiotherapist during several exercises that belong to international protocols for rehabilitation of ACL injuries. Finally, section 5.5 presents the chapter summary regarding the results and possible future works.

5.1 Requirements of the control algorithm

The following is a list of requirements to be met by the movement control algorithm:

- The sampling period of the algorithm should be lower than 300 ms.
- The algorithm should control the movement during different rehabilitation exercises.
- The movement control algorithm should be fast and light so it may be implemented in real-time.
- The algorithm should not need high performance computing features, *i.e.*, the amount of processor time required during one sampling period should be low.
- The movement control algorithm should be implemented online as an HIL simulation.
- The motion control algorithm should control the three joints at the same time.

5.2 Modeling the rehabilitation system Nukawa

The mathematical model of Nukawa, stated in [40]–[42], is a set of three rigid bodies connected in a serial chain, with friction at each of the joints. Each joint has a sensor to measure joint position, and an actuator to apply torque to the link. The dynamics of Nukawa were mathematically modeled using the Newton-Euler method, stated in [102]. The plant model includes the weight and dimensions of both the 3-DOF mechatronic device and the subject.

The mathematical model of a 3-DOF serial robot is described by the rigid body dynamic equation, stated in [6], as Equation (2.4). The friction term may be decomposed into two terms which are given by

$$F(\dot{q}) = F_v \dot{q} + F_d(\dot{q}), \quad (5.1)$$

where F_v is the coefficient matrix of viscous friction which is proportional to the velocity of joint motion, and F_d a dynamic friction term or Coulomb friction which is constant except for a sign dependance on the joint velocity. Therefore, Equation (2.4) can be expressed as

$$M(q)\ddot{q} + V(q, \dot{q}) + F_v \dot{q} + F_d(\dot{q}) + G(q) + \tau_d = \tau. \quad (5.2)$$

On one hand, the viscous friction may be assumed as

$$F_v \dot{q} = \text{vec}\{v_i \dot{q}_i\} = \begin{pmatrix} v_1 \dot{q}_1 \\ v_2 \dot{q}_2 \\ v_3 \dot{q}_3 \end{pmatrix}, \quad (5.3)$$

with v_i constant coefficients for each $i \in \{1, 2, 3\}$, and $\text{vec}\{\cdot\}$ the vectorization of a matrix. On the other hand, the dynamic friction may be assumed to have the form

$$F_d(\dot{q}) = \text{vec}\{k_i \text{sgn}(\dot{q}_i)\}, \quad (5.4)$$

with k_i constant coefficients for each $i \in \{1, 2, 3\}$. Taking into account that

$$N(q, \dot{q}) = V(q, \dot{q}) + F_v \dot{q} + F_d(\dot{q}) + G(q), \quad (5.5)$$

where the $N(q, \dot{q})$ are the nonlinear terms, the mathematical model that describes both the 3-DOF mechatronic device and the subject is given by

$$M(q)\ddot{q} + N(q, \dot{q}) + \tau_d = \tau. \quad (5.6)$$

The conventions for the mathematical model are presented in Figure 5.1. Each joint has a coordinate axis, and a counterclockwise movement is the convention for a positive arc of movement. The base of the robot is the hip joint. Let q_1 , q_2 , and q_3 be the hip, knee and ankle joint angles, respectively. q_1 is measured taking into account the horizontal plane. q_2 and q_3 are measured relative to the previous segment of the robot. For example, the position in Figure 5.1 is expressed as

$q = (q_1, q_2, q_3)^T = (45^\circ, -30^\circ, 80^\circ)^T$, in this figure L_1 , L_2 , and L_3 are the link lengths. For this work, the plant model includes the weight of both the 3-DOF mechatronic device and the subject. Therefore, the total weight of Link 1 is expressed as $m_1 = m_{1p} + m_{1e}$, where m_{1p} is the weight of the subject's thigh and m_{1e} is the weight of the mechatronic device's thigh. Also, the total weight of Link 2 is given by $m_2 = m_{2p} + m_{2e}$, where m_{2p} is the weight of the subject's shank and m_{2e} is the weight of the mechatronic device's shank. In addition, the total weight of Link 3 is expressed as $m_3 = m_{3p} + m_{3e}$, where m_{3p} is the weight of the subject's foot and m_{3e} is the weight of the mechatronic device's foot. Finally, g represents the gravity.

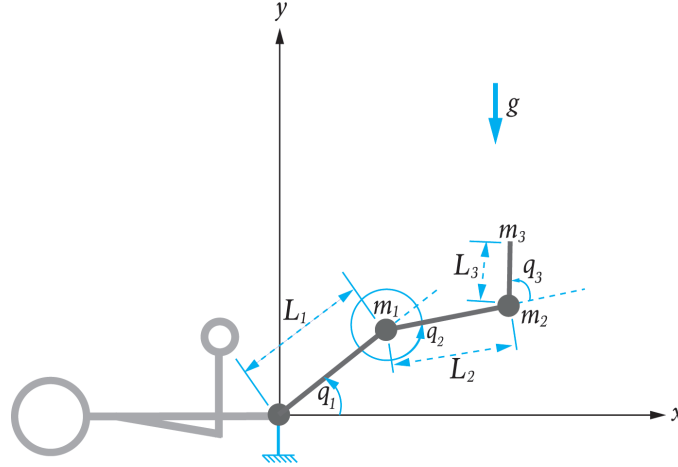


Figure 5.1: Conventions for the mathematical model of Nukawa

For this work, assumption 1, 2, 3, 4, and 5 were considered.

Assumption 1 The base of the robot is fixed to the platform as a stationary element, see Figure 5.1.

Assumption 2 The center of mass is located in the distal point of each limb, *i.e.*, being this the worst-case scenario, see Figure 5.1.

Assumption 3 The robot is moving in free space, without contact with its environment.

Assumption 4 The disturbance torques τ_d are zero, *i.e.*, there are no torques exerted by the subject or any inaccurately modeled dynamics.

Assumption 5 The dynamic friction $F_d(\dot{q})$ is neglected.

Finally, Assumptions 4 and 5 turn Equation (5.5) into

$$N(q, \dot{q}) = V(q, \dot{q}) + F_v \dot{q} + G(q), \quad (5.7)$$

and the robot dynamics presented in Equation (5.2) can be expressed as

$$M(q)\ddot{q} + V(q, \dot{q}) + F_v \dot{q} + G(q) = \tau, \quad (5.8)$$

In (5.8), the symmetric and positive definite rigid body inertia matrix $M(q)$ can be expressed as

$$M(q) = \begin{pmatrix} M_{11} & M_{12} & M_{13} \\ M_{21} & M_{22} & M_{23} \\ M_{31} & M_{32} & M_{33} \end{pmatrix} \quad (5.9)$$

where

$$\begin{aligned} M_{11} = & m_3 L_3 (L_1 \cos(q_2 + q_3) + L_2 \cos(q_3) + L_3) + m_2 L_2 (L_1 \cos(q_2) + L_2) + m_3 L_2 (L_1 \cos(q_2) + \\ & L_2 + L_3 \cos(q_3)) + m_1 L_1^2 + m_2 L_1 (L_1 + L_2 \cos(q_2)) + m_3 L_1 (L_1 + L_2 \cos(q_2) + \\ & L_3 \cos(q_2 + q_3)), \end{aligned} \quad (5.10)$$

$$\begin{aligned} M_{12} = & m_3 L_3 (L_2 \cos(q_3) + L_3) + m_2 L_2^2 + m_3 L_2 (L_2 + L_3 \cos(q_3)) + m_2 L_1 L_2 \cos(q_2) + \\ & m_3 L_1 (L_2 \cos(q_2) + L_3 \cos(q_2 + q_3)), \end{aligned} \quad (5.11)$$

$$M_{13} = m_3 L_3^2 + m_3 L_2 L_3 \cos(q_3) + m_3 L_1 L_3 \cos(q_2 + q_3), \quad (5.12)$$

$$\begin{aligned} M_{21} = & m_3 L_3 (L_1 \cos(q_2 + q_3) + L_2 \cos(q_3) + L_3) + m_2 L_2 (L_1 \cos(q_2) + L_2) + m_3 L_2 (L_1 \cos(q_2) + \\ & L_2 + L_3 \cos(q_3)), \end{aligned} \quad (5.13)$$

$$M_{22} = m_3 L_3 (L_2 \cos(q_3) + L_3) + m_2 L_2^2 + m_3 L_2 (L_2 + L_3 \cos(q_3)), \quad (5.14)$$

$$M_{23} = m_3 L_3^2 + m_3 L_2 L_3 \cos(q_3), \quad (5.15)$$

$$M_{31} = m_3 L_3 (L_1 \cos(q_2 + q_3) + L_2 \cos(q_3) + L_3), \quad (5.16)$$

$$M_{32} = m_3 L_3 (L_2 \cos(q_3) + L_3), \quad (5.17)$$

$$M_{33} = m_3 L_3^2. \quad (5.18)$$

The coriolis and centripetal vector $V(q, \dot{q})$ is given by

$$V(q, \dot{q}) = \begin{pmatrix} V_{11} \\ V_{21} \\ V_{31} \end{pmatrix} \quad (5.19)$$

where

$$\begin{aligned} V_{11} = & m_3 L_3 (L_1 \sin(q_2 + q_3) \dot{q}_1^2 + L_2 \sin(q_3) (\dot{q}_1 + \dot{q}_2)^2) + m_2 L_1 L_2 \sin(q_2) \dot{q}_1^2 \\ & + m_3 L_2 (L_1 \sin(q_2) \dot{q}_1^2 - L_3 \sin(q_3) (\dot{q}_1 + \dot{q}_2 + \dot{q}_3)^2) - m_2 L_1 L_2 \sin(q_2) (\dot{q}_1 + \dot{q}_2)^2 \\ & - m_3 L_1 L_2 \sin(q_2) (\dot{q}_1 + \dot{q}_2)^2 - L_3 \sin(q_2 + q_3) (\dot{q}_1 + \dot{q}_2 + \dot{q}_3)^2, \end{aligned} \quad (5.20)$$

$$\begin{aligned} V_{21} = & m_3 L_3 (L_1 \sin(q_2 + q_3) \dot{q}_1^2 + L_2 \sin(q_3) (\dot{q}_1 + \dot{q}_2)^2) + m_2 L_1 L_2 \sin(q_2) \dot{q}_1^2 \\ & + m_3 L_2 (L_1 \sin(q_2) \dot{q}_1^2 - L_3 \sin(q_3) (\dot{q}_1 + \dot{q}_2 + \dot{q}_3)^2), \end{aligned} \quad (5.21)$$

$$V_{31} = m_3 L_3 (L_1 \sin(q_2 + q_3) \dot{q}_1^2 + L_2 \sin(q_3) (\dot{q}_1 + \dot{q}_2)^2). \quad (5.22)$$

Finally, the gravitational effects $G(q)$ are represented by

$$G(q) = g \begin{pmatrix} G_{11} \\ G_{21} \\ G_{31} \end{pmatrix} \quad (5.23)$$

where

$$\begin{aligned} G_{11} = & m_3 L_3 \cos(q_1 + q_2 + q_3) + m_2 L_2 \cos(q_1 + q_2) + m_3 L_2 \cos(q_1 + q_2) + m_1 L_1 \cos(q_1) \\ & + m_2 L_1 \cos(q_1) + m_3 L_1 \cos(q_1), \end{aligned} \quad (5.24)$$

$$G_{21} = m_3 L_3 \cos(q_1 + q_2 + q_3) + m_2 L_2 \cos(q_1 + q_2) + m_3 L_2 \cos(q_1 + q_2), \quad (5.25)$$

$$G_{31} = m_3 L_3 \cos(q_1 + q_2 + q_3). \quad (5.26)$$

5.3 Control law

The problem of controlling a 3-DOF robot is a multi-input, multi-output (MIMO) problem. That is, there is a *vector* of desired joint positions, velocities, and accelerations. Moreover, the control law must compute a *vector* of torques [103]. The desired trajectory is denoted by $q_d(t) \in \mathbb{R}^{3 \times 1}$, $\dot{q}_d(t) \in \mathbb{R}^{3 \times 1}$, and $\ddot{q}_d(t) \in \mathbb{R}^{3 \times 1}$ in the joint space. The tracking control objective is that the actual position $q_m(t) \in \mathbb{R}^{3 \times 1}$ follows the desired position $q_d(t)$, the actual velocity $\dot{q}_m(t) \in \mathbb{R}^{3 \times 1}$ follows the desired velocity $\dot{q}_d(t)$, and the actual acceleration $\ddot{q}_m(t) \in \mathbb{R}^{3 \times 1}$ follows the desired acceleration $\ddot{q}_d(t)$.

The computed torque control law $\tau_u \in \mathbb{R}^{3 \times 1}$ for Nukawa is represented by

$$\tau_u = M(q)(\ddot{q}_d - u(t)) + N(q, \dot{q}), \quad (5.27)$$

and replacing Equation (5.7) in (5.27), the control law can be expressed as

$$\tau_u = M(q)(\ddot{q}_d - u(t)) + V(q, \dot{q}) + F_v \dot{q} + G(q) \quad (5.28)$$

where $u(t) \in \mathbb{R}^{3 \times 1}$ is the output of the *outer loop feedback*, which is based on a derivative on process variable PID algorithm, stated in [104], and computed as

$$u(t) = -K_p e(t) - (K_p/T_i) \int_0^t e(t) dt - T_d K_p (-\dot{q}_m), \quad (5.29)$$

where $K_p = \text{diag}\{K_{p_i}\}$ is the proportional gain, $T_i = \text{diag}\{T_{i_i}\}$ is the integral time, and $T_d = \text{diag}\{T_{d_i}\}$ is the derivative time for each $i \in \{1, 2, 3\}$, *i.e.*, the gains of the PID controller. Also, the tracking error is defined as

$$e(t) = q_d(t) - q_m(t). \quad (5.30)$$

Algorithm 1 summarizes the CTC algorithm implementation which is responsible for computing the necessary torque τ_u to control the movement of each joint. The algorithm includes both the *outer loop feedback* and the *nonlinear inner loop*. Algorithm 1 receives q_m , \dot{q}_m , \ddot{q}_m , \dot{q}_d , \ddot{q}_d , and the model parameters P . This algorithm computes the torque τ_u each sampling period. The development of this algorithm was based on the CTC algorithm reported by Kirby [41], however, the

implementation was conducted to work in real-time as an HIL simulation.

Algorithm 1: CTC algorithm

1 $Tu = \text{ComputeTorque}(q_m, \dot{q}_m, \ddot{q}_m, \dot{q}_d, \ddot{q}_d, P)$;

Input :

q_m Actual position (rad, rad, rad)
 \dot{q}_m Actual speed (rad/s, rad/s, rad/s)
 \ddot{q}_m Actual acceleration (rad/s², rad/s², rad/s²)
 q_d Desired position (rad, rad, rad)
 \dot{q}_d Desired speed (rad/s, rad/s, rad/s)
 \ddot{q}_d Desired acceleration (rad/s², rad/s², rad/s²)
 P Model parameters

Output :

τ_u Actuators torque (Nm, Nm, Nm)
 /* Outer loop feedback */
 2 $e(t) = q_d(t) - q_m(t)$; // Compute position error (rad, rad, rad)
 3 $u(t) = -K_p e(t) - (K_p/T_i) \int_0^t e(t) dt - T_d K_p (-\dot{q}_m)$; // Use PID control action
 /* Nonlinear inner loop */
 4 Compute $M(q)$, $V(q, \dot{q})$, F_v , and $G(q)$
 5 $\tau_u = M(q)(\ddot{q}_d - u(t)) + V(q, \dot{q}) + F_v \dot{q} + G(q)$; // Compute torque (Nm, Nm, Nm)
 6 return τ_u ; // Return actuators torque

5.4 HIL simulation

In order to test the mathematical model and the movement control algorithm, without interacting with the actual robot, an HIL implementation was used. Figure 5.2 unveils the HIL implementation, which has two main components. The first component is the mathematical model placed on a computer. The second component is the CTC algorithm placed on a BBB Rev C, which communicates with the computer through TCP/IP. The communications are conducted within a predefined communication port to perform a remote execution.

The mathematical model of the plant, represented by Equation (5.8), was implemented in the computational programming environment Matlab. Also, a graphical model was implemented to visualize the behavior of the system [40]–[42].

The CTC algorithm was implemented using Python in a BBB Rev C, such as the HIL simulation of the sEMG signal processing algorithm presented in Section 4.4. This process was conducted taking into account the control law defined by Equation (5.28). The CTC algorithm was used to get gravitational compensation and to remove, or to attenuate, the nonlinearities effects of the system

The sampling period was set to $TS = 0.02$ s, therefore, the sampling frequency was $fs = 50$ Hz. The computer used for the tests was the same as the one used in Section 4.4. The simulation of the dynamics, in Matlab, is slow compared to the sampling period. Nonetheless, the control algorithm is designed so that it is not affected by the time taken by the dynamics simulation.

Table 5.1 presents the parameters for the simulations, including both the 3-DOF mechatronic device and a subject of 1.85 m height and 83 kg weight. In order to define the lengths and weights of the segments, models proposed by Plagenhoef [105] and De Leva [106] were used. These models contain anatomical data for analyzing human motion. Table 5.2 presents the percentages of total body weight for each lower limb segment. Table 5.3 presents the segment length as a percentage of

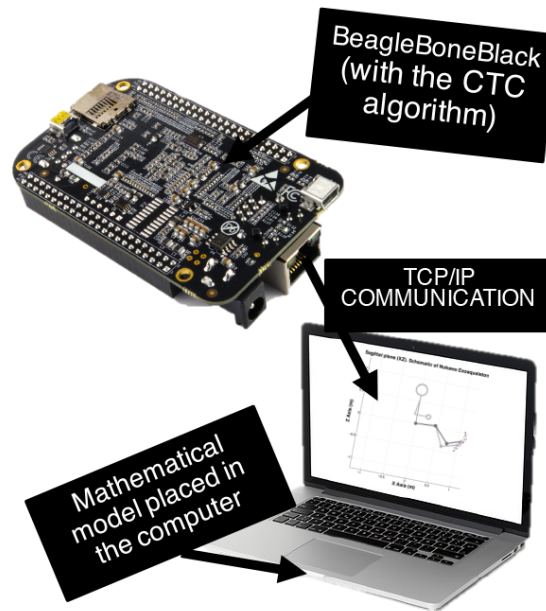


Figure 5.2: HIL implementation in order to test the movement control algorithm. Made by the author and copyrighted to [42]

total height. However, several models has been proposed in order to compute body measurements.

In this work, the viscous friction $\text{vec}\{v_i\}$ was assumed in a heuristic way, taking into account that the simulation showed a three-segment pendulum behavior when the CTC algorithm is deactivated. It was assumed in this way, so that the model behaved with a pendulum that oscillated three times, before stabilizing, when it was dropped from the position $q = (0^\circ, 0^\circ, 90^\circ)$, as expected in the mechatronic system. Also, an heuristic method was used to tune the gains of the PID controller, *i.e.*, the *outer loop feedback*. These gains were configured in order to reduce the error and the oscillations.

The backrest of the mechatronic system is not an actuated joint. However, it is imperative to report the backrest angle B_r of the mechatronic system for each test, since it determines in which position the mechatronic system is. Figure 5.3 presents the conventions for the B_r . A counterclockwise movement is the convention for a positive arc of movement, and B_r is measured taking into account the horizontal plane.

The main positions of the mechatronic system Nukawa are presented in Figure 5.4. Figure 5.4a presents the supine position, *i.e.*, lying horizontally facing up by means of a $q = (0^\circ, 0^\circ, 90^\circ)$ position, and $B_r = 180^\circ$. Figure 5.4b presents a sitting position by means of a $q = (0^\circ, -90^\circ, 90^\circ)$ position, and $B_r = 90^\circ$. Finally, Figure 5.4c presents a standing position by means of a $q = (-90^\circ, 0^\circ, 90^\circ)$ position, and $B_r = 90^\circ$. The ROM of the three joints of the lower limbs during the HIL simulations should be within the values presented in Table 5.4.

5.5 Test with ACL rehabilitation exercises

In order to validate that the movement control algorithm works properly during actual exercises for rehabilitation of ACL injuries, a physiotherapist, with a specialization in Biomedical Engineering,

Table 5.1: Nukawa parameters for simulation including a subject of 1.85 m height and 83 kg weight

Variable	Description	Value	Unit
v_1	Viscous Friction in hip joint	40	$\text{Nm} \frac{s}{\text{rad}}$
v_2	Viscous Friction in knee joint	40	$\text{Nm} \frac{s}{\text{rad}}$
v_3	Viscous Friction in ankle joint	40	$\text{Nm} \frac{s}{\text{rad}}$
L_1	Link 1 length	0.4607	m
L_2	Link 2 length	0.4755	m
L_3	Link 3 length	0.3278	m
m_{1p}	Thigh weight	12.2674	kg
m_{2p}	Shank weight	3.9923	kg
m_{3p}	Foot weight	1.1371	kg
m_{1e}	Link 1 weight	19	kg
m_{2e}	Link 2 weight	9	kg
m_{3e}	Link 3 weight	11	kg
m_1	Total weight of Link 1	31.2674	kg
m_2	Total weight of Link 2	12.9923	kg
m_3	Total weight of Link 3	12.1371	kg
g	Gravity	9.8	$\frac{m}{s^2}$
K_p	Proportional gain	150	-
T_i	Integral time	150	-
T_d	Derivative time	0.1	-
$m_{1\text{Saturation}}$	Motor 1 saturation	768.458	Nm
$m_{2\text{Saturation}}$	Motor 2 saturation	371.377	Nm
$m_{3\text{Saturation}}$	Motor 3 saturation	102.689	Nm

Table 5.2: Segment weight as a percentage of total body weight [106]

Segment	Men (%)	Women (%)	Average (%)
Thigh	14.16	14.78	14.47
Shank	4.33	4.81	4.57
Foot	1.37	1.29	1.33

Table 5.3: Segment length as a percentage of total height [105]

Segment	Men (%)	Women (%)	Average (%)
Thigh	23.2	24.9	24.05
Shank	24.7	25.7	25.2
Foot	4.25	4.25	4.25

performed six exercises from the ones presented in Section 4.2.9, *i.e.*, exercises 13 to 18.

The movements performed by the physiotherapist were recorded with the wearable body sensing platform BiosignalPlux, *i.e.*, the commercial acquisition device presented in Section 4.2. During

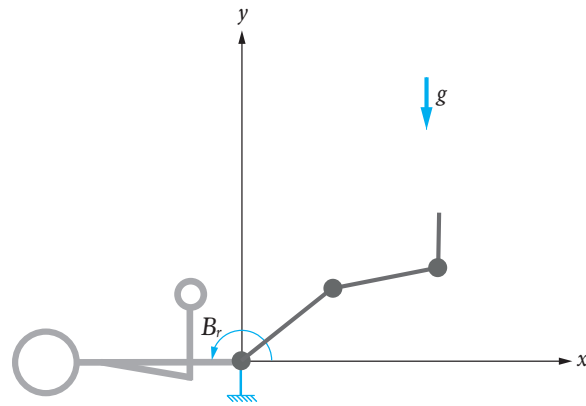


Figure 5.3: Backrest angle conventions

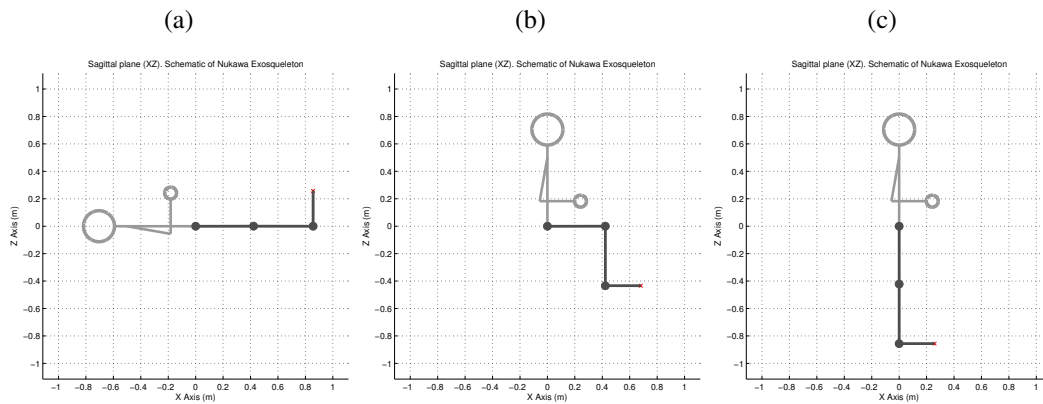


Figure 5.4: Main positions for the mechatronic system, (a) supine, (b) sitting, and (c) standing. Made by the author and copyrighted to [42]

Table 5.4: Lower extremity range of motion [107]

Joint	Movement	Range of Motion (°)
Hip	Flexion	122 ± 12
	Extension	22 ± 8
Knee	Flexion	134 ± 9
	Extension	-1 ± 2
Ankle	Dorsiflexion	12 ± 4
	Plantar flexion	54 ± 6

each exercise, the expert was asked to conduct the movements the best way possible, *i.e.*, as it should be done so that the subject is induced to rehabilitation.

The sampling rate was also set to $f_s = 1000$ Hz. The sensed data was stored in a text file using the OpenSignals software. With the purpose of capturing the movements performed by the physiotherapist during the selected exercises, three twin axis goniometers (SG150) were used.

However, the tests with the HIL simulation only used the FE channels of each goniometer to measure hip FE, knee FE, and ankle DP flexion movements. The goniometers were placed in the right leg, *i.e.*, the dominant lower limb member of the physiotherapist. The process to locate the goniometers was the same as in the experimental protocol presented in Section 4.2, however, the sEMG sensors were not used.

Subsequently, the trajectories extracted with the goniometers were softened in order to obtain a smooth position set-point (SP). The pre-recorded angles of each joint were conducted to an offline simulator to validate the trajectories of the simulation that would be used with the HIL simulation. Figure 5.5 presents one of the six cases, which is the simulation of Exercise 13. This offline simulation was conducted using a 3D CAD model of Nukawa. This simulation included the kinematics of the robot as stated in the simulation-based methodology proposed in [100], [101].

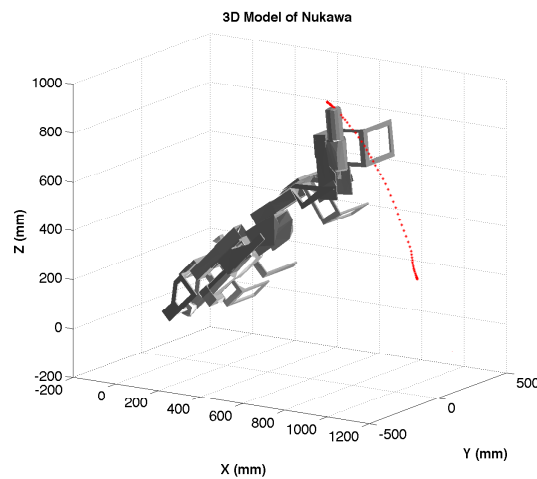


Figure 5.5: 3D Simulation with pre-recorded trajectories in order to validate the movements in the right limb of Nukawa. Made by the author and copyrighted to [42].

Finally, the trajectories were conducted to the HIL simulation. These movements were a position SP, *i.e.*, the angles of the hip, knee, and ankle were conducted as a position reference for the three joints of the robotic system.

Table 5.5 presents the numerical results of the six HIL simulation tests that were performed with pre-defined references. This table shows that the supposed motors were not saturated since the maximum torques exerted by the controller are smaller than the ones presented in Table 5.1. Therefore, the motors must meet these torque requirements, either by construction or employing gears, so that Nukawa may follow the proposed trajectories. Moreover, the motors must ensure the speed at those torques.

Also, Table 5.5 presents the maximum and minimum angle for each joint during the six tests. In this table it can be noticed that the angles executed by the robotic system Nukawa are within the ROM of the lower limbs according to the values presented in Table 5.4.

Table 5.5 shows the results of computing the position MAE for each test. Moreover, it presents the MAE in a percentage of joint motion, *i.e.*, the error relative to the motion performed by each joint during each test. As indicated in the table, the maximum MAE for each joint is 2.79° , 2.6° ,

1.2° and the maximum MAE in a percentage of the joint motion is 5.7 %, 4.9 %, and 9.5 %, for the hip, knee, and ankle joints, respectively. Thus, the error is lower in the knee, which is where the injury is. However, it tolerates small errors, which are needed for the PID controller to work.

Table 5.5: Results of the six HIL simulations using pre-recorded trajectories extracted from ACL rehabilitation exercises

Exercise	B_r (°)	Position MAE (°, °, °)	Maximum Torque (Nm, Nm, Nm)	Minimum Torque (Nm, Nm, Nm)	Maximum Angle (°, °, °)	Minimum Angle (°, °, °)	Joint motion (°, °, °)	MAE in percentage of joint motion (%, %, %)
1	180	(2.7919, 0.4355, 0.5823)	(664.5950, 243.8630, 39.2040)	(174.5030, 47.9520, -24.2410)	(49.5001, -0.8597, 68.2314)	(0.8272, -18.6657, 58.6880)	(48.6729, 17.8060, 9.5434)	(5.7360, 2.4458, 6.1016)
		(2.5994, 2.3389, 1.2640)	(435.4620, 163.4860, 47.7150)	(49.3990, 50.1630, -22.8660)	(86.5538, -9.5109, 78.1261)	(31.9709, -57.4554, 61.0364)	(54.5829, 47.9445, 17.0897)	(4.7623, 4.8783, 7.3963)
3	90	(0.4244, 1.9864, 0.1640)	(500.3780, 179.1210, 44.8750)	(53.2350, -63.7530, -12.8190)	(15.1249, -8.7834, 97.8625)	(1.5625, -72.1193, 94.7839)	(13.5624, 63.3359, 3.0786)	(3.1292, 3.1363, 5.3271)
		(0.3027, 1.4723, 0.1289)	(454.9370, 144.5800, 45.4950)	(275.4570, 68.5650, 9.3080)	(14.8908, -24.7428, 90.4839)	(5.5589, -64.5651, 87.2635)	(9.3319, 39.8223, 3.2204)	(3.2437, 3.6972, 4.0026)
5	90	(0.5625, 2.4139, 0.4282)	(381.4440, 156.2180, 36.0430)	(282.3270, 66.0580, 7.2290)	(12.6574, -20.1280, 96.8261)	(-1.5469, -69.6521, 87.1468)	(14.2043, 49.5241, 9.6793)	(3.9601, 4.8742, 4.4239)
		(1.1319, 2.6511, 0.1548)	(431.7540, 166.2320, 56.4060)	(156.2670, 68.1360, 14.4760)	(50.7972, -48.6990, 91.6108)	(27.5392, -102.3704, 89.9920)	(23.2580, 53.6714, 1.6188)	(4.8667, 4.9395, 9.5626)

Figure 5.6 contains six sub figures. Each sub figure presents the graphical result of one of the six tests. The red and dotted line represents the actual position for the end-point of the robot, *i.e.*, the distal point of the third link (L3). The blue and dotted line represents the desired position for the end-point of the robot. In this figure it can be seen that the desired and actual position are overlapped in the six sub figures. Consequently, it is proposed that the robotic system may conduct mechatronic-assisted rehabilitation based on exercises and movements associated with therapies for ACL injuries.

In order to exemplify the trajectory tracking error, Figures 5.7a, 5.7b, and 5.7c, present the results of the HIL simulation of Exercise 13. Figure 5.7a presents the desired position with a continuous line and the actual position with a dotted line. In this figure, it is possible to observe that the system can follow the SP in joint space, since both curves are almost overlapped. Also, it is possible to denote that the system followed the imposed reference not only visualizing Figure 5.7a but for the error presented in Figure 5.7b. Figure 5.7c shows the desired speed in a continuous line and the actual speed in dotted line. Both curves look alike with a small delay, except at the beginning of the trial.

The mean execution time (M) and the standard deviation (SD) taken by the motion control algorithm within the BBB was measured. The controller does not take more than $M = 12.6$ ms on average with a maximum standard deviation of $SD = 2.3$. Therefore, it is proposed that the implementation of the movement control algorithm may be tested with the real-time system, without any significant delays generated by the calculation of the control law.

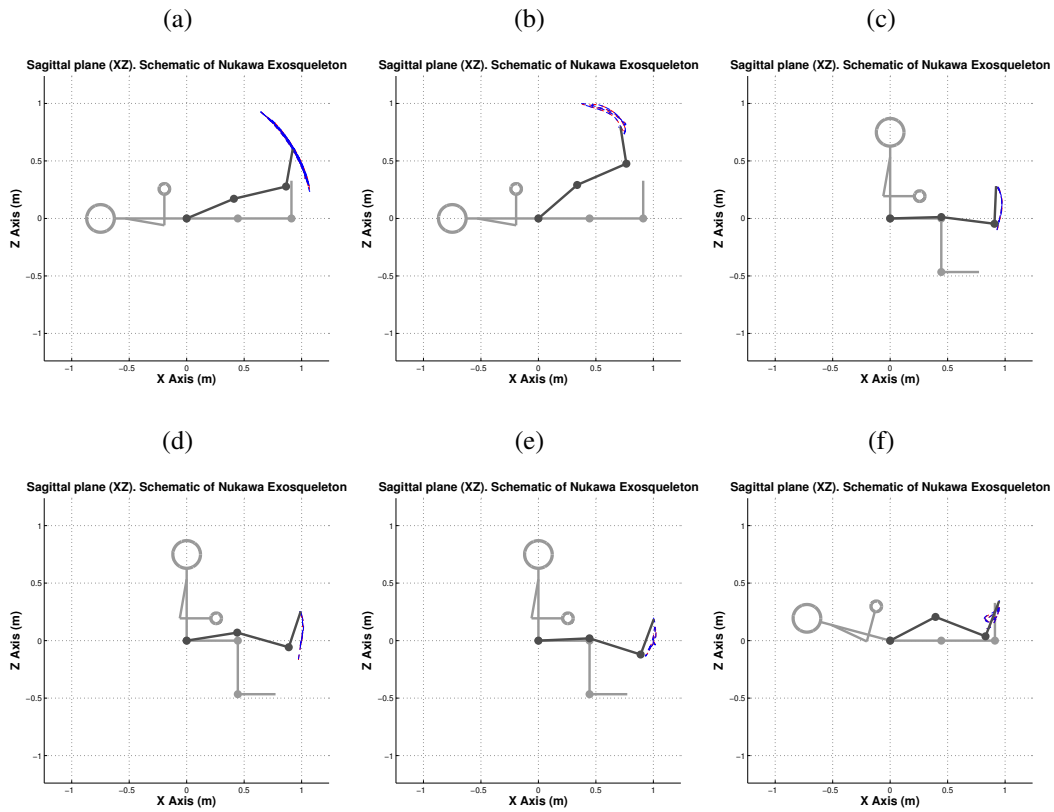


Figure 5.6: HIL Simulation using pre-recorded trajectories

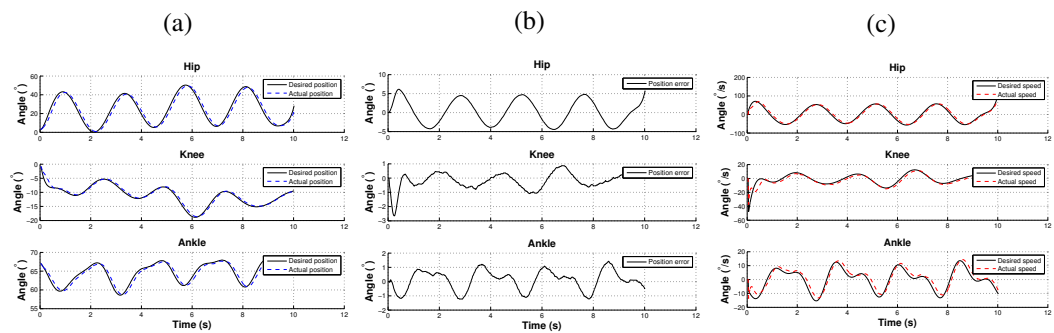


Figure 5.7: Results of the HIL simulation using a trajectory extracted during a straight leg raise, (a) desired position vs. actual position, (b) position error, and (c) desired speed vs. actual speed

For the aforementioned, the movement control algorithm is validated for the parameters presented in Table 5.1. Moreover, the movement control algorithm is validated in the case in which the controller knows the exact parameters of the plant model.

Chapter Summary

These simulations have shown the feasibility of implementing an HIL simulation to control the movements of a simplified model of Nukawa. However, the computational model may differ from the actual robot, due to the fact of simplifications or inaccuracies. Therefore, a future work requires conducting these tests with the actual robotic system.

The HIL simulation of the mathematical model of Nukawa was a useful tool in order to validate the CTC algorithm without interacting with the actual robot. Thus, making variations in the control parameters was a simple task in order to evaluate the system response.

The system is capable of reproducing trajectories associated with ACL rehabilitation protocols. Therefore, due to the ability to reproduce these trajectories, it will be possible to validate different types of exercises that include several paths, *i.e.*, isotonic, assisted, resisted, among others.

With the purpose of obtaining a model closer to the real one, it is imperative to configure the system with known lengths and weights and to drop it from the position $q = (0^\circ, 0^\circ, 0^\circ)$, without restrictions or mechanical limits enabled. During this test, the position of each joint must be recorded, and then, an optimization algorithm must be used to tune the friction coefficients.

It is considered as a future work the inclusion of the entire friction term in the mathematical model. Therefore, the model would take into account the force that is opposed to the beginning of the movement, *i.e.*, the effects that may generate a dead zone for the controller. Even though a slightly larger torque is exerted, no movement will be generated until it can overcome the friction. Also, it is possible to include the friction that occurs between the robot and the patient with the medium, *i.e.*, the friction with the air during high-speed exercises, for example, with athletes finishing a rehabilitation process.

Some of the perturbations of the system may be known a priori. Therefore, it is proposed that in the future they may be included in the CTC algorithm, to make a feed-forward control. Therefore, the *outer loop feedback* would not be responsible for dealing with these perturbations.

The center of mass was assumed at the distal point of each limb, *i.e.*, being this the worst-case scenario. Therefore, the computed torques are greater than the real ones. Consequently, another future work is to use the 3D model of Nukawa or even to do experimental tests with the actual robot, to estimate the inertial parameters of each limb to obtain a mathematical model closer to the real one.

In the future, an HIL simulation can be performed using torque references rather than position SP. These test may be conducted to control the torque of the motors to perform another type of exercises, *e.g.*, isotonic exercises.

Further work, also includes implementing the control algorithm in the Robot Operating System (ROS) and applying the simulations in an environment other than Matlab such as Gazebo, V-REP, Peekabot, Webots, Drake, among others.

The constants of the *outer loop feedback* were set using a heuristic PID tuning method, this method and values were appropriate for the current application. However, it could be a better approach if an optimization method is used for each joint controller, *i.e.*, an autotuning method.

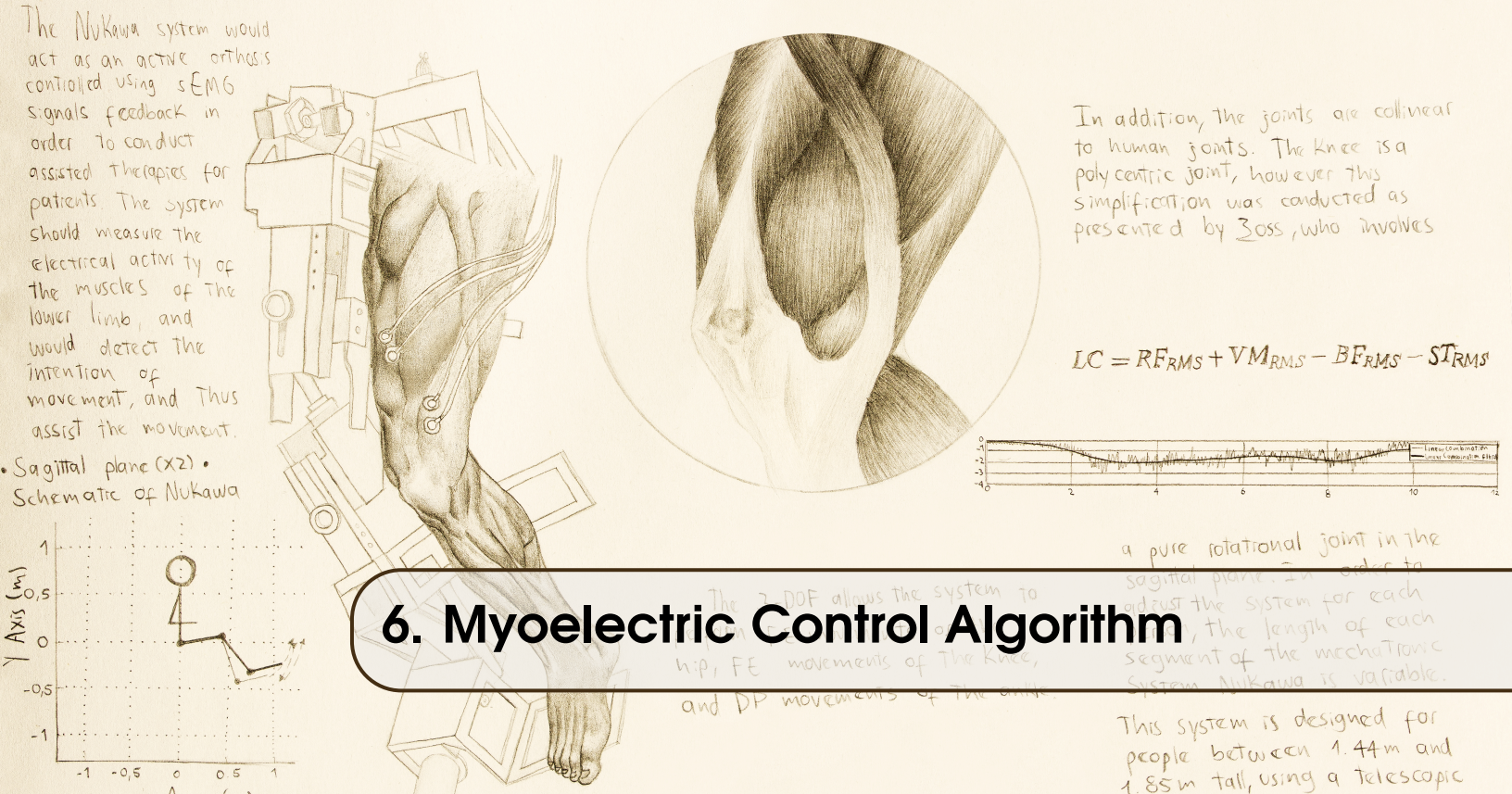
With the purpose of characterizing the trajectories that fit all subjects, a future work is to acquire the same trajectories during the six exercises with a group of physiotherapists, healthy, and unhealthy subjects.

As mentioned in Section 2.3, CTC is a model-based control which enables compliant robot control with small tracking errors for accurate robot models. Nevertheless, in order to assesses the robustness of the movement control algorithm, future work includes several tests changing the parameters of the mathematical model implemented in Matlab. However, during these trials, the

CTC algorithm should not be tuned each time but it should be left the same way for each test. It is imperative to emphasize that these tests are intended to verify the robustness of the control system which is subjected to uncertainties. Testing the robustness as an HIL simulation helps to ensure that the actual implementation of the mechatronic system is robust enough, despite the usual uncertainties during construction and use. The robustness to changes of each parameter should be tested separately, and finally, all the combinations of the parameters should be modified at the same time to verify the robustness to multiple factors. The following model parameters should be changed during the tests:

- Patient height between 1.44 m and 1.85 m.
- Weight of the subjects between 50 kg and 100 kg.
- Weight uncertainty for each link of the exoskeleton between 0 % and 10 %.
- Friction coefficient between 0 and 200.
- Percentage of variability of the sensor between 0 % y 10 %.

Finally, a future work includes to develop an adaptive control algorithm for Nukawa, so that the mechatronic system is stable for any given user regardless of the parameter uncertainties.



6. Myoelectric Control Algorithm

A test protocol was conducted to assess the behavior of the MEC algorithm for mechatronic-assisted rehabilitation and its possibilities to support rehabilitation therapies for ACL injuries, *i.e.*, fulfilling the fifth objective of this thesis. To do so, the algorithms presented in Chapter 4 and Chapter 5 were joined together as an HIL simulation. The first algorithm corresponds to the sEMG signal processing algorithm to assess the detection of motion intention. The second algorithm is the movement control algorithm for mechatronic-assisted rehabilitation based on exercises and movements associated with therapies for ACL injuries.

The protocol of tests was carried out in real-time conducting the pre-recorded sEMG signals from the Nukawa Database to the MEC. The tests assessed if the movement developed by the mechatronic system corresponds to the movement intention executed by the subject during the experimental protocol. Therefore, the tests did not involve individuals or animals but pre-recorded signals from the Nukawa Database.

6.1 Protocol of tests

A four component architecture was used to conduct the protocol of tests. Figure 6.1 presents a block diagram of the interaction of all four components. In this figure, the custom-made sEMG signal simulator presented in Chapter 4 is the first element. This component is placed in the same computer as the one used in that chapter. This simulator communicates with the BBB through TCP/IP within a predefined communication port to perform a remote execution. The custom-made sEMG signal simulator reads the signal from the Nukawa Database, and sends a window of 20 ms each time to the sEMG signal processing algorithm.

The sEMG signal processing algorithm presented in Chapter 4 is the second component. This element, runs in the BBB, and receives a window of 20 ms each time, and computes the movement intention, *i.e.*, the intensity and orientation of the knee joint motion intention. The motion intention is sent through TCP/IP to the third component, which is the movement control algorithm presented in Chapter 5 and is also located in the BBB. However, a set-point conversion is conducted as shown

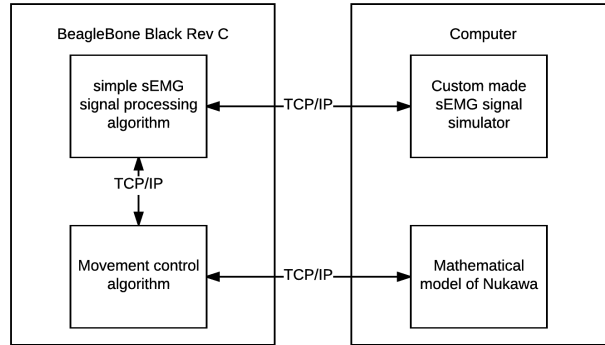


Figure 6.1: Block diagram of the interaction of all of the four components of the architecture used for the protocol of tests

in Figure 6.2, *i.e.*, the output of the motion intention algorithm is scaled taking into account that

$$\dot{q}_d \text{Knee} = \alpha LC + \beta, \quad (6.1)$$

where $\dot{q}_d \text{Knee}$ is the scaled motion intention, and the desired speed for the knee joint, α is the amplitude scaling factor, and β is the offset. Subsequently, the scaled motion intention is derived for the knee joint and the desired trajectory for the hip and ankle joints are given by the goniometers. In this figure the notation $[n \times m]$ is the size of the signal bus where n is the number of signals and m is the number of samples in the observation window. The movement control algorithm is responsible for computing the torque τ_u . The calculated torque is sent back to the computer through TCP/IP, to the fourth component, which is the mathematical model of Nukawa presented in Chapter 5. The simulation of the dynamics of the Nukawa is performed in the computer, in Matlab. Therefore, the graphical model moves as the desired path indicates it. Finally, an acknowledge is sent back and the loop is repeated each sampling period.

In order to validate that the MEC algorithm works properly during actual exercises for rehabilitation of ACL injuries, six tests were conducted using the six dynamic exercises presented in Section 4.2.9, *i.e.*, exercises 7 to 12. The graphical and numerical results of the six tests are shown in Section 6.1.1 and 6.1.2. These tests were carried out randomly, *i.e.*, the combination of subject and trial was randomized.

6.1.1 Graphical Results

With the purpose of exemplifying the behavior of the MEC, the implementation with the signals obtained during trial 9 with the seventh subject (S7) is presented below.

Figures 6.3a, 6.3b, 6.3c, 6.3d, 6.3e, and 6.3f presents the result of an HIL simulation for trial 9 with S7. As explained in Section 4.2.9, during trial 9, the subject was in prone position over a flat bench with the knee flexed 90° , hip at 0° . Their ankle was fastened with a belt to a crossover machine. However, the simulations were conducted with the subject in supine position, since Nukawa is not designed to perform therapies in prone position. The above is acceptable for rehabilitation purposes,

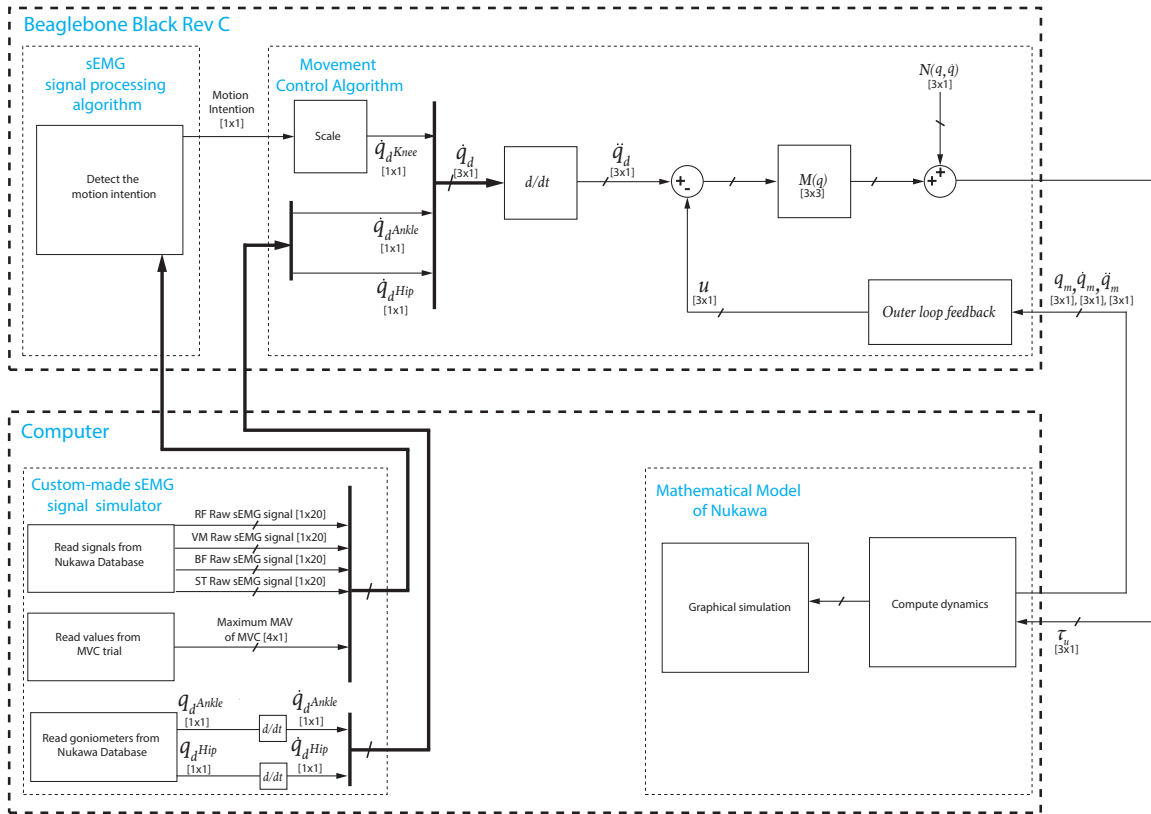


Figure 6.2: Set-point conversion for the myoelectric control

since the selection process, of the exercises belonging to international protocols for rehabilitation of ACL injuries, presented in Section 4.2.9, was performed with the assistance of a physiotherapist.

The online simulation presented in Figure 6.3a was conducted using a 3D CAD model of Nukawa. This simulation included the kinematics of the robot. The simplified model of the robot was used as well, to reduce the computational time of the real-time tests. Figure 6.3b presents the result of the HIL simulation with the simplified model. In both figures, the red and dotted line represents the actual endpoint of the robot, *i.e.*, the distal point of the third limb. In Figure 6.3b, the blue and dotted line represents the desired position trajectory for the endpoint of the robot. Both curves are almost overlapped. Therefore, the robot is able to follow the desired trajectory in cartesian space.

Figure 6.3c compares the desired position in a continuous line, and the actual position with a dotted line. Both curves are almost overlapped. Therefore, the position error is small compared to the motion of each joint, as seen in Figure 6.3d.

Figure 6.3e presents the desired speed in a continuous line and the actual speed in a dotted line. In this figure, it is possible to observe that the system can follow the desired speed, *i.e.*, the motion intention, since both have a similar behavior. Also, it can be denoted that the system follows the imposed reference visualizing the error presented in Figure 6.3f.

6.1.2 Numerical Results

The numerical results of the behavior of the MEC algorithm are shown in Table 6.1. This table shows that the hip motor saturates to compensate the counter-torque when the maximum motion

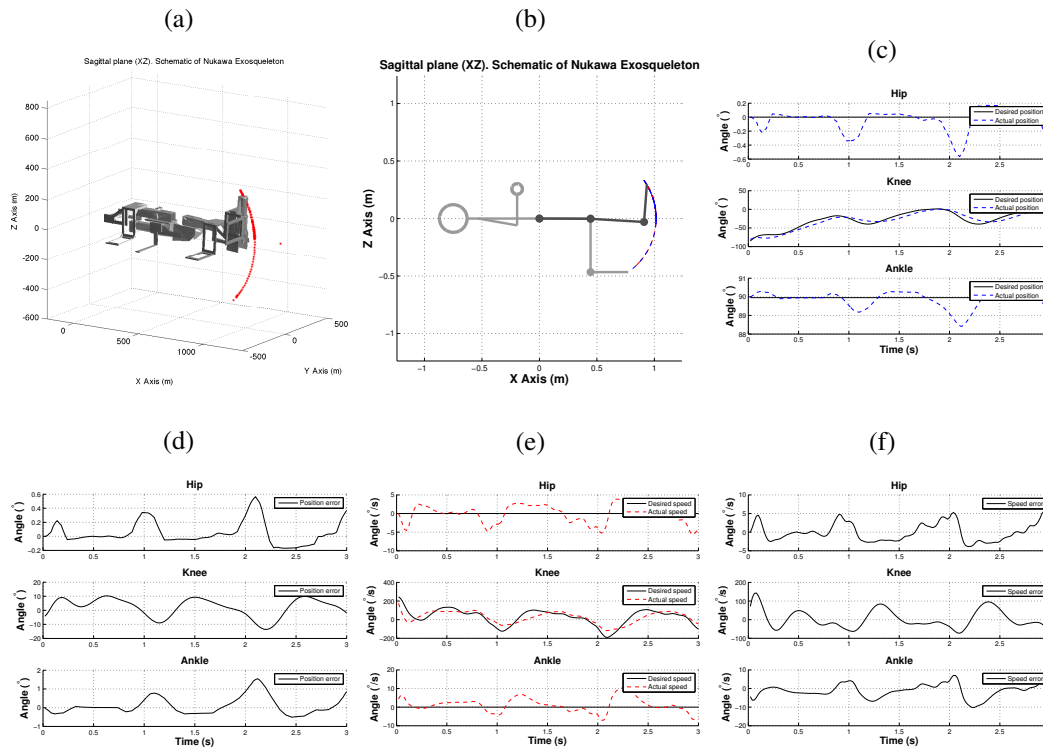


Figure 6.3: Results of the HIL simulation using a trajectory extracted during trial 9 with S7 (a) 3D simulation, (b) simplified simulation, (c) desired position vs. actual position, (d) position error, (e) desired speed vs. actual speed, and (f) speed error

intention is above $180^\circ/s$ for the knee joint. However, notwithstanding the saturated motor, the system followed the specific trajectories. Also, when the motion intention was lower than $180^\circ/s$, no motor was saturated, and the trajectories were also followed. This table presents the MAE in a percentage of joint motion, *i.e.*, the error relative to the motion performed by each joint during each test. As indicated in the table, the maximum position MAE is 0.1° , 6.3° , and 0.3° and maximum error in percentage of the joint motion 15.3% , 7.3% , and 40.2% , for the hip, knee, and ankle joints, respectively. Thus, the error is lower in the knee.

For the aforementioned, the contribution of the MEC algorithm was validated for the implementation of mechatronic-assisted rehabilitation of ACL injuries. During these therapies, the MEC algorithm would detect when the subject tries to make a knee movement, but due to the pain caused by the ACL injury, the subject is not able to execute the motion. Therefore, the MEC algorithm would assist its movement using the mechatronic system.

Chapter Summary

The results of the HIL simulations shown that the MEC algorithm is a potentially useful tool for the implementation of a mechatronic-assisted rehabilitation protocol for ACL injuries. However, this proposal can not be generalized for the entire population, but can only be considered for the

Table 6.1: Results of the behavior of the MEC during the six trials

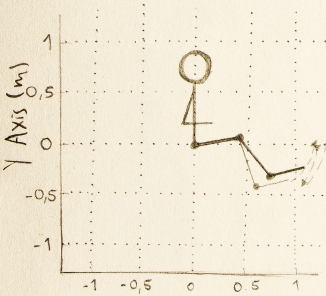
Subject	Trial	B_r (°)	MAE position (°, °, °)	MAE speed (°/s, °/s, °/s)	Maximum Torque (Nm, Nm, Nm)	Minimum Torque (Nm, Nm, Nm)	Maximum Angle (°, °, °)	Minimum Angle (°, °, °)	Maximum speed (°/s, °/s, °/s)	Minimum speed (°/s, °/s, °/s)	Joint motion (°, °, °)	Error in percentage of joint motion (%, %, %)
7	9	180	(0.110681,	(2.063316,	(505.691000,	(-228.730000,	(0.169230,	(-0.565129,	(3.855275,	(-5.706177,	(0.734359,	(15.071819,
			5.953059,	40.039538,	212.092000,	-237.333000,	0.414328,	-80.830241,	174.878598,	-117.829666,	81.244569,	7.327331,
11	10	90	(0.002591,	(0.158922,	(428.287000,	(222.409000,	(0.031580,	(-0.004412,	(1.733209,	(-0.239346,	(0.035992,	(7.199068,
			1.209047,	6.572052,	108.651000,	-36.946000,	-92.386863,	-118.322922,	13.171678,	-47.466899,	25.936059,	4.661644,
14	8	180	(0.008853,	(0.493991,	(400.706000,	(-30.582000,	(0.019747,	(-0.037883,	(1.076965,	(-2.108435,	(0.057629,	(15.361139,
			2.270075,	13.945526,	157.942000,	-120.116000,	-46.943581,	-84.191193,	112.004572,	-46.700015,	37.247612,	6.094551,
18	12	90	(0.004550,	(0.262892,	(515.771000,	(195.202000,	(0.047169,	(-0.012811,	(2.551169,	(-0.739407,	(0.059980,	(7.586011,
			2.031967,	12.376163,	142.567000,	-63.046000,	-93.771189,	-126.763046,	26.451387,	-74.859648,	32.991857,	6.158995,
20	11	90	(0.012189,	(0.402754,	(768.458600,	(120.964000,	(0.224307,	(-0.088015,	(5.565006,	(-5.062804,	(0.312322,	(3.902838,
			6.355364,	32.913905,	313.521000,	-206.097000,	-99.788344,	-205.465005,	162.896545,	-180.169962,	105.676661,	6.013971,
12	7	180	(0.048044,	(1.364740,	(487.982000,	(-169.482000,	(0.055215,	(-0.489126,	(2.971292,	(-4.771509,	(0.544340,	(8.826098,
			4.997653,	32.172227,	214.976000,	-200.942000,	-2.436364,	-81.240685,	167.477468,	-95.696145,	78.804321,	6.341852,

sample, *i.e.*, the subjects of the population who participated in the study and are part of the Nukawa Database.

Future work includes several tests with signals from the Nukawa Database and the actual robot, *i.e.*, to test the MEC with the actual robot and pre-recorded signals. Also, it is possible to extend the endorsement from the ethics committee to conduct a clinical trial to assess the behavior of the MEC algorithm but with patients, not just with healthy-subjects. Finally, a future work includes to test and assess the MEC with patients during a rehabilitation process with Nukawa.

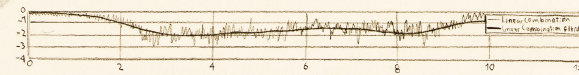
The Nukawa system would act as an active orthosis controlled using sEMG signals feedback in order to conduct assisted therapies for patients. The system should measure the electrical activity of the muscles of the lower limb, and would detect the intention of movement, and thus assist the movement.

• Sagittal plane (x2) •
Schematic of Nukawa



In addition, the joints are collinear to human joints. The knee is a polycentric joint, however this simplification was conducted as presented by Zoss, who involves

$$LC = RF_{RMS} + VM_{RMS} - BF_{RMS} - ST_{RMS}$$



7. Overall Conclusions

The 3 DOF allows the system to adjust the system for each person, the length of each segment of the mechatronic system Nukawa is variable.

a pure rotational joint in the sagittal plane. In order to adjust the system for each person, the length of each segment of the mechatronic system Nukawa is variable.

This system is designed for people between 1.44m and 1.85m tall, using a telescopic

This Chapter presents the general conclusions of the thesis, contributions, and possible future work. The hypothesis of this thesis proposed that an active orthosis controller can be implemented using electromyography (EMG) signals feedback to conduct assisted therapies for persons with anterior cruciate ligament (ACL) injuries, where the movement intention of the patient controls the motion of the rehabilitation mechatronic-assisted system Nukawa. Taking into account the results and analysis proposed in this study it is possible to conclude that the hypothesis should be accepted for the sample, *i.e.*, the population who participated in the study and are part of the Nukawa Database. However, the conclusions cannot be generalized to the entire population.

7.1 Conclusions

In conclusion, within this study, a sEMG signal processing algorithm and a movement control algorithm for mechatronic-assisted rehabilitation of ACL injuries were developed.

A literature review of sEMG signal processing algorithms was presented in Chapter 3. This study showed that there are several sEMG signal processing algorithms to detect the motion intention. Moreover, some of them are very complex, and some of them are very simple. The sEMG signal processing algorithm proposed by Hayashi et al. [65] was selected to be used in this thesis. The selection was made due to the fact that it detects the motion intention in the knee joint. Moreover, it was tested in the commercial robotic system HAL. Finally, it is a simple algorithm which requires no prior training with sEMG signals from other subjects. The only problem with this approach is that it requires a long calibration process with an additional torque sensor to estimate the conversion coefficients.

Subsequently, Chapter 4 presented the development of a sEMG signal processing algorithm, based on the algorithm stated in [65], in order to assess the detection of motion intention. Experimental tests with healthy-subjects were conducted with the purpose of obtaining a collection of sEMG signals for its use in the study. This collection contains kinematic and sEMG data, and it was called the "Nukawa Database". Several tests were conducted in order to assess the sEMG signal processing algorithm. The tests were conducted in the offline programming environment Matlab, and as a

Hardware-In-The-Loop (HIL) simulation in Python within a Beaglebone Black (BBB) Rev C. The results showed that the *LC* algorithm detected the intensity of the movement intention, approximately, in a comparable way to the MVC. Moreover, the algorithm detected the orientation of the movement intention, *i.e.*, flexion or extension. Also, it requires no prior training with sEMG signals from other subjects. Moreover, no additional torque sensor is required to estimate the conversion coefficients.

Also, a literature review of movement control algorithms for mechatronic-assisted rehabilitation was presented in Chapter 4. The Computed Torque Control (CTC) algorithm was selected since several studies reported to have small position, speed, and torque tracking errors [5], [41]. Moreover, the offline simulations presented by Kirby [41] have shown the feasibility of implementing the CTC algorithm to control the movements of Nukawa, and they were validated by a group of physiotherapists. The only problem with this approach is that it requires an accurate model of the system. However, for the purpose of this thesis, the parameter uncertainties were neglected.

In addition, Chapter 5 presented the movement control algorithm for mechatronic-assisted rehabilitation based on exercises and movements associated with therapies for ACL injuries. The implementation of the CTC algorithm was conducted as an HIL simulation in Python within a BBB Rev C. The HIL simulation used a computational model of Nukawa in order to test the mechatronic system without having to use the actual robot. Several tests were conducted in order to test and assess the movement control algorithm implemented as an HIL simulation and the model itself. The test showed that the system is capable of reproducing trajectories associated with ACL rehabilitation protocols.

Finally, Chapter 6 tested and assessed the behavior of the myoelectric control algorithm for mechatronic-assisted rehabilitation and its possibilities to support rehabilitation therapies for ACL injuries through a protocol of tests. To do so, both algorithms were joined together, *i.e.*, the sEMG signal processing algorithm and the movement control algorithm. A protocol of tests was conducted as an HIL simulation conducting the pre-recorded sEMG signals from the Nukawa Database to the myoelectric control. The results of the HIL simulations shown that the MEC algorithm is a potentially useful tool for the implementation of a mechatronic-assisted rehabilitation protocol for ACL injuries.

7.2 Contributions

The main contribution of this thesis is the combination of two algorithms in order to propose a myoelectric control (MEC) algorithm. The arrangement reveals something useful to perform mechatronic-assisted rehabilitation for ACL injuries. The algorithm detects the motion intention and controls a mechatronic rehabilitation system to assist the knee movement, *i.e.*, such as in active-assisted extension exercises but with an exoskeleton. During the development of this thesis, other secondary contributions presented below were achieved:

7.2.1 Publications and scientific production

Appendix B presents a list of scientific production and publications that were achieved by the author and its co-authors within the framework of this thesis. The products include two software registered with the “Dirección Nacional de Derechos de Autor (DNDA)” and seven in the process of being registered, four international publications, the best student paper award, a methodology, and diffusion in a webpage, a newspaper, and a radio program.

7.2.2 State of the art

The state of the art presented in Chapter 3 gives an overview of advances in sEMG signal processing algorithms and movement control algorithms.

7.2.3 Nukawa Database

An experimental protocol with 20-healthy-subjects was conducted with the purpose of obtaining a collection of sEMG signals for its use in the study. This database contains kinematic and sEMG data, and it was titled “Nukawa Database”. The experimental tests were conducted in order to acquire and record sEMG signals and its respective kinematics during exercises and movements associated with therapies for ACL injuries.

7.2.4 sEMG signal processing algorithm

This thesis offers a sEMG signal processing algorithm that detects the knee joint movement intention. The algorithm requires no additional torque sensor to estimate the conversion coefficients such as the algorithm stated in [65]. Moreover, it requires no prior training with sEMG signals from other subjects such as the ones that use machine learning algorithms. Moreover, this thesis presents a custom-made sEMG signal simulator that uses pre-recorded signals from the Nukawa Database to test the algorithms as an HIL simulation.

7.2.5 Movement control algorithm

This thesis confirmed the feasibility of implementing the CTC algorithm in order to control the movements of Nukawa in real-time with a BBB Rev C. The system is capable of reproducing trajectories associated with ACL rehabilitation protocols.

7.3 Recommendations for future work

The main proposed future work are:

7.3.1 Nukawa Database

It is proposed to conduct the experimental protocol with more healthy-subjects and with patients with ACL injuries in order to increase the data of the Nukawa Database. Also, it is possible to conduct the experimental protocol along with other exercises and movements associated with therapies for ACL injuries.

7.3.2 sEMG signal processing algorithms

Also, in the next studies, the detection of the motion intention of the hip and the ankle may be included, to perform mechatronic-assisted rehabilitation exercises which include movements of these joints.

In the future, the sEMG signal processing algorithm may be developed and implemented using several models such as white models or even black-box models.

Future work also includes the evaluation of the behavior of the algorithm using, not just pre-recorded signals extracted from a database, but from healthy-subjects with the BiosignalPlux or any acquisition device. These tests should be given to assess if the intention was detected correctly.

Future work includes to test and evaluate the sEMG signal processing algorithm with signals from patients with ACL injuries with the BiosignalPlux or any acquisition device.

It is considered as a future work the inclusion of mechatronic-resisted rehabilitation exercises, where the algorithm detects the intended movement and does not perform an assistive action, but a resistive.

Future work includes several tests such as 25 % isometric contractions with the knee flexed 90° and the hip flexed 90°. In addition, tests with multiple repetitions of isometric tests may be conducted, *e.g.*, performing an isometric contraction multiple times and in a row.

Future work may include testing the sEMG signal processing algorithm to compute the torque of the knee joint using sEMG signals. The tests may be conducted taking into account the actual torque exerted by the subject. The tests may be conducted using an isokinetic dynamometer or an estimation of the torque using the free-body diagram of the machine and the subject, and the angle of each limb recorded with the goniometers. These tests should be conducted to modify the current algorithm so it can estimate the exact torque exerted by the subject.

7.3.3 Movement control algorithms

With the purpose of obtaining a model closer to the real one, it is imperative to configure the system with known lengths and weights and to drop it from the position $q = (0^\circ, 0^\circ, 0^\circ)$, without restrictions or mechanical limits enabled. During this test, the position of each joint must be recorded, and then, an optimization algorithm must be used to tune the friction coefficients.

It is considered as a future work the inclusion of the entire friction term in the mathematical model. Therefore, the model would take into account the force that is opposed to the beginning of the movement, *i.e.*, the effects that may generate a dead zone for the controller. Even though a slightly larger torque is exerted, no movement will be generated until it can overcome the friction. Also, it is possible to include the friction that occurs between the robot and the patient with the medium, *i.e.*, the friction with the air during high-speed exercises, for example, with athletes finishing a rehabilitation process.

Some of the perturbations of the system may be known a priori. Therefore, it is proposed that in the future they may be included in the CTC algorithm, to make a feed-forward control. Therefore, the *outer loop feedback* would not be responsible for dealing with these perturbations.

The center of mass was assumed at the distal point of each limb, *i.e.*, being this the worst-case scenario. Therefore, the computed torques are greater than the real ones. Consequently, another future work is to use the 3D model of Nukawa or even to do experimental tests with the actual robot, to estimate the inertial parameters of each limb to obtain a mathematical model closer to the real one.

In the future, an HIL simulation can be performed using torque references rather than position SP. These test may be conducted to control the torque of the motors to perform another type of exercises, *e.g.*, isotonic exercises.

Further work, also includes implementing the control algorithm in the Robot Operating System (ROS) and applying the simulations in an environment other than Matlab such as Gazebo, V-REP, Peekabot, Webots, Drake, among others.

The constants of the *outer loop feedback* were set using a heuristic PID tuning method, this method and values were appropriate for the current application. However, it could be a better approach if an optimization method is used for each joint controller, *i.e.*, an autotuning method.

With the purpose of characterizing the trajectories that fit all subjects, a future work is to acquire the same trajectories during the six exercises with a group of physiotherapists, healthy, and unhealthy subjects.

In order to assess the robustness of the movement control algorithm, future work includes several

tests changing the parameters of the mathematical model implemented in Matlab. However, during these trials, the CTC algorithm should not be tuned each time but it should be left the same way for each test. It is imperative to emphasize that these tests are intended to verify the robustness of the control system which is subjected to uncertainties.

Finally, a future work includes to develop an adaptive control algorithm for Nukawa, so that the mechatronic system is stable for any given user regardless of the parameter uncertainties.

7.3.4 Mechatronic-Assisted Rehabilitation for ACL injuries

Future work includes several tests with signals from the Nukawa Database and the actual robot, *i.e.*, to test the MEC with the actual robot and pre-recorded signals. Also, it is possible to extend the endorsement from the ethics committee to conduct a clinical trial to assess the behavior of the MEC algorithm but with patients, not just with healthy-subjects.

Finally, a future work includes to test and assess the MEC with patients during a rehabilitation process with Nukawa, to perform assisted rehabilitation exercises.

The Nukawa system would act as an active orthosis controlled using sEMG signals feedback in order to conduct assisted therapies for patients. The system should measure the electrical activity of the muscles of the lower limb, and would detect the intention of movement, and thus assist the movement.

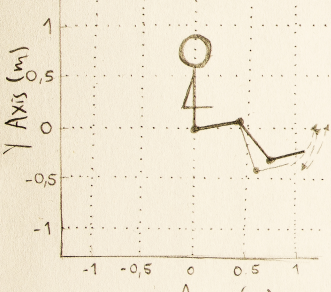


In addition, the joints are collinear to human joints. The knee is a polycentric joint, however this simplification was conducted as presented by Zoss, who involves

$$LC = RF_{RMS} + VM_{RMS} - BF_{RMS} - ST_{RMS}$$



• Sagittal plane (x2) •
Schematic of Nukawa



8. References

The 3-DOF allows the system to simulate FE movements of the hip, FE movements of the knee, and DP movements of the ankle.

a pure rotational joint in the sagittal plane. In order to adjust the system for each person, the length of each segment of the mechatronic system Nukawa is variable.

This system is designed for people between 1.44m and 1.85m tall, using a telescopic

- [1] American Academy of Orthopaedic Surgeons, *Sports Medicine Media Guide an Illustrated Resource on the Most Common Injuries and Treatments in Sports*. 2011.
- [2] E. Mora and R. De Rosa, *Fisioterapia del Aparato Locomotor*, Síntesis, Ed. 1999.
- [3] J. M. Brotzman and K. E. Wilk, *Rehabilitación Ortopédica Clínica*, Edición 2d, M. Elsevier and Editorial, Eds. Elsevier, 2010.
- [4] D. Nguyen-Tuong and J. Peters, "Learning robot dynamics for computed torque control using local gaussian processes regression", *Proceedings of the 2008 ECSIS Symposium on Learning and Adaptive Behaviors for Robotic Systems, LAB-RS 2008*, pp. 59–64, 2008. DOI: 10.1109/LAB-RS.2008.16.
- [5] I. L. Lasso, M. Masso, and O. A. Vivas, "Exoesqueleto para reeducación muscular en pacientes con imoc tipo diplejía espástica moderada", pp. 1–88, 2010. [Online]. Available: <http://www.unicauca.edu.co/deic/Documentos/Monograf%EDA%20exoesqueleto.pdf>.
- [6] F. L. Lewis, D. M. Dawson, and C. T. Abdallah, *Manipulator Control Theory and Practice*. 2004, ISBN: 0824740726.
- [7] J. a. Blaya and H. Herr, "Adaptive control of a variable-impedance ankle-foot orthosis to assist drop-foot gait", *IEEE Transactions on Neural Systems and Rehabilitation Engineering*, vol. 12, no. 1, pp. 24–31, 2004. DOI: 10.1109/TNSRE.2003.823266.
- [8] W. R. Eby, "Feasibility analysis of a powered lower-limb orthotic for the mobility impaired user", *Simulation*, 2005.
- [9] J. Pratt, B. Krupp, C. Morse, and S. Collins, "The roboknee: An exoskeleton for enhancing strength and endurance during walking", *IEEE International Conference on Robotics and Automation, 2004. Proceedings. ICRA '04. 2004*, vol. 3, no. April, pp. 2430–2435, 2004. DOI: 10.1109/ROBOT.2004.1307425.

-
- [10] W. Hassani, S. Mohammed, H. Rifaï, and Y. Amirat, “Powered orthosis for lower limb movements assistance and rehabilitation”, *Control Engineering Practice*, vol. 26, no. 1, pp. 245–253, 2014. DOI: 10.1016/j.conengprac.2014.02.002.
- [11] J. C. Z. Cortés, “Valoración isocinética de los músculos rotadores del complejo articular del hombro en jugadores de balonmano playa”, *Tesis Doctoral*, 2014. [Online]. Available: <http://dspace.uah.es/dspace/bitstream/handle/10017/22719/Tesis%20Juan%20Carlos%20Zapardiel.pdf?sequence=1>.
- [12] S. Kagawa, T. Koyama, M. Hosomi, T. Takebayashi, K. Hanada, F. Hashimoto, and K. Domen, “Effects of constraint-induced movement therapy on spasticity in patients with hemiparesis after stroke”, *Journal of Stroke and Cerebrovascular Diseases*, vol. 22, no. 4, pp. 364–370, 2013. DOI: 10.1016/j.jstrokecerebrovasdis.2011.09.021.
- [13] Y. Mon and A. Al-Jumaily, “Estimation of upper limb joint angle using surface emg signal”, *International Journal of Advanced Robotic Systems*, p. 1, 2013. DOI: 10.5772/56717.
- [14] R. Merletti and P. A. Parker, *Electromyography: Physiology, Engineering, and Non-Invasive Applications*. 2004, p. 506. DOI: 10.1002/0471678384.
- [15] R. B. R. Randall Q. Huber, *Vocabulario Comparativo: Palabras Selectas de Lenguas Indígenas de Colombia*, First. Bogotá: Instituto Lingüístico de Verano, 1992. [Online]. Available: <https://www.sil.org/resources/archives/18886>.
- [16] Eurostat, “Disability statistics - prevalence and demographics”, vol. 2011, no. September, pp. 1–5, 2014. [Online]. Available: http://ec.europa.eu/eurostat/statistics-explained/index.php/Disability_statistics_-_prevalence_and_demographics.
- [17] World Health Organization, “World report on disability”, Tech. Rep., 2011, p. 27. [Online]. Available: http://www.who.int/disabilities/world_report/2011/report.pdf.
- [18] D. Alméras and V. Milosavljevic, “Informe regional sobre la medición de la discapacidad. Una mirada a los procedimientos de medición de la discapacidad en América Latina y el Caribe”, *CEPAL Decimotercera reunión del Comité Ejecutivo de la Conferencia Estadística de las Américas de la Comisión Económica para América Latina y el Caribe*, vol. 3860, no. Discapacidad en America Latina, p. 48, 2014. [Online]. Available: <http://www.cepal.org/deype/noticias/documentosdetrabajo/0/53340/LCL3860e.pdf>.
- [19] Organización Panamericana de la Salud, *Aplicación de la Clasificación Internacional del Funcionamiento, de la Discapacidad y de la Salud en estudios de prevalencia de discapacidad en las Américas*. 2012. [Online]. Available: <http://publicaciones.ops.org.ar/publicaciones/otras%20pub/informeCIF.pdf>.
- [20] Departamento Administrativo Nacional de Estadística, *Defunción por grupo de edad, sexo, según departamento, municipio y área de residencia*, 2014. [Online]. Available: http://www.dane.gov.co/files/investigaciones/poblacion/defunciones/defun_2014/Cuadro4_oct31.xls.
- [21] Instituto Nacional de Medicina Legal y Ciencias Forenses, “Muertes y lesiones por accidentes de transporte, colombia, 2012”, *Forensis*, p. 281, 2011. [Online]. Available: <http://www.medicinalegal.gov.co/documents/10180/34861/7+transporte+forensis+2012.pdf/2fbb18b6-2ae7-4f58-8c25-220cb4d3be37>.

- [22] I. N. de Medicina Legal y Ciencias Forenses, “Datos para la vida”, *Forensis*, 2017. [Online]. Available: <http://www.medicinalegal.gov.co/documents/88730/4023454/Forensis+2016+-+Datos+para+la+Vida.pdf/af636ef3-0e84-46d4-bc1b-a5ec71ac9fc1>.
- [23] S. M. N. Arosha Senanayake, O. A. Malik, P. M. Iskandar, and D. Zaheer, “A knowledge-based intelligent framework for anterior cruciate ligament rehabilitation monitoring”, *Applied Soft Computing Journal*, vol. 20, pp. 127–141, 2014. DOI: 10.1016/j.asoc.2013.11.010.
- [24] A. Y. Li and G. Y. Ng, “Overview of anterior cruciate ligament rehabilitation and its evolution in hong kong in the past 8 years”, *Hong Kong Physiotherapy Journal*, vol. 22, no. 1, pp. 14–21, 2004. DOI: 10.1016/S1013-7025(09)70045-4.
- [25] F. Cimino, B. S. Volk, and D. Setter, “Anterior cruciate ligament injury: Diagnosis, management, and prevention”, *American Family Physician*, vol. 82, no. 8, pp. 917–922, 2010. [Online]. Available: <http://www.aafp.org/afp/2010/1015/p917.pdf>.
- [26] R. Visbal, O. Yamhure, J. González, A. Colina, C. Serverini, and M. López, “Reconstrucción de ligamento cruzado anterior con autoinjerto semitendinoso-recto interno fijado con tornillos de interferencia bioabsorbibles: Evaluación clínica y funcional”, *Revista Colombiana de Ortopedia y Traumatología*, vol. 25, no. 4, pp. 345–355, 2011. [Online]. Available: <http://www.sccot.org.co/pdf/RevistaDigital/25-04-2011/05ReconstruccionLigamento.pdf>.
- [27] T. J. Ganley, “Preface: ACL injuries in the young athlete: A focus on prevention and treatment”, *Clinics in Sports Medicine*, vol. 30, no. 4, pp. xv–xviii, 2011. DOI: 10.1016/j.csm.2011.08.006.
- [28] A. M. Dollar and H. Herr, “Lower extremity exoskeletons and active orthoses: Challenges and state-of-the-art”, *IEEE Transactions on Robotics*, vol. 24, no. 1, pp. 144–158, 2008. DOI: 10.1109/TR0.2008.915453.
- [29] E. Guizzo and H. Goldstein, “The rise of the body bots [robotic exoskeletons]”, *IEEE Spectrum*, vol. 42, no. 10, pp. 50–56, Oct. 2005. DOI: 10.1109/MSPEC.2005.1515961.
- [30] E. Akdogan and M. A. Adli, “The design and control of a therapeutic exercise robot for lower limb rehabilitation: Physiotherabot”, *Mechatronics*, vol. 21, no. 3, pp. 509–522, 2011. DOI: 10.1016/j.mechatronics.2011.01.005.
- [31] D. Villanueva, “Técnicas de asistencia para la recuperación de la locomoción funcional después de una lesión de médula espinal”, vol. XXII, pp. 89–100, 2001. [Online]. Available: <http://www.medigraphic.com/pdfs/inge/ib-2001/ib012h.pdf>.
- [32] C. Hu, Q. Huang, L. Yu, and M. Ye, “The immediate intervention effects of robotic training in patients after anterior cruciate ligament reconstruction.”, *Journal of physical therapy science*, vol. 28, no. 7, pp. 2031–2033, 2016, ISSN: 0915-5287 (Print). DOI: 10.1589/jpts.28.2031.
- [33] M. Geary, “ACL non-operative protocol”, *South Shore Hospital Orthopedic, Spine and Sports Therapy*, pp. 1–10,
- [34] Chester Knee Clinic and Cartilage Repair Centre, “The Guide to Rehabilitation of Anterior Cruciate Ligament (ACL) Reconstruction”,

-
- [35] Chester Knee Clinic and Cartilage Repair Center, *Accelerated ACL Reconstruction Rehabilitation Program*, 2014.
- [36] P. Lonnie, F. Noyes, E. Grood, and D. Buttlar, “Rehabilitation after anterior cruciate *”, pp. 140–149,
- [37] P. J. Millett, “ACL Reconstruction Rehabilitation Protocol”,
- [38] I. K. Evans, “ACL Reconstruction Rehabilitation Protocol”, no. 978, [Online]. Available: <https://www.sportsmednorth.com/sites/sportsmednorth.com/files/ACL-Reconstruction-Protocol.pdf>.
- [39] M. F. Lucas, A. Gaufriau, S. Pascual, C. Doncarli, and D. Farina, “Multi-channel surface emg classification using support vector machines and signal-based wavelet optimization”, *Biomedical Signal Processing and Control*, vol. 3, no. 2, pp. 169–174, 2008. DOI: 10.1016/j.bspc.2007.09.002.
- [40] J. G. Patiño, E. E. Bravo, J. J. Perez, and V. Perez, “Lower limb rehabilitation system controlled by robotics, electromyography surface and functional electrical stimulation”, *Pan American Health Care Exchanges, PAHCE*, no. 2002, p. 6257, 2013. DOI: 10.1109/PAHCE.2013.6568341.
- [41] F. A. Kirby, “Simulación de los algoritmos de control de un sistema de rehabilitación de miembro inferiro (legsys)”, Master’s thesis, Universidad Pontificia Bolivariana, 2016.
- [42] J. C. Yepes, A. J. Saldarriaga, J. M. Vélez, V. Z. Pérez, and M. J. BETANCUR, “A Hardware-in-the-loop Simulation Study of a Mechatronic System for Anterior Cruciate Ligament Injuries Rehabilitation”, in *BIODEVICES 2017 - 10th International Conference on Biomedical Electronics and Devices*, vol. 1, 2017.
- [43] A. B. Zoss, H. Kazerooni, and A. Chu, “Biomechanical Design of the Berkeley Lower Extremity Exoskeleton (BLEEX)”, *IEEE/ASME Transactions on Mechatronics*, vol. 11, no. 2, pp. 128–138, 2006, ISSN: 1083-4435. DOI: 10.1109/TMECH.2006.871087.
- [44] C. F. van Eck, M. P. J. van den Bekerom, F. H. Fu, R. W. Poolman, and G. M. M. J. Kerkhoffs, “Methods to diagnose acute anterior cruciate ligament rupture: A meta-analysis of physical examinations with and without anaesthesia”, *Knee Surgery, Sports Traumatology, Arthroscopy*, vol. 21, no. 8, pp. 1895–1903, 2013. DOI: 10.1007/s00167-012-2250-9.
- [45] H. Makhmalbaf, A. Moradi, and F. Omid-Kashani, “Accuracy of lachman and anterior drawer tests”, vol. 94, no. 2, pp. 94–97, 2013. [Online]. Available: <https://www.ncbi.nlm.nih.gov/pmc/articles/PMC4151408/pdf/ABJS-1-94.pdf>.
- [46] C. R. Wheelless, *Pivot shift test*, 2015. [Online]. Available: http://www.wheellessonline.com/ortho/pivot_shift_test.
- [47] J. M. Reynolds, T. J. Gordon, and R. A. Robergs, “Prediction of one repetition maximum strength from multiple repetition maximum testing and anthropometry”, *Journal of Strength and Conditioning Research*, vol. 20, no. 3, pp. 584–592, 2006.
- [48] L. J., “Maximum based on reps.”, *National Strength and Conditioning Association (NSCA) Journal*, vol. 6, pp. 60–61, 1985.
- [49] M. Brzycki, “Strength testing—predicting a one-rep max from reps-to-fatigue”, *Journal of Physical Education, Recreation & Dance*, vol. 64, no. 1, pp. 88–90, 1993. DOI: 10.1080/07303084.1993.10606684.

- [50] R. O'Connor, B. O'Connor, J. Simmons, and P. O'Shea, *Weight Training Today*. West, 1989, ISBN: 9780314689511. [Online]. Available: <https://books.google.com.co/books?id=eHqfwq6o18oC>.
- [51] B. Epley, *Boyd Epley Workout*. 1985, p. 86.
- [52] P. Theresa Chiaia, *ACL injury prevention tips and exercises: Stay off the sidelines!*, 2009. [Online]. Available: https://www.hss.edu/conditions_acl-injury-prevention-stay-off-sidelines.asp.
- [53] N. O. Centre, "A patient's guide to anterior cruciate ligament (ACL) reconstruction", 2015. [Online]. Available: <http://www.ouh.nhs.uk/hipandknee/information/documents/acl-reconstruction.pdf>.
- [54] American Academy of Orthopaedic Surgeons, *Management of Anterior Cruciate Ligament Injuries*. 2014. [Online]. Available: <http://www.aaos.org/research/guidelines/ACLGuidelineFINAL.pdf>.
- [55] L. Frey, C. Krishnan, and K. Avin, "Modeling nonlinear errors in surface electromyography due to baseline noise: A new methodology", *Journal of Biomechanics*, vol. 44, no. 1, pp. 202–205, 2011. DOI: 10.1016/j.jbiomech.2010.09.008.
- [56] M. E. M. De Biase, F. Politti, E. T. Palomari, T. E. P. Barros-Filho, and O. P. De Camargo, "Increased EMG response following electromyographic biofeedback treatment of rectus femoris muscle after spinal cord injury", *Physiotherapy*, vol. 97, no. 2, pp. 175–179, 2011. DOI: 10.1016/j.physio.2010.05.005.
- [57] G. Wei, F. Tian, G. Tang, and C. Wang, "A wavelet-based method to predict muscle forces from surface electromyography signals in weightlifting", *Journal of Bionic Engineering*, vol. 9, no. 1, pp. 48–58, 2012. DOI: 10.1016/S1672-6529(11)60096-6.
- [58] A. R. Merletti and P. Torino, "Standards for reporting EMG data", *Journal of Electromyography and Kinesiology*, vol. 7, no. 2, pp. I–II, 1999. DOI: 10.1016/S1050-6411(97)90001-8.
- [59] SENIAM, *Welcome at seniam.org*, 2015. [Online]. Available: <http://www.seniam.org/>.
- [60] National Institute of Neurological Disorders and Stroke, *Emglab projects*, 2008. [Online]. Available: <http://www.emglab.net/emglab/Projects/projects.php#standarts>.
- [61] National Institute of Biomedical Imaging and Bioengineering, *Neuroelectric and myoelectric databases*, 2014. [Online]. Available: <http://physionet.org/physiobank/database/#neuro>.
- [62] M. Asghari Oskoei and H. Hu, "Myoelectric control systems-a survey", *Biomedical Signal Processing and Control*, vol. 2, no. 4, pp. 275–294, 2007. DOI: 10.1016/j.bspc.2007.07.009.
- [63] A. L. Delis, J. L. a. J. Carvalho, and A. F. Rocha, "Myoelectric knee angle estimation algorithms for control of active transfemoral leg prostheses", *Self Organizing Maps - Applications and Novel Algorithm Design*, no. 1977, pp. 401–424, 2006. [Online]. Available: http://cdn.intechopen.com/pdfs/13310/InTech-Myoelectric_knee_angle_estimation_algorithms_for_control_of_active_transfemoral_leg_prostheses.pdf.

-
- [64] K. Kiguchi, T. Tanaka, and T. Fukuda, "Neuro-fuzzy control of a robotic exoskeleton with emg signals", *IEEE Transactions on Fuzzy Systems*, vol. 12, no. 4, pp. 481–490, 2004. DOI: 10.1109/TFUZZ.2004.832525.
- [65] T. Hayashi, H. Kawamoto, and Y. Sankai, "Control method of robot suit hal working as operator's muscle using biological and dynamical information", *2005 IEEE/RSJ International Conference on Intelligent Robots and Systems, IROS*, vol. 2, no. 1, pp. 3455–3460, 2005. DOI: 10.1109/IROS.2005.1545505.
- [66] P. Konrad, *The ABC of EMG*, March. 2006, pp. 1–61. [Online]. Available: <http://noraxonusa.wpengine.com/wp-content/uploads/2014/12/ABC-EMG-ISBN.pdf>.
- [67] S. Wasala and T. Dulantha, "A study of controlling upper-limb exoskeletons using EMG and EEG signals", 2014. [Online]. Available: http://portal.dl.saga-u.ac.jp/bitstream/123456789/121916/1/zenbun_fulltext_lalitharatne.pdf.
- [68] K. Englehart and B. Hudgins, "A robust, real-time control scheme for multifunction myoelectric control", *IEEE Transactions on Bio-Medical Engineering*, vol. 50, no. 7, pp. 848–854, 2003. DOI: 10.1109/TBME.2003.813539.
- [69] A. Subasi, "Classification of EMG signals using combined features and soft computing techniques", *Applied Soft Computing*, vol. 12, no. 8, pp. 2188–2198, 2012. DOI: 10.1016/j.asoc.2012.03.035.
- [70] A. Phinyomark, C. Limsakul, and P. Phukpattaranont, "A novel feature extraction for robust EMG pattern recognition", *Journal of Computing*, vol. 1, no. 1, pp. 71–80, 2009. [Online]. Available: <https://arxiv.org/abs/0912.3973>.
- [71] A. Alkan and M. Günay, "Identification of EMG signals using discriminant analysis and SVM classifier", *Expert Systems with Applications*, vol. 39, no. 1, pp. 44–47, 2012. DOI: 10.1016/j.eswa.2011.06.043.
- [72] N. P. Reddy and V. Gupta, "Toward direct biocontrol using surface EMG signals : Control of finger and wrist joint models", vol. 29, pp. 398–403, 2006. DOI: 10.1016/j.medengphy.2005.10.016.
- [73] H. Andrade, J. Saenz, M. Giraldo, D. Cuartas, and O. Torres, "Sistema de biofeedback basado en pda para rehabilitación ambulatoria de pacientes con disfunción motora en extremidad superior", *III Congreso Nacional de Ingeniería Biomédica*, no. x, pp. 1–6, 2008.
- [74] A. F. Ruiz-olaya and A. López-delis, "Surface EMG signal analysis based on the empirical mode decomposition for human-robot interaction", 2011. DOI: 10.1109/STSIWA.2013.6644943.
- [75] R. a. R. C. Gopura and K. Kiguchi, "Application of surface electromyographic signals to control exoskeleton robots", *Applications of EMG in Clinical and Sports Medicine*, pp. 69–94, 2011. [Online]. Available: http://cdn.intechopen.com/pdfs/25819/InTech-Application_of_surface_electromyographic_signals_to_control_exoskeleton_robots.pdf.
- [76] A. López Delis and A. E. Ruiz, "Métodos computacionales para el reconocimiento de patrones mioeléctricos en el control de exoesqueletos robóticos : Una revisión", 2012. [Online]. Available: <http://csifesvr.uan.edu.co/index.php/ingewan/article/view/262>.

- [77] L. Mayeta Revilla, A. Lopez Delis, and A. F. Ruiz Olaya, "Evaluation of the hilbert-huang transform for myoelectric pattern classification: Towards a method to detect movement intention", *Pan American Health Care Exchanges, PAHCE*, pp. 1–6, 2013. DOI: 10.1109/PAHCE.2013.6568259.
- [78] N. López, C. Soria, E. Orosco, F. Sciascio, and M. Valentinuzzi, "Control mioeléctrico para movimientos en 2D de un manipulador robótico industrial", *Control*, vol. 1, no. Control mioeléctrico, pp. 1–4, [Online]. Available: http://ebanov.inaut.unsj.edu.ar/publicaciones/1840_07.pdf.
- [79] M. A. Romero Sacoto, "Diseño y construcción de una órtesis de rodilla, destinada a la rehabilitación automatizada de la extremidad inferior", PhD thesis, 2012. [Online]. Available: <http://dspace.ups.edu.ec/bitstream/123456789/2814/1/UPS-CT002463.pdf>.
- [80] S. Thongpanja, A. Phinyomark, P. Phukpattaranont, and C. Limsakul, "Mean and median frequency of emg signal to determine muscle force based on time-dependent power spectrum", *Electronics and Electrical Engineering*, vol. 19, no. 3, pp. 51–56, Mar. 2013. DOI: 10.5755/j01.eee.19.3.3697.
- [81] A. Rainoldi, G. Melchiorri, and I. Caruso, "A method for positioning electrodes during surface emg recordings in lower limb muscles", *Journal of Neuroscience Methods*, vol. 134, no. 1, pp. 37–43, 2004. DOI: 10.1016/j.jneumeth.2003.10.014.
- [82] A. F. Ruiz, E. Rocon, and A. Forner-Cordero, "Exoskeleton-based robotic platform applied in biomechanical modelling of the human upper limb", *Applied Bionics and Biomechanics*, vol. 6, no. 2, pp. 205–216, 2009. DOI: 10.1080/11762320802697380.
- [83] H. S. Lo and S. Q. Xie, "Exoskeleton robots for upper-limb rehabilitation: State of the art and future prospects", *Medical Engineering and Physics*, vol. 34, no. 3, pp. 261–268, 2012. DOI: 10.1016/j.medengphy.2011.10.004.
- [84] P. Masarati, "Computed torque control of redundant manipulators using general-purpose software in real-time", *Multibody System Dynamics*, pp. 1–26, 2013. DOI: 10.1007/s11044-013-9377-4.
- [85] A. Kyrylova, T. Desplenter, A. Escoto, S. Chinchalkar, and A. L. Trejos, "Simplified EMG-driven model for active-assisted therapy", in *IROS 2014 Workshop on Rehabilitation and Assistive Robotics: Bridging the Gap Between Clinicians and Roboticians*, 2014, p. 6. [Online]. Available: <http://users.eecs.northwestern.edu/~argall/14rar/submissions/kyrylova.pdf>.
- [86] Q. Ding, A. Xiong, X. Zhao, and J. Han, "A novel emg-driven state space model for the estimation of continuous joint movements", in *2011 IEEE International Conference on Systems, Man, and Cybernetics*, IEEE, Oct. 2011, pp. 2891–2897. DOI: 10.1109/ICSMC.2011.6084104.
- [87] D. Pan, F. Gao, Y. Miao, and R. Cao, "Co-simulation research of a novel exoskeleton-human robot system on humanoid gaits with fuzzy-pid/pid algorithms", *Advances in Engineering Software*, vol. 79, pp. 36–46, 2015. DOI: 10.1016/j.advengsoft.2014.09.005.
- [88] A. F. Ruiz Olaya, "Sistema robótico multimodal para análisis y estudios en biomecánica, movimiento humano y control neuromotor", pp. 1–256, 2008. [Online]. Available: <http://e-archivo.uc3m.es/handle/10016/5636>.

-
- [89] T. Lenzi, S. M. M. De Rossi, N. Vitiello, and M. C. Carrozza, "Intention-based emg control for powered exoskeletons", *IEEE Transactions on Biomedical Engineering*, vol. 59, no. 8, pp. 2180–2190, 2012. DOI: 10.1109/TBME.2012.2198821.
- [90] Q. Zhang, R. Hosoda, and G. Venture, "Human joint motion estimation for electromyography (EMG)-based dynamic motion control.", *Conference proceedings : ... Annual International Conference of the IEEE Engineering in Medicine and Biology Society. IEEE Engineering in Medicine and Biology Society. Annual Conference*, vol. 2013, pp. 21–4, Jan. 2013. DOI: 10.1109/EMBC.2013.6609427.
- [91] H. Kazerooni, J.-l. Racine, L. Huang, and R. Steger, "On the Control of the Berkeley Lower Extremity Exoskeleton (BLEEX)", no. April, pp. 4353–4360, 2005.
- [92] A. Belkadi, H. Oulhadj, Y. Touati, S. A. Khan, and B. Daachi, "On the Robust PID Adaptive Controller for Exoskeletons: A Particle Swarm Optimization Based Approach", *Applied Soft Computing Journal*, 2017, ISSN: 1568-4946. DOI: 10.1016/j.asoc.2017.06.012. [Online]. Available: <http://dx.doi.org/10.1016/j.asoc.2017.06.012>.
- [93] Z. Chen, Z. Li, S. Member, and C. L. P. Chen, "Disturbance Observer-Based Fuzzy Control of Uncertain MIMO Mechanical Systems With Input Nonlinearities and its Application to Robotic Exoskeleton", pp. 1–11, 2016.
- [94] B. Brahmi, M. Saad, S. M. Ieee, C. Ochoa-luna, and H. Mohammad, "Adaptive Control of an Exoskeleton Robot with Uncertainties on Kinematics and Dynamics", pp. 1369–1374, 2017.
- [95] A. Riani, T. Madani, A. E. Hadri, and A. Benallegue, "Adaptive Control Based on an On-line Parameter Estimation of an Upper Limb Exoskeleton", 2017.
- [96] H.-b. Kang and J.-h. Wang, "Adaptive control of 5 DOF upper-limb exoskeleton robot with improved safety", *ISA Transactions*, vol. 52, no. 6, pp. 844–852, 2013, ISSN: 0019-0578. DOI: 10.1016/j.isatra.2013.05.003. [Online]. Available: <http://dx.doi.org/10.1016/j.isatra.2013.05.003>.
- [97] V. Florimond, "Basics of surface electromyography applied to physical rehabilitation and biomechanics", vol. 1, no. March, pp. 1–50, 2010.
- [98] A. E. Clements, "Neuromuscular Consequences Following Anterior Cruciate Ligament Reconstruction", 2013. [Online]. Available: <http://utdr.utoledo.edu/cgi/viewcontent.cgi?article=1069&context=theses-dissertations>.
- [99] Biometrics Ltd, "Goniometer and torsionmeter operating manual", Tech. Rep., 1998, pp. 1–24.
- [100] S. Bustamante, J. C. Yepes, Z. P. Vera, J. C. Correa, and U. P. Bolivariana, "A simulation-based methodology to test and assess designs of mechatronic neural interface systems", vol. 4, no. Biostec, pp. 78–87, 2016.
- [101] S. Bustamante, J. C. Yepes, V. Z. Pérez, J. C. Correa, and M. J. Betancur, "Online simulation of mechatronic neural interface systems: Two case-studies", in *Biomedical Engineering Systems and Technologies: 9th International Joint Conference, BIOSTEC 2016, Rome, Italy, February 21–23, 2016, Revised Selected Papers*, A. Fred and H. Gamboa, Eds. Cham: Springer International Publishing, 2017, pp. 255–275, ISBN: 978-3-319-54717-6. DOI: 10.1007/978-3-319-54717-6_15. [Online]. Available: https://doi.org/10.1007/978-3-319-54717-6_15.

-
- [102] K. Fu, R. Gonzalez, and C. Lee, *Robotics: control, sensing, vision and intelligence*. McGraw-Hill, 1987, p. 1, ISBN: 0-07-022625-3.
- [103] J. Craig, *Introduction to Robotics: Pearson New International Edition: Mechanics and Control*. Pearson Education Limited, 2013, ISBN: 9781292052526. [Online]. Available: <https://books.google.com.co/books?id=ZTqpBwAAQBAJ>.
- [104] M. King, *Process Control: A Practical Approach*. Wiley, 2016, ISBN: 9781119157755. [Online]. Available: <https://books.google.com.co/books?id=4ZIfDAAAQBAJ>.
- [105] S. Plagenhoef, F. G. Evans, and T. Abdelnour, “Anatomical Data for Analyzing Human Motion”, *Research Quarterly for Exercise and Sport*, vol. 54, no. 2, pp. 169–178, 1983, ISSN: 0270-1367. DOI: 10.1080/02701367.1983.10605290.
- [106] P. De Leva, “Adjustments to zatsiorsky-seluyanov’s segment inertia parameters”, *Journal of Biomechanics*, vol. 29, no. 9, pp. 1223–1230, 1996, ISSN: 00219290. DOI: 10.1016/0021-9290(95)00178-6. eprint: 0021-92909600178-6.
- [107] W. D. B. P. Nancy Berryman, *Joint Range of Motion and Muscle Length Testing*, 1st., 2002, ISBN: 9780721689425,0721689426.

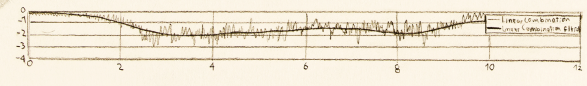
Appendices

The Nukawa system would act as an active orthosis controlled using sEMG signals feedback in order to conduct assisted therapies for patients. The system should measure the electrical activity of the muscles of the lower limb, and would detect the intention of movement, and thus assist the movement.

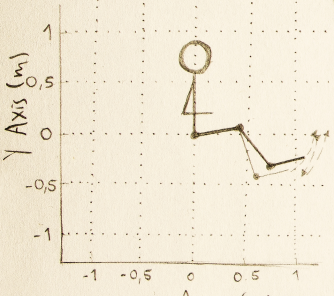


In addition, the joints are collinear to human joints. The knee is a polycentric joint, however this simplification was conducted as presented by Zoss, who involves

$$LC = RF_{RMS} + VM_{RMS} - BF_{RMS} - ST_{RMS}$$



• Sagittal plane (x2) •
Schematic of Nukawa



A. Ethics Committee Approval

The 3 DOF allows the system to adjust the system for each person, the length of each segment of the mechatronic system Nukawa is variable. The 3 DOF allows the system to adjust the system for each person, the length of each segment of the mechatronic system Nukawa is variable. The 3 DOF allows the system to adjust the system for each person, the length of each segment of the mechatronic system Nukawa is variable.

a pure rotational joint in the sagittal plane. In order to adjust the system for each person, the length of each segment of the mechatronic system Nukawa is variable.

This system is designed for people between 1.44m and 1.85m tall, using a telescopic

Medellín, Julio 9 de 2015

Doctora
VERA Z. PÉREZ
Investigador principal

Proyecto: MYOLEGSYS: PRUEBAS DE FACTIBILIDAD DE UN SISTEMA ROBÓTICO DE REHABILITACIÓN DE MIEMBRO INFERIOR PARA VÍCTIMAS DE ACCIDENTES DE TRÁNSITO

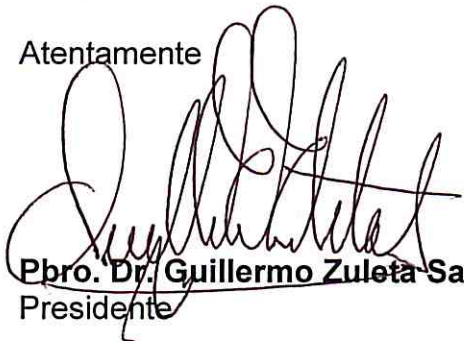
La presente comunicación tiene por objetivo informarle que el Comité de Ética de Investigación en Salud de la Universidad Pontificia Bolivariana ha evaluado el proyecto presentado por usted y ha decidido darle la **aprobación ética** respectiva.

Los miembros del Comité se ponen a su disposición para resolver cualquier inquietud de tipo ético que surja durante la ejecución de la investigación. De igual manera, le recuerda que toda modificación que se le haga al proyecto debe ser sometida a nueva consideración del Comité.

Para finalizar, es importante que tenga en cuenta que el Comité, en el cumplimiento de sus funciones, podrá realizar visitas de seguimiento que permitan verificar que todo se esté llevando a cabo adecuadamente desde el punto de vista ético.

Se anexa a la presente comunicación el formato de consentimiento informado aprobado.

Atentamente

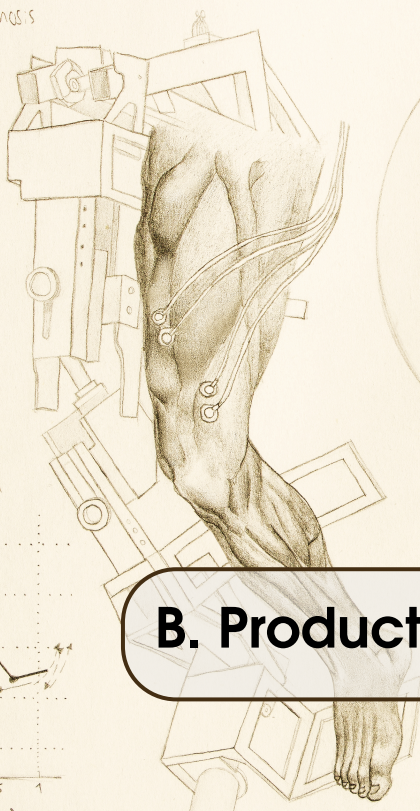


Pbro. Dr. Guillermo Zuleta Salas
Presidente



Mg Gloria Ángel Jiménez
Secretaria

The Nukawa system would act as an active orthosis controlled using sEMG signals feedback in order to conduct assisted therapies for patients. The system should measure the electrical activity of the muscles of the lower limb, and would detect the intention of movement, and thus assist the movement.

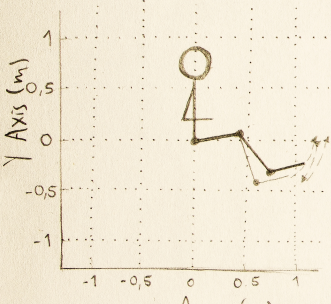


In addition, the joints are collinear to human joints. The knee is a polycentric joint, however this simplification was conducted as presented by Zoss, who involves

$$LC = RF_{RMS} + VM_{RMS} - BF_{RMS} - ST_{RMS}$$



• Sagittal plane (x2) •
Schematic of Nukawa



B. Product List

The 3-DOF allows the system to perform FE movements of the hip, FE movements of the knee, and DP movements of the ankle.

a pure rotational joint in the sagittal plane. In order to adjust the system for each person, the length of each segment of the mechatronic system Nukawa is variable.

This system is designed for people between 1.44m and 1.85m tall, using a telescopic

Below is a list of publications and scientific production that were achieved by the author and its co-authors within the framework of this thesis. The products includes two registered software and seven in the process of being registered with the "Dirección Nacional de Derechos de Autor", four international conference proceedings, a best student paper award, a methodology, and diffusion in a webpage, newspaper, and a radio program.

Software

- **EMG-NUKAWA Software**, Authors: Juan C. Yepes, Samuel Bustamante, Vera Z. Pérez, and Julio C. Correa, registered with the *Dirección Nacional de Derechos de Autor (DNDA)*, Date: 18 september 2017, Register Number: 13-63-186.
- **EMG-KUKA Software**, Authors: Juan C. Yepes, Samuel Bustamante, Vera Z. Pérez, Manuel J. Betancur, and Julio C. Correa, registered with the DNDA, Date: 18 september 2017, Register Number: 13-63-185.
- **VisorEMG_real-time**, Authors: Juan C. Yepes, Álvaro J. Saldarriaga, Vera Z. Pérez, and Manuel J. Betancur, Current State: Software in the process of being registered with the DNDA.
- **Nukawa Database Viewer**, Authors: Juan C. Yepes, Mario A. Portela, Álvaro J. Saldarriaga, Vera Z. Pérez, and Manuel J. Betancur, Current State: Software in the process of being registered with the DNDA.
- **EMG Features**, Authors: Juan C. Yepes, Álvaro J. Saldarriaga, Vera Z. Pérez, and Manuel J. Betancur, Current State: Software in the process of being registered with the DNDA.
- **EMG-Motion-BBB**, Authors: Juan C. Yepes, Mario A. Portela, Álvaro J. Saldarriaga, Vera Z. Pérez, and Manuel J. Betancur, Current State: Software in the process of being registered with the DNDA.
- **EMG-Motion**, Authors: Juan C. Yepes, Mario A. Portela, Álvaro J. Saldarriaga, Vera Z. Pérez, and Manuel J. Betancur, Current State: Software in the process of being registered with the DNDA.

- **CTC-BBB**, Authors: Juan C. Yepes, Álvaro J. Saldarriaga, Vera Z. Pérez, and Manuel J. Betancur, Current State: Software in the process of being registered with the DNDA.
- **EMG-Simulator**, Authors: Juan C. Yepes, Álvaro J. Saldarriaga, Vera Z. Pérez, and Manuel J. Betancur, Current State: Software in the process of being registered with the DNDA.

Publications

- **Springer**, Biomedical Engineering Systems and Technologies, BIOSTEC 2016. Communications in Computer and Information Science, volume: 690. Editor: Springer International Publishing, Authors: Samuel Bustamante, Juan C. Yepes, Vera Z. Pérez, Julio C. Correa and Manuel J. BETANCUR, doi:10.1007/978-3-319-54717-6_15, Date: 4 March, 2017, Editors: Ana Fred, Hugo Gamboa, ISBN: 978-3-319-54716-9 (Print) 978-3-319-54717-6 (Online), Title: Online Simulation of Mechatronic Neural Interface Systems, Two Case-Studies.
- **PAHCE 2017**, Global Medical Engineering Physics Exchanges (GMEPE) & Pan American Health Care Exchanges (PAHCE) 2017, Tuxtla Gutiérrez - San Cristóbal de las Casas, Chiapas, Mexico, Date: 20-25 March, 2017, Authors: Juan C. Yepes, Mario A. Portela, AJ Saldarriaga, Vera Z. Pérez, and Manuel J. BETANCUR, Title: Surface Electromyography Signal Processing Algorithm for the Detection of the Knee Joint Movement Intention.
- **BIOSTEC 2017 Conference Proceedings**, 10th International Conference on Biomedical Electronics and Devices (Part of BIOSTEC 2017), Porto, Portugal, Date: 21-23 February, 2017, Chapter in memory with ISBN: 978-989-758-216-5, Authors: Juan C. Yepes, AJ Saldarriaga, Jorge M. Vélez, Vera Z. Pérez, and Manuel J. BETANCUR, doi:10.5220/0006252800690080, Title: A Hardware-in-the-loop Simulation Study of a Mechatronic System for Anterior Cruciate Ligament Injuries Rehabilitation.
- **BIOSTEC 2016 Conference Proceedings**, BIOSIGNALS 2016, 9th International Joint Conference on Biomedical Engineering Systems and Technologies, Rome, Italy, Date: 21-23, February 2016, ISBN 978-989-758-170-0, Authors: Samuel Bustamante, Juan C. Yepes, Vera Z. Pérez and Julio C. Correa, doi:10.5220/0005698200780087, Title: A Simulation-based Methodology to Test and Assess Designs of Mechatronic Neural Interface Systems.

Awards

- **Best Student Paper Award**, Best Student Paper Award by the paper entitled *A Simulation-based Methodology to Test and Assess Designs of Mechatronic Neural Interface Systems*, Received in: 9th International Joint Conference on Biomedical Engineering Systems and Technologies, Rome, Italy, Date: February 21 - 23, 2016. Authors: Samuel Bustamante, Juan C. Yepes, Vera Z. Pérez and Julio Correa.

Methodologies

- **EMG-KUKA Methodology**, Title: *Metodología Basada en Simulación para probar y Evaluar Diseños de Interfaces Neuronales Mecatrónicas*, Date: February 2016, Authors: Juan C. Yepes, Samuel Bustamante, Vera Z. Pérez and Julio C. Correa. Universidad Pontificia Bolivariana.

Diffusion

- **Universitas Científica Paper**, Title: *Legsys: Un Primer Paso Hacia el Sueño de Volver a Caminar*. Vol. 18, Universitas Científica, Num. 2 (2015), ISSN 1692-01550120-131X, pages 38 - 41, Date: March 2016.
- **Web Portal of the UPB**, Disclosure in the news of the Web Portal of the Universidad Pontificia Bolivariana of the award “Best Student Paper Award” obtained in: 9th International Joint Conference on Biomedical Engineering Systems and Technologies, Rome, Italy. Date: 10 march, 2016. Authors: Juan C. Yepes, Samuel Bustamante, Vera Z. Pérez and Julio C. Correa. Universidad Pontificia Bolivariana. url: <https://www.upb.edu.co/es/noticia/proyecto-de-biose%C3%B1ales-triunfo-en-roma>.
- **Newspaper La Crónica**, Disclosure in the newspaper *La Crónica del Quindío (Armenia)*, of the award “Best Student Paper Award” obtained in: 9th International Joint Conference on Biomedical Engineering Systems and Technologies, Rome, Itay. Date: 14 march 2016. Authors: Juan C. Yepes, Samuel Bustamante, Vera Z. Pérez and Julio C. Correa. Universidad Pontificia Bolivariana. url: <http://www.prensanet.com/upb/index.php?res=1366&linknoticia=4727150§or=16088&codigo=7443223418112/2>.
- **Radio UPB**, Radio program *Ingeniando* in the *Radio Bolivariana* station, Auditory Report on Rehabilitation Engineering - Biomechatronics, Authors: Vera Z. Pérez, Abelardo Escoto and Juan C. Yepes, Date: 19 May 2015.